LEVERAGING EMI SIGNALS FOR APPLIANCE DETECTION AND ENERGY HARVESTING

Submitted in partial fulfillment of the requirements
of the degree of

Doctor of Philosophy

by

Manoj Gulati
(Roll No. PhD1327)

Supervisors:

Prof. Shobha Sundar Ram
Prof. Amarjeet Singh

INDRAPRASTHA INSTITUTE *of*
INFORMATION TECHNOLOGY **DELHI**

Department of Electronics and Communication Engineering
INDRAPRASTHA INSTITUTE OF INFORMATION TECHNOLOGY
DELHI
2020

Leveraging EMI Signals for Appliance Detection and Energy Harvesting

by

Manoj Gulati

Submitted to the Department of Electronics and Communication Engineering
in partial fulfillment of the requirements for the degree of

Doctor of Philosophy

at the

INDRAPRASTHA INSTITUTE OF INFORMATION TECHNOLOGY, DELHI

2013-19

Author .....
Department of Electronics and Communication Engineering
December 03, 2019

Certified by .....
Dr. Amarjeet Singh
Assistant Professor, IIIT-Delhi
Thesis Supervisor

Certified by .....
Dr. Shobha Sundar Ram
Associate Professor, IIIT-Delhi
Thesis Supervisor

Accepted by .....
Department of Electronics and Communication Engineering
IIIT Delhi

Leveraging EMI Signals for Appliance Detection and Energy Harvesting

by

Manoj Gulati

Submitted to the Department of Electronics and Communication Engineering
on December 03, 2019, in partial fulfillment of the
requirements for the degree of
Doctor of Philosophy

Abstract

Electromagnetic interference (also known as EMI) is a byproduct of high-speed switching circuits used inside most of present-day electrical and electronic appliances. EMI propagates through conduction along the power lines and through radiation to limited distances. Due to its intrusive nature, EMI signals are generally suppressed or filtered out. Despite this, these signals are fairly ubiquitous. Hence, we explore the possibility of leveraging the weak EMI signals for two applications - appliance detection and energy harvesting.

There has been increased research, in recent years, in appliance detection for *non-intrusive load monitoring* (NILM). NILM facilitates consumers with direct energy feedback, information regarding daily activities, and supports data-driven load scheduling for realizing the long-term goal of optimization of energy consumption in buildings. Traditionally, appliance detection has relied on low-frequency smart meter data. However, in current literature, NILM has been unsuccessful in identifying many information technology loads - such as laptops, desktop computers, modems, and projectors - due to their complex time-varying power consumption patterns. In our thesis, we have investigated the use of conducted and radiated EMI, arising from the switching circuits within these loads, as unique and time-invariant features for detection and classification.

Differential mode (DM) conducted EMI signals were first proposed in 2010 as possible features for identifying appliances having complex power consumption patterns. However, these EMI signals were not robustly characterized to ascertain their effectiveness in real world scenarios. In my thesis, we conducted an in-depth study of DM EMI signals through both measurements and simulations for 24 different appliances. Our studies showed that the performance of DM EMI is impacted significantly by the power line impedance, the filters present in the switching power supply circuitry of neighboring appliances on a common power line and power line harmonics.

Based on our findings with DM EMI, our follow-up work proposed common-mode (CM) conducted EMI for appliance detection. CM EMI originates from capacitive coupling from the switching circuitry and flows along the earth conductor. Hence, the signal is not affected by power line harmonics. Also, most appliances are not fitted with common mode chokes because of which the signals from multiple appliances do not interfere with each other. Hence, the CM EMI is a far more robust feature for appliance detection. In order to experimentally test our hypothesis, we designed an EMI sensor to simultaneously monitor both DM and CM EMI from appliances. We evaluated the detection performance, across multiple instances of five commonly used electronic appliances typically found in office setups. We used statistical features derived from the histograms of measured EMI signals to differentiate across the various classes of appliances. We found that the CM EMI indeed serves as a superior feature, having higher detection accuracy of 87% in comparison to lower accuracy of 45% in the case of DM EMI. Expanding on this line of work, we envision CM EMI data to be combined with instantaneous, low-frequency power data gathered from smart meters to provide actionable insights to energy stakeholders.

Along with conducted EMI, we also explored radiated emissions (also known as RFI) from appliances with an end goal of providing personalized energy apportionment (PEA). PEA is a process of attributing energy consumption to individual stakeholders in a shared space. As radiated emissions can propagate as far as 30cm, they can be leveraged using a wearable sensing device for mapping appliance usage to the instantaneous power data from smart meters. In our study, we characterized RFI from 10 electrical and electronic appliances, in multiple test scenarios, at variable distances. Our test setup consisted of custom-off-the-shelf components like software defined radio and ultra-wideband antennas. We found that a simple peak finder algorithm yielded 72% accuracy for detecting these appliances using RFI signals.

Taking our initial exploration with EMI signals one step further, we employed low-frequency stray emissions from AC power lines for energy harvesting. Energy harvesting is a process of scavenging energy from ambient physical sources - such as mechanical load, vibrations, temperature gradients, and light - to support battery-less low-power sensing in the nW-mW range. Since the advent of cyber-physical systems and the internet of things, energy harvesting has been a topic of interest. However, the intermittent nature of existing natural sources restricted the applications of energy harvesting.

In this thesis, we leveraged the ubiquitous and continuous nature of stray electric fields from power lines, for facilitating 24x7 energy harvesting for long-term, self-powered deploy and forget sensor networks. Stray electric field signals do not require an isolating wire bundle or an active appliance for harvesting, unlike stray magnetic field signals. We proposed a novel capacitive energy harvester (CapHarvest) with an ultra-low-power management circuit connected to the harvesting electrodes to effectively gather energy from this nano-watt source. Furthermore, we demonstrated the efficiency of our circuit for powering two applications. The first application, called

ApplianceTag, is a new stick-on sensing system which monitors appliance state using stray magnetic field signals present around the power line. The second application, called FarmCheck, monitors all the ambient physical parameters like temperature, light intensity, and relative humidity for vertical farming applications.

This thesis paves a new dimension of sensing and repurposing the otherwise ignored ubiquitous EMI signals for appliance detection and energy harvesting to support the long-term goal of energy sustainability. In the future, the blend of simultaneous sensing and energy harvesting - as demonstrated with CapHarvest - may enable more such exciting applications.

Thesis Supervisor: Dr. Amarjeet Singh
Title: Assistant Professor, IIIT-Delhi

Thesis Supervisor: Dr. Shobha Sundar Ram
Title: Associate Professor, IIIT-Delhi

Acknowledgements

Salute to the mother (Smt. Shanti Devi Gulati), who dedicated herself to his son's betterment and stands like a rock for son's protection. Thanks to her for showing the path of patience and perseverance.

My Father (Lt. Shri Mukesh Gulati) supported my studies, despite all the hurdles he faced in his life, sacrificing his bread and his life too!

I also acknowledge all my great mentors who have nurtured me over the years, like a self-less gardener. I will try to give back directly or indirectly for the betterment of society.

Finally, I would love to thank my friends, who were always there during not-so-good patches of my life.

A special thanks to all my spiritual masters for showing the path whenever and wherever I required it.

And my prospective wife (Nikki Rai) waited patiently and let me finish my Ph. D.

With Sincere Gratitude,
Manoj Gulati

Contents

List of Figures

List of Tables

Acronyms

Abbreviation	Full Form
AC	Alternating Current
AD	Appliance Detection
ADL	Activities of Daily Living
AUT	Appliance Under Test
BGN	Background Noise
CapHarvest	Capacitive energy Harvester
CFL	Compact Fluorescent Lamp
CM EMI	Common Mode Conducted EMI
DAQ	Data Acquisition Systems
DC	Direct Current
DM EMI	Differential Mode Conducted EMI
DPP	Distant Plug Point
EH	Energy Harvesting
EM	Electro-Magnetic
EMI	Electro-Magnetic Interference
EMC	Electromagnetic Compatibility
HPF	High Pass Filter
HVAC	Heating, Ventilation and Air Conditioning
IOT	Internet of Things
kNN	k-nearest neighbor

Continued on next page

Table 1 – continued from previous page

Abbreviation	Full Form
LPF	Low Pass Filter
LT	Linear Technology
NILM	Non-Intrusive Load Monitoring
NPP	Nearby Plug Point
PEA	Personalized Energy Apportionment
PL	Power Line
RFI	Radio Frequency Interference
SDR	Software-Defined Radio
SMPS	Switched-Mode Power Supplies
SPP	Sensing Plug Point
TI	Texas Instruments
UPS	Uninterrupted Power Supply
USRP	Universal Software Radio Peripheral
UWB	Ultra-Wide Band

Chapter 1

Introduction

"Your Noise is My Signal,"

Shwetak N. Patel, University of Washington,

Since the early days of radio and telegraph communications, it has been known that switching circuits generate electromagnetic waves, rich in spectral content, that can interfere with electronic and electrical devices in the neighborhood [3, 4]. This phenomenon, known as EMI, may propagate through electrostatic coupling, electromagnetic induction, conduction, or radiation depending on the frequency [3]. A major portion of EMI transmits in the form of conducted EMI. Conducted EMI can further be categorized as DM conducted EMI or CM conducted EMI depending on the mode of coupling [5]. Present-day power electronic circuits are specifically designed with filters, chokes, and shields to mitigate EMI and adhere to EMC guidelines laid down by the International Electro-technical Commission. However, these signals can never be entirely suppressed [3]. Due to the ubiquitous nature of these signals, a recent research question that has emerged is whether these electrical signals can be used to some benefit [6]. In this thesis, we examine the possibility of using EMI for two applications - appliance detection and monitoring and energy harvesting. We discuss the research questions, methodology, and results pertaining to each of these applications in greater detail.

1.1 EMI for Appliance Detection

Appliance detection has been a popular research topic under the broader ambit of NILM. NILM is a process of analyzing changes in the voltage and current at the mains level to deduce appliance level energy consumption patterns [7]. Furthermore, NILM provides a low-cost alternative to attaching individual monitors on each appliance [7, 8]. Such appliance level consumption information, can facilitate actionable insights on activities of daily living (ADLs) [9], provide personalized energy feedback [8] and support data driven load scheduling. Darby et al. in her review paper suggested that direct energy feedback can yield up to 5-15% of energy savings and is quite effective in optimizing energy consumption [10].

Most of the present-day appliances rely on high-speed switching circuits (also known as SMPS[1]) to power-up, which consume power in a non-linear and time-varying manner to improve efficiency [5]. Current NILM techniques, based on machine learning algorithms [8, 11, 12], often underperform or fail to identify these appliances due to their complex power consumption behavior [13].

In recent years, along with our exploration with HF EMI signals in commercial and office buildings, several other research groups also investigated other HF approaches for NILM and AD. There are several attempts to design low-cost HF sensing systems that can measure voltage and current waveforms at higher sampling rates typically around a few kHz in comparison to conventional LF smart meters [14, 15, 16, 17, 18, 19, 20, 21]. Most of these systems are built using commodity and open-source hardware to facilitate ease of scalability, repair, and maintenance. This has also resulted in several HF energy datasets ranging from tens of kHz to hundreds of kHz specifically logged for NILM research.

PLAID is a high resolution (30 kHz) energy dataset [22, 23] having 17 distinct types of individually metered appliances, having 330 different makes and models. Likewise, it also contains data for the combined operation of 13 of these appliance types. Kahl proposed NoFaRe, a non-intrusive facility resource monitoring system

[1]Switched-Mode Power Supplies

[24] to enable low-cost monitoring of electrical devices in buildings using advanced Non-Intrusive Load Monitoring (NILM) techniques. In this work, authors specifically target facility management based on the Building Management System (BMS) prototypes.

One more work proposed a model to generate a realistic synthetic dataset for commercial buildings [25, 26], to circumvent the need for real-world data for commercial buildings. In this work, authors account for both public and private real-world energy datasets to generate this model. Along with this, the authors also presented a detailed statistical analysis of ED in commercial buildings [27] similar to [28]. Statistically analyzing residential and commercial buildings, especially for clustering them using their load curves, is a new research thread. It can lead to collective optimization strategies customized and implemented on a set of buildings having identical load profiles [29, 30].

Another dataset, WHITED [31, 32], measured transients of both voltage and current waveforms recorded for the first 5 seconds of appliance start-up around 110 appliances (47 different categories). These measurements are taken in households and small industry settings in different regions around the world. In addition to this, there are few more HF energy datasets like COOLL [33], REDD [34], BLUED [35], UK-Dale [36], and LIT-Dataset [37].

Apart from this, this expedition has led to several analytical techniques using HF data for NILM and AD. Giri et al. proposed an energy estimation framework for event-based methods used in NILM [38]. This framework automatically builds appliance models using classification labels and aggregate power consumption in time-series data. The underlying model relies on feature extraction, clustering, perturbation of extracted states to mimic appliance behavior, creation of FSM models, correction of errors in classification [39], and estimation of energy based on corrected labels. Another extension of this work proposes an error correction framework for sequences resulting from known state-transition models [40]. Bolt [41], introduced an online binary matrix factorization of current waveforms for ED and evaluated this on a publicly available dataset. Once the model is trained, the algorithm can perform

inference in real-time on inexpensive general-purpose hardware, which allows leveraging high-frequency information without offloading it for computation. These authors also proposed a neural algorithm performing variational identification and filtering for stochastic non-linear dynamical systems [42]. They have applied this to NILM by enforcing domain-constraints of the state variable. The algorithm makes use of an approximate inference technique called Variational Inference in conjunction with Deep Neural Networks as the optimization engine. Authors of the BOLT framework also proposed an extension, Dyna-BOLT [43] recently. In this work, Domain Adaptive Binary Factorization of current waveforms for NILM is proposed. Authors provide private decoders for the source and target domains to account for the differences in the current waveforms. Also, they tie the weights between the two decoders using a specifically trained metric to distinguish between appliance classes.

Kahl et al. performed a comprehensive feature study for appliance recognition on high-frequency energy data [44]. Authors evaluate a broad set of features consisting of 36 signatures for electrical appliance recognition, extracted from HF start-up events. An extension of this work attempted appliance classification across multiple HF energy datasets [45]. In this work, the authors experimented with four different classifiers on 36 spectral and temporal features to perform a cross-, mixed-, and intra-dataset validation. The same authors also proposed an Unsupervised Multi-Environment Event Detection framework (MEED) leveraging multi-variate supervised classification of SMPS based appliances [46, 47].

Henriet proposed a matrix factorization technique based on Semi Non-Negative Matrix Factorization (SNMF) for NILM in commercial buildings [48]. This optimization problem is constrained with total variation penalization (TV-SNMF). Experiments on a simulated commercial building dataset show significant improvements compared to other approaches such as Independent Component Analysis (ICA) and classic SNMF. Furthermore, Henriet also explored Independent-Variation Matrix Factorization for NILM and tested it against Independent Component Analysis (ICA) and Semi Nonnegative Matrix Factorization (SNMF) [49]. Experiments performed on a synthetic source separation problem, and a practical NILM application for large

commercial buildings show that IVMF outperforms competing methods. This algorithm is particularly appropriate for recovering positive sources with a strong temporal dependency and sources whose variations are independent of each other.

One significant difference with these HF techniques is that all of them are focused on capturing voltage and current waveforms at a few kHz. While, in our case, we measured HF EMI signals which are in the range of 10 kHz to 5 MHz. Within the EMI domain, several attempts [11, 9] have been made to investigate the possibility of using DM EMI - generated by SMPS between phase and neutral wires of power lines - as a unique signature for appliance detection. However, despite the initial promise, some fundamental questions regarding the effectiveness and robustness of DM EMI for appliance detection remained unanswered. In our first study on DM EMI, we specifically set out to answer the following questions:

- Do the EMI characteristics of an appliance vary when observed at different places within a home?
- Do conducted EMI from multiple appliances interfere with each other? Are the interference mechanisms unique to an appliance, or will they vary depending on the other appliances that are connected to the power-line?
- Does background noise from the power-line infrastructure that may differ from one home to another, significantly impact the observed EMI from an appliance?
- Do all appliances follow specified EMI standards?
- Do all appliances of the same category exhibit similar EMI characteristics?

To address this, we performed systematic empirical evaluation and designed physics-based simulation models to study the characteristics of DM EMI. We created multiple experiments to characterize conduction of DM EMI signals in different scenarios to test (1) the impact of line impedance on the conducted DM EMI signal; (2) the effect of EMI filters of the neighboring appliances on the EMI generated by the appliance under test; (3) and the impact of background noise present on the power lines due to the harmonics of the power supply. The results of our first study are the following:

- The impedance of a power-line attenuates the conducted DM EMI. Consequently, the EMI characteristics of an appliance vary when observed at different plug points within a home.
- The DM EMI signals from the appliances interfere with each other, resulting in distorted signatures when multiple appliances are connected to a common power supply.
- The DM EMI signals are significantly impacted by background noise from the power-line infrastructure - such as the harmonics of the main power signal.
- Not all appliances follow the specified EMI standards.
- All appliances of the same category, e.g. CFLs from different manufacturers, may not exhibit similar EMI characteristics.

To address the challenges associated with DM EMI, we explored the use of CM conducted EMI in our follow up study. CM EMI also originates from SMPS based power supplies and circulates through the power-line [3]; however, it is less likely to suffer interference from power-line noise and attenuation from EMI filters as it propagates through the earth wire which is only meant for leakage currents (stray signals) unlike phase and neutral conductors. Additionally, most of the present-day appliances carry bidirectional EMI filters, which are meant to suppress DM EMI, but common-mode EMI chokes are mostly limited to medical equipment and rarely used on residential and office devices such as the information and technology (IT) loads.

IT and office loads such as LCD monitors, laptops, printers, desktop CPUs, and CFL lamps constitute a significant proportion of energy wastage in office spaces when they are left operational during non-working hours. Currently, IT plug loads account for 12%-50% of commercial building energy consumption, and they are expected to increase in both proportion of energy use and actual energy use, as office equipment energy consumption is expected to rise at a rate of 0.8% per year [50, 51].

Current single point sensing solutions with smart energy meters have been unsuccessful in detecting these IT and electronic loads, due to their dynamic power

consumption patterns [7, 13, 8]. Quite a few attempts have been made to model this power behavior [13, 8] like using time-domain voltage and current transients as appliance signatures [52], utilizing event window to label individual non-overlapping electrical activities [53] and modeling distinct topology of front-end of electronic circuits to identify power signatures [54]. Employing frequency-domain EMI signals for appliance classification [55, 11] and leveraging wavelet-based models to uniquely assign labels to the union of transient and steady-state power signatures of these sophisticated appliances are other techniques being adopted [56]. However, even with so many attempts, very few have taken off from the lab settings to the real-world deployments and commercial adoption in the NILM framework. One such promising effort is using EMI signatures from appliances for appliance identification. These appliances (and many more) generate CM EMI on the phase and neutral power-lines with respect to the earth at low frequencies through capacitive coupling as well as DM EMI between the phase and neutral at higher frequencies through inductive coupling.

Such behavior makes them appropriate for comparing the effectiveness of CM and DM EMI for NILM in a real-world environment. In this thesis, we designed a small portable sensor made of commercial, off-the-shelf components to simultaneously measure both CM and DM EMI generated by these IT and office loads. We used a nearest neighbor-based classification algorithm on the statistical features extracted from histograms of the measured EMI signals. Our experimental evaluations showed 87% detection accuracy using CM EMI signals when compared to 45% accuracy with the DM EMI signals from the same set of appliances. We further demonstrated that the CM EMI signals gathered from a single instance of an appliance can be used to detect other appliances of the same make and model. This is particularly relevant in an office scenario where multiple instances of appliances having the same make and model are likely to exist.

Continuing with this idea, we also explored radiated emissions (also known as RFI) from appliances and power-lines for appliance detection. Radiated emissions are also part of EM noise signals generated from switching circuits in appliances with a difference that their mode of transmission is radiation rather than conduction.

These signals also carry a significant amount of information about the type of appliance from which they are radiated. Our idea of using radiated emissions for appliance detection was to design a wearable sensing system, which can help in inferring the appliance being used and also allow us to assign this energy usage to the individual who has operated this appliance. Typically this process is known as *personalized energy apportionment*, which is quite useful for shared spaces having multiple stakeholders, and net energy consumption has to be attributed to all of them in a personalized manner.

Prior work in radiated emissions involved using a copper plate as an antenna [57], capacitive [58] and magnetically coupled sensors [59]. However, most of these sensors required touching the appliance to capture the stray electric or magnetic field. Also, the lower sensitivity of these sensors to the electromagnetic field strength affected the detection of the appliance at long ranges. To overcome these challenges and in order to capture these stray emissions effectively, we developed an RFI sensor using off-the-shelf UWB antennas and a SDR system from Ettus Research[2] for sensing. UWB antennas can provide a higher gain over a wider bandwidth along with better impedance matching. Also, ultra-low noise circuitry in SDR allows us to monitor weak signals, which were otherwise hard to capture with conventional analog DAQs.

In our work, we precisely worked on answering the following questions -

- How do the characteristics of RFI signatures vary for the different classes of appliances?
- How do RFI signatures vary with an increase in distance between the source and sensor?
- How do signatures vary for different electrical states (such as standby, active, shut-off) of the same appliances?

This study allowed us to characterize the weak RFI signals in a controlled manner before establishing them for appliance detection with a contactless wearable sensor.

[2]https://www.ettus.com/

We did a rigorous empirical evaluation of RFI signal measurements from ten electrical and electronic appliances at varying distances. Additionally, we found that a simple peak-finder algorithm could yield 72% accuracy in detecting these appliances using RFI signals, which could be subsequently employed for energy apportionment in shared spaces.

1.2 EMI for Energy Harvesting

The second application of EMI that we investigated was for energy harvesting. According to the 2017 forecasts by Gartner Inc, a total of 20.4 billion IoT devices will be connected to the Internet by 2020[3]. These devices demand frequent battery replacement, adding to overall deployment and maintenance costs. As the number of connected devices continues to grow, the need for scalable power management poses a major concern. Self-powered sensor nodes have emerged as a possible solution to the problem, relying on energy harvesting to continuously power them up. Energy harvesting is a process of scavenging energy from ambient physical sources - such as mechanical load, vibrations, temperature gradients, and light - to support battery-less low-power sensing in the nW-mW range [60]. However, none of these sources can be used reliably for continuous sensing applications due to the intermittent nature of these physical signals. Instead, in our research, we focus on stray fields (electric field and magnetic field) generated from low-voltage AC power-lines. The ubiquitous AC power-lines can be used to harvest energy 24x7 for ambient sensing nodes without any hassle of replacing batteries, connecting power adapters and their additional maintenance.

Previous works, that discussed harvesting stray magnetic field from AC power-lines, required bulky electromagnetic harvesters like inductive coils or transformers placed around the phase wire to gather energy. The sensing mechanism also required isolating the phase wire from the rest of the conductors (neutral and earth) in case all three wires were bundled together [61, 62, 63]. In the case of stray electric field harvesters,

[3]https://www.gartner.com/newsroom/id/3598917

the circuits derived local earth ground by making Ohmic contact with the earth wire by running additional wires from the harvester to a nearby ground terminal, or by scraping off the paint to create contact with concrete walls to generate an earth ground [64, 65]. Thus, all of these solutions are inherently intrusive and require mechanical modifications to the electrical circuitry.

In our work, we designed our harvester in a manner that it overcomes these challenges. Our configuration carries an additional ultra-low-power management circuit, which continuously harvests from this nano-watt energy source. The main advantage of our system design is that it does not require bulky transducers or isolating conductors like magnetic field harvesting. Additionally, we created an effective earth ground by designing novel double-layer stacked capacitive electrodes. The inner electrode acts as a high potential electrode placed right next to the shielded wire carrying alternating AC voltage. The outer electrode was kept at some distance with an air-gap to serve as a local ground that is loosely coupled with a nearby earth ground. This design allowed us to make a stick-on capacitive energy harvester, which can be deployed on any wire bundle carrying AC voltage for energy scavenging. We used our harvester to collect sufficient energy from the stray electric field around different types of AC power-lines (wires) in various scenarios such that we can enable ambient sensing applications like appliance detection. Also, we could sense physical parameters like temperature, pressure, and relative humidity for smart-home and for indoor farming applications.

1.3 Thesis Impact and Organization

In the future, both appliance detection and energy harvesting using EMI can be fused to enable the broader goal of energy sustainability, connected and smart devices, and ubiquitous sensing. Some examples:

1. Energy harvesting can aid numerous self-powered sensor nodes deployed inside the building during construction.

2. They can be used for supporting distributed sensing of ambient parameters such as room temperature and relative humidity for controlling heating ventilation and air conditioning (HVAC) systems.

3. They can be used to monitor state of appliances and provide real-time feedback to the end electricity consumers. Apart from this, they can help in locating, identifying, and rectifying the malfunctioned and failed instances of appliances.

4. They can serve as active beacons, which can enable indoor localization and fingerprinting applications inside buildings.

This thesis is organized as following: Chapter-2 provides an overview of EMI signals and mechanisms of propagation. Also, it describes methodology and findings from our study where we evaluated DM EMI signals for appliance detection. In Chapter-3, we propose the use of CM EMI signals over DM EMI for appliance detection. Also, the chapter highlights the design of a novel sensor to measure both DM and CM EMI. In this chapter, we present the performance of appliance detection using both of these signals measured from IT and office loads. In Chapter-4, we discuss the characteristics of radiated emissions from shared appliances and assess the efficacy of appliance detection using RFI with an end goal to attribute net energy consumption to the individuals. Chapter-5 introduces a new stick-on CapHarvester leveraging stray EM emissions from AC power lines. The circuit continuously harvests energy to enable appliance detection and ambient sensing applications. Furthermore, we present a comparison of the existing techniques for harvesting energy from AC power lines. We conclude the thesis with Chapter-6 where we highlight some of the future research directions that have been enabled with the work carried out in this thesis.

Chapter 2

Differential Mode Conducted EMI Signals for Appliance Detection

EMI are stray electromagnetic fields, ranging from a few Hz to 10 GHz, that adversely impact the functioning of electrical devices in the neighborhood [3, 66]. Naturally existing sources of EMI are lightning and atmospheric noises while man-made sources include communication devices emitting radio signals, heavy machinery, and HVAC equipment that switch large currents during operation [67].

In this thesis, we focus on exploiting man-made EMI generated from SMPS circuits that are found within many modern electronic appliances. As shown in Figure-2-1, the first stage in an SMPS is an AC to DC converter with a rectifier and filter. A high-frequency switching circuit that generates square-shaped pulses follows this AC-DC circuit. These pulses cause a rapid inrush of current when the load is connected at the output of the SMPS, leading to the generation of EMI [68, 69, 70]. Due to the highly nonlinear nature of these switching circuits, the dominant component of EMI from an appliance consists of the switching frequency and its harmonics. The switching frequencies of these circuits are determined by the output power requirements of the appliance and hence may be unique to an appliance [5]. The size of the power transformer, required to step down the voltage in the second stage of the SMPS circuit, reduces as the switching frequency increases. Therefore, modern compact SMPS are characterized by high switching frequencies (of the order of MHz) unlike

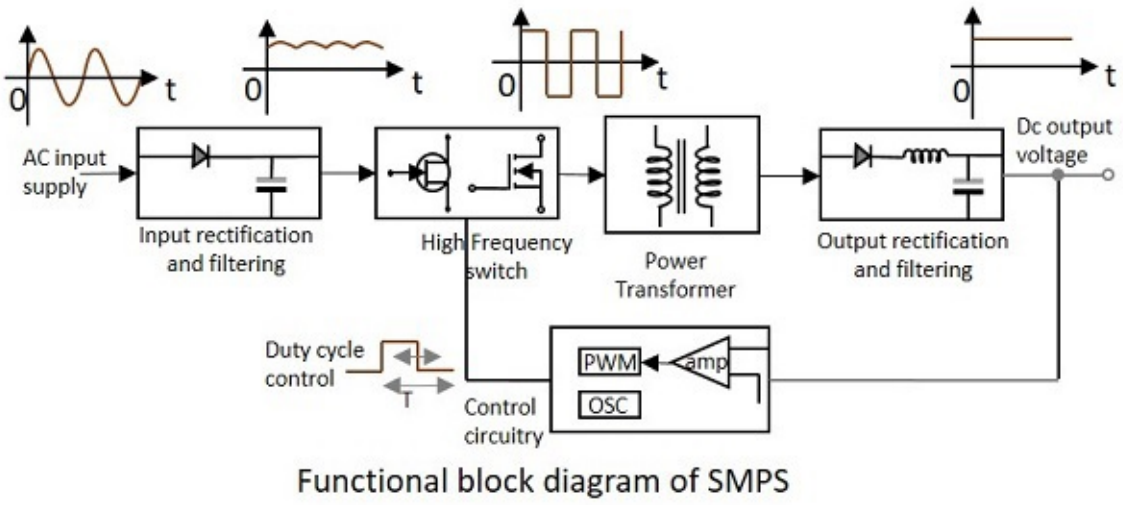

Figure 2-1: Functional block diagram of SMPS highlighting five power conversion stages of an SMPS [1].

traditional linear regulation based power supplies where the step-up or step-down voltage conversion is done at AC power line frequencies of 50 or 60 Hz. Post power conversion, the output high-frequency AC voltage is rectified and filtered back to DC in the final stage. A feedback and control circuit drives the duty cycle of the high-frequency switching stage through a pulse width modulation based error-feedback amplifier [3, 71]. EMI generated by these SMPS based power supplies is propagated either in the form of conducted EMI through the transmission power lines or radiated into the ambient environment as RFI. Conducted EMI is generated when there is a direct conduction route along which these signals can travel [72] and is further categorized into DM EMI and CM EMI.

DM EMI signals appear on the phase and neutral power lines in opposite directions. The time-domain voltage and current differential signals are highlighted as V_{diff} and I_{diff} in Figure-2-2. This kind of interference primarily appears in series with the 110/230V AC power signal [73]. CM EMI signals of identical magnitude and phase occur on the phase and neutral lines with respect to the earth. The voltage and current common-mode signals are shown as V_{cm} and I_{cm} in the figure. The direction of flow of CM EMI currents (I_{cm}) propagating through the phase and neutral conductors towards the earth conductor is identical. The signal on each line returns

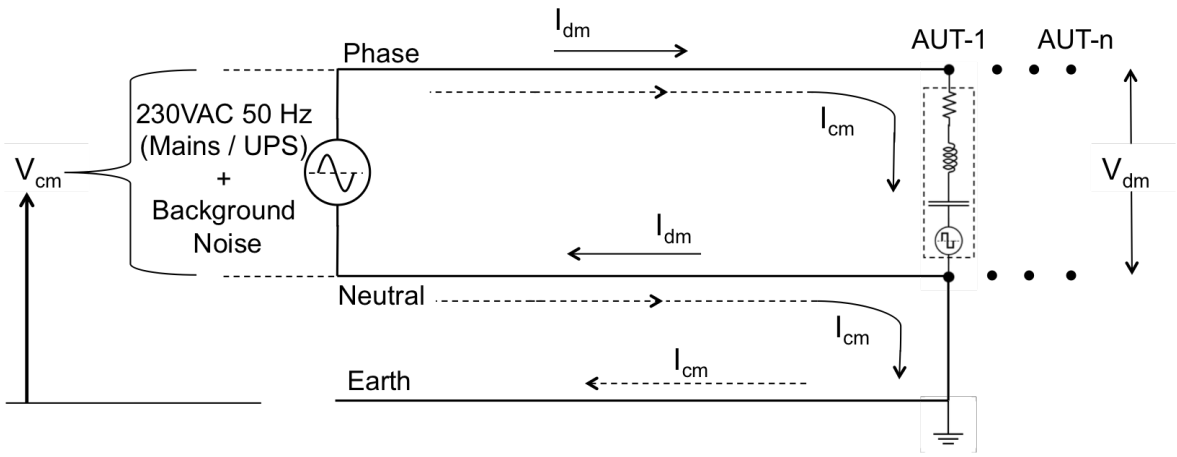

Figure 2-2: Differential mode and common-mode voltage along with the direction of flow of EMI currents (both DM and CM) [2].

through a common ground. In this chapter, we focus on DM EMI from SMPS power supplies for appliance detection. In the subsequent chapters, we discuss CM EMI signals and radiated emissions.

2.1 DM EMI for Appliance Detection and NILM

Appliance detection forms the basis of the NILM. NILM is a technique used to disaggregate the electric load composition of a household using single point sensing usually at the mains power feed. Though NILM was originally introduced more than two decades ago [7], recent large-scale deployments of smart meters by electrical utilities across the world have resulted in increased research interest [74]. However, due to limited data collection capabilities of smart meters being deployed, significant NILM research in the recent past are driven by low frequency data (1 Hz or lower).

While there is some work involving NILM using higher frequency (few kHz - MHz) power consumption data, much of it is limited to controlled laboratory experiments [75]. In 2010, Gupta et al [11] proposed indirectly identifying disaggregated energy consumption using high frequency DM EMI that emanate from electronic appliances. They showed that DM EMI propagates through the power infrastructure and hence can be measured from a single point installation at the home level. A follow up work [76] showed that DM EMI signals can be further used to get detailed information re-

garding the operational state of an appliance e.g. the type of programs being watched on a television. In this chapter, we present the key challenges towards exploiting DM EMI as a unique and deterministic signature for appliance disaggregation. While prior work in power line EMI sensing for NILM may sound promising, much of this work is based upon certain assumptions derived from limited set of experiments. For instance, Gupta et al. [11] observed that SMPS based appliances conduct unique and observable DM EMI. However, their study was restricted to a small set of appliances. Furthermore, they stated that appliances with DM EMI filters will also conduct observable EMI but the actual impact of such filters on the DM EMI signature of the appliance and other devices on the power line was not well studied. Miro and Froehlich et al in their work [55, 76], limited to televisions, observed that DM EMI signatures remain time-invariant and robust to background noise.

Through an extensive set of experiments performed both in lab setting and in a real home, on a wide range of appliances, we show some of the limitations of the above mentioned assumptions.

2.2 Empirical study highlighting implications of using DM EMI for appliance detection

2.2.1 Experimental Setup

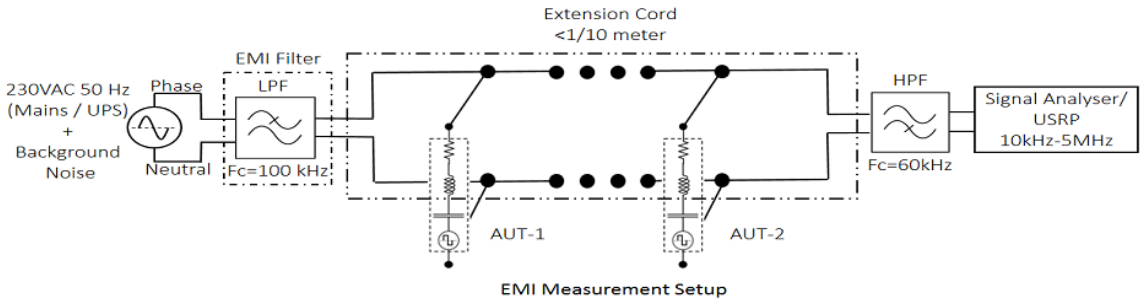

Figure 2-3: Test setup used for DM EMI measurements. AUTs were connected through an optional LPF to the mains power line. Observations after filtering through a differential high pass filter (HPF), shown in detail in Figure 2-4, were made either with a signal analyser or a universal software radio peripheral (USRP).

Figure 2-3 shows details of the experimental setup used for collecting DM EMI data from the 230V power line, for multiple appliances, in both the laboratory and the residential settings. The mains power line consists of 50 Hz power signal, background noise from the electrical infrastructure of the building (such as air handling units, variable speed drives and lighting sources) and DM EMI introduced by the AUTs. To isolate the background noise for some experiments, the mains power supply is replaced with Luminous 600VA UPS. AUTs are connected to the mains either through an off-the-shelf power extension cord, having a distance of few centimeters between plug points or, a custom built 10 meter long extension cord, with a plug point at every 2 meters. Some off-the-shelf extension cords come with built-in low-pass EMI filters, to isolate the appliances from noise in the power supply. To analyze the impact of such filters, an Elcom EP-15AP power line DM EMI filter offering an attenuation of approximately 10 to 20 dB from 1 MHz to 100 MHz is used for some of the experiments. Though IEC specifies the range of conducted EMI from 9 kHz to 30

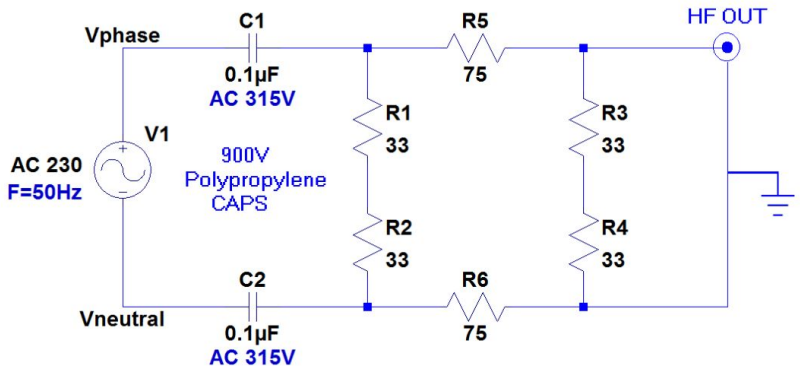

Figure 2-4: Differential High Pass Filter schematic and it's interconnection to the mains power supply.

MHz, the AUTs, in our measurements, show DM EMI only up to 5 MHz. A custom built differential HPF shown in detail in Figure-2-4, with a cutoff frequency of 60 kHz, is used to pass this high frequency DM EMI noise to the measurement equipment (either a signal analyser or a USRP). The high cutoff frequency is chosen in order to prevent the 50 Hz power signal and its harmonics from damaging the sensitive analog front end of the measurement devices. The detailed schematic of the high pass filter

is shown in Figure-2-4. While the circuit is similar to the one previously used in [11], the component values are slightly modified for 230V operation. EMI is measured using either the Agilent N9000A CXA signal analyser or a USRP[1] N200.

DM EMI measurements in the lab settings are carried out with four different configurations of the experimental setup. In setup-1, an AUT is connected to a NPP on the off-the-shelf extension cord. Therefore, the NPP, is a few centimeters from the SPP where the signal analyzer is connected. In setup-2, the AUT is connected to a DPP, 10 meters from the SPP, on the custom extension cord. This test is performed to study the impact of power line impedance on the DM EMI measurements. In both the cases described above, the low-pass DM EMI filter is not connected to the experimental setup. In setup-3, the impact of a power line DM EMI filter is studied by incorporating a low-pass filter to setup-1. In these three cases, extension cords are connected directly to the AC mains power supply. In setup-4, a UPS having 3 power outlets, few centimeters apart, is used to power the AUTs. Since the UPS is independently powered, it is isolated from the noise in the building's electrical infrastructure. Due to the limited power capacity of the UPS, DM EMI measurements with setup-4 could only be carried out for medium and the low power AUTs. In all four cases, DM EMI measurements are carried out with both individual AUT or a combination of AUTs, from 10 kHz to 5 MHz. Additionally, background noise on the power line is measured for each case with the AUTs disconnected from the extension cord. Setup-1 described above is repeated in residential settings while replacing the signal analyzer with the USRP. Table-2.1 shows the list of 24 AUTs used in lab and residential settings along with their manufacturer details and power ratings.

2.2.2 Observations and Analysis

Appliance Specific DM EMI Signatures

In Figure-2-5, we display the DM EMI measurements taken from four AUTs, from test setup-1, along with background noise from the power line. Each appliance conducts

[1] `https://en.wikipedia.org/wiki/Universal_Software_Radio_Peripheral`

S.No.	AUTs	Brand	Category	Power Ratings (in Watts)	Location Used
1	CFL-1, 2, 3, 4	Crompton Greaves [1], Bajaj [2, 3, 4]	SMPS	18, 15, 15, 5	L, R
2	LED Lamp-1, 2, 3	Genre India [1], Unbranded [2], Crompton Greaves [3]	SMPS	5, NA, 0.5	L, R
3	Laptop Charger-1, 2	Dell [1], HP [2]	SMPS	90, 65	L, R
4	Phone Charger-1, 2, 3	Samsung [1], Asus [2], LG [3]	SMPS	NA, 7, 6	L, R
5	LCD Monitor	HP	SMPS	NA	L, R
6	Printer	HP	SMPS	5	L, R
7	Speakers	Harman Kardon	SMPS	24	L, R
8	Modem	Asus Router	SMPS	18	L, R
9	Induction Cooktop -1, 2	Philips [1], Maharaja Whiteline [2]	SMPS	[500,1300], [600,1000]	L, R
10	Microwave	Kenstar	NOT SURE	1250	R
11	Refrigerator	LG	NON SMPS	1020	R
12	Blender	Inalsa	NON SMPS	180	L, R
13	Iron	Philips	NON SMPS	535	L
14	Room Heater	North Star	NON SMPS	1500	L
15	Television	LG	SMPS	60	R

Table 2.1: List of appliances used in Lab and Residential settings

DM EMI in a specific band of frequencies. CFL1 (Figure-2-5a) conducts high DM EMI up to -25 dBm from 80 kHz to 3 MHz; the induction cooktop (Figure-2-5b) conducts DM EMI from 3.5 MHz to 5 MHz; the LED lamp (Figure-2-5c), conducts EMI from 1 MHz to 4 MHz; CFL2 (Figure-2-5d) does not show any noticeable DM EMI. The DM EMI data from CFL1, CFL2 and induction cooktop were collected in the lab while the LED lamp data was collected in the home. The background noise traces clearly indicate that the harmonics of the 50 Hz power signal are suppressed by the high pass filter. Also, the background noise level in the lab data was consistently higher than the background noise level at home. We believe this is because of the complex electrical

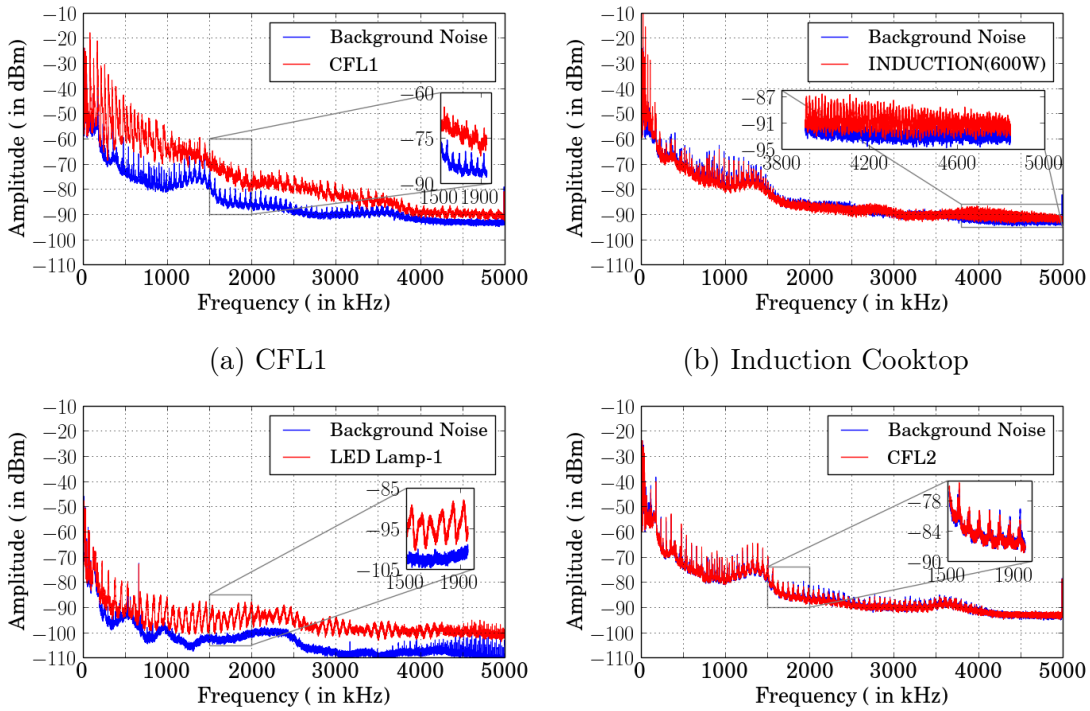

(a) CFL1

(b) Induction Cooktop

(c) Led Lamp-1

(d) CFL2

Figure 2-5: Measured DM EMI from different AUTs connected independently to mains power supply along with background noise traces measured with AUTs disconnected from the setup.

infrastructure in the building where our laboratory is located. Besides CFL2, other appliances such as CFL3 and laptop chargers 1&2 did not conduct any observable DM EMI.

It is worth noting, although identical, even a minute change in switching circuits or passive components used inside SMPS based power supplies cause a distinct EMI signal [3]. Also, most appliance manufacturers follow their custom designs for different SMPS-based supplies with discrete components, leading to separate DM EMI signals across the same class of appliances. For e.g. there are several CFL manufacturers across the globe, but none of them follow identical switching circuits to protect trademarks and copyrights. Hence, even the same CFL (18W) may have a distinct EMI signature depending on SMPS topology's nature and the exact design parameters chosen for that particular model.

These results provide two useful insights - (1) All SMPS based appliances may not

conduct significant DM EMI; (2) DM EMI signatures of the same class of appliances such as CFLs (Figures-2-5a, 2-5d and 2-6a) may not be consistent across different manufacturers.

Effect of Background Noise

Two appliances - a CFL and a router, are used to examine the effect of background noise on the measurable DM EMI from an AUT. Figure-2-6 illustrates observed DM EMI for both the AUTs when connected to mains power supply (setup-1) and UPS (setup-4). The DM EMI from both the appliances are hardly noticeable when they are connected to the mains power supply (see Figure-2-6a for CFL4 and 2-6c for router). This is because of the high interference feature arising from the background appliances on the same power line, resulting in poor signal to interference ratio. When connected to an independently powered UPS, that is isolated from the electrical infrastructure of the building, both the appliances show significant DM EMI (see Figure-2-6b and 2-6d for CFL4 and router respectively). The thermal noise floor is uniform in both the cases and is limited by the bandwidth of the measurement device. These results indicate that in certain sensing configurations, with high background interference, disaggregation of individual appliances with low DM EMI may be challenging.

Effect of Power Line Impedance

Next we study the impact of power line impedance on the DM EMI conducted by AUTs. We measure the DM EMI trace of an AUT, connected at a NPP from the SPP where the measurement device is connected (setup-1). Then the measurement is repeated with the AUT connected at a DPP, 10 meters from the SPP (setup-2). Figure-2-7 shows that DM EMI from CFL1 was attenuated at DPP in comparison to DM EMI observed at NPP especially at high frequencies above 2 MHz. This can be attributed to the transmission line effects of the long extension cord. An in-depth analysis of higher order effects of the transmission line is required to better understand the impact of line impedance on DM EMI measurements. Some extension cords have inbuilt DM EMI filters, to protect the appliances from noise in the power supply.

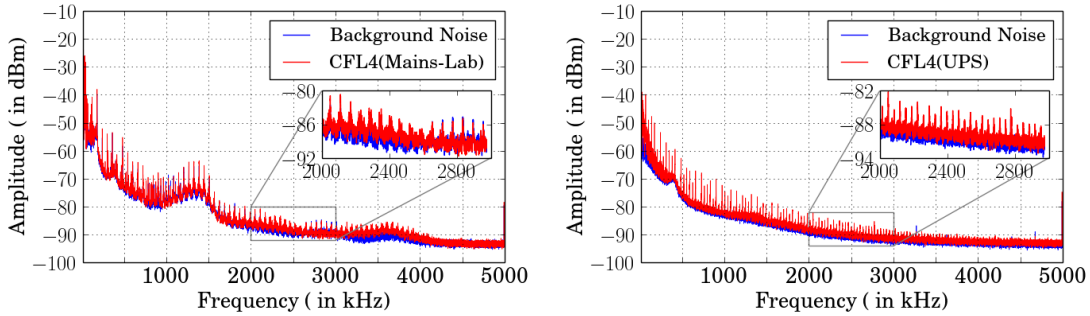

(a) CFL4 connected to the mains power supply

(b) CFL4 connected to the UPS

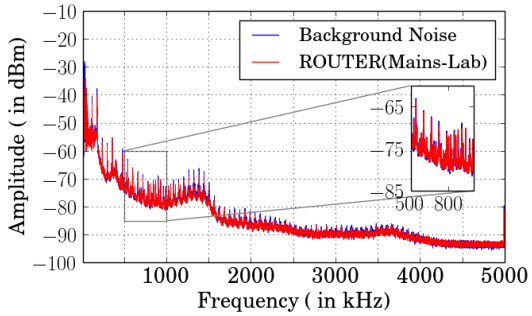

(c) Router connected to the mains power supply

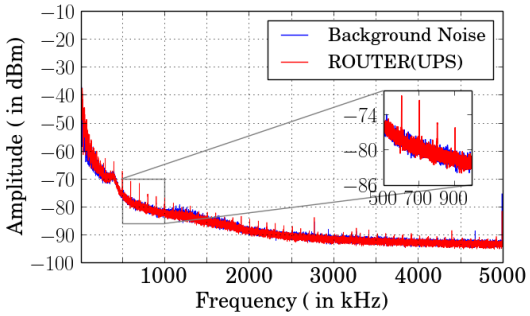

(d) Router connected to the UPS

Figure 2-6: Background noise from mains interferes with EMI from (a) and (c). However, EMI from (b) and (d) can be observed when they are connected to the UPS with a much lower background noise as it is independently powered.

In order to study their impact, we measured the EMI from CFL1 when an external DM EMI filter is connected between the off-the-shelf extension cord and mains power supply (setup-3). This result is shown in Figure-2-8 and compared with the DM EMI, shown earlier in Figure-2-5a, from setup-1 which did not have an DM EMI filter on the extension cord. We observe two effects of the power line filter. First, the strength of background interference features from the power supply is lowered. Second, the DM EMI from the AUT is also lowered. We postulate that this phenomenon occurs because DM EMI currents from the AUT flow into the low impedance path of the filter and hence cannot be measured at the sensing point. Thus the power line DM EMI filters impact the measurability of EMI, of an appliance connected to the power line.

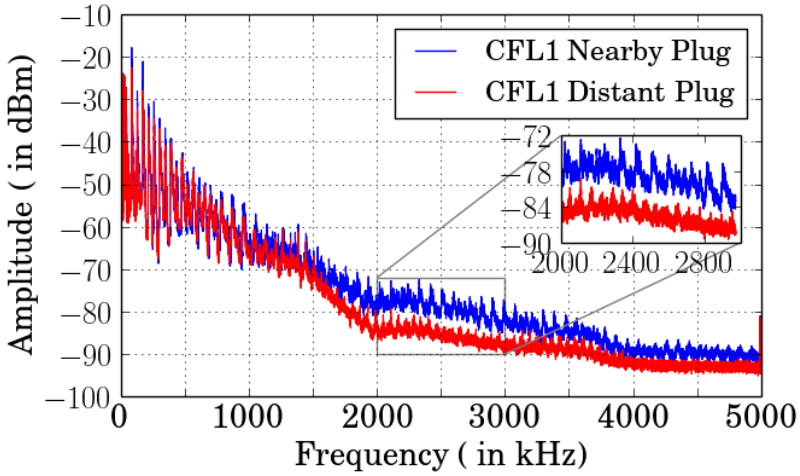

Figure 2-7: Effect of line impedance on DM EMI from CFL1 on a nearby and a distant plug point

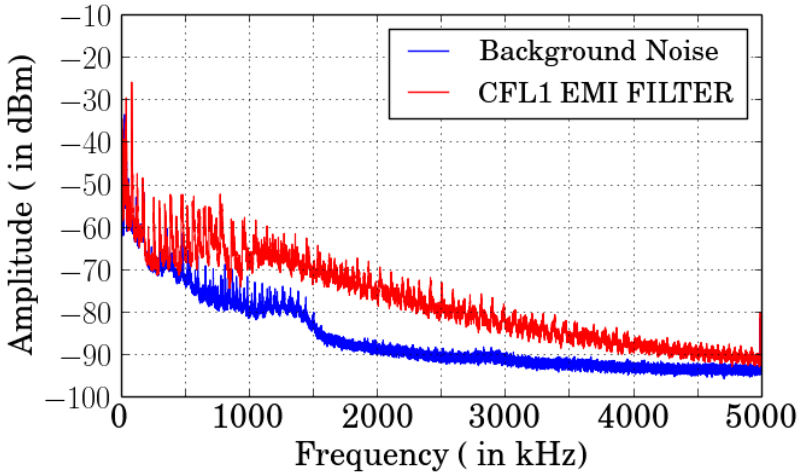

Figure 2-8: Impact of inbuilt DM EMI filter of the extension cord on the EMI observed from CFL1 connected to the mains power supply

Effect of Multiple Appliances on a Common Power Line

Finally, we consider the case, when multiple AUTs are connected on the same power line. This is a common setting in a home where different appliances may operate simultaneously, during some time intervals. Figure-2-9a shows the DM EMI conducted by CFL1 and laptop charger when powered independently and when connected together. As mentioned earlier when connected independently, the DM EMI from the CFL1 is clearly observed while the DM EMI from the laptop charger is weak due

to its inbuilt DM EMI filter. Interestingly, when the two appliances are connected together, the DM EMI of the CFL1 is suppressed from 40 kHz to 1.5 MHz. We postulate that this phenomenon is the result of the low impedance path offered, to the DM EMI currents from CFL1, by the inbuilt DM EMI filter in the laptop charger. Similar behavior is observed when an LED lamp and a laptop charger are connected together (Figure-2-9b). We further investigate this phenomenon, by measuring the DM EMI (as shown in Figure-2-9c) when the CFL1 is connected to NPP with respect to SPP, while the laptop charger is connected at DPP. In this case, the DM EMI currents from CFL1 do not flow through the filter in the laptop charger and instead flow through the sensing point, where they can be measured. This is due to the line impedance introduced between the two AUTs. The damping effect of the inbuilt DM EMI filters of an appliance on the EMI signatures of neighbouring appliances on the power line is significant only when the appliances are in close proximity.

2.3 Simulation Models for DM EMI

During DM EMI measurements, we observed certain factors that affected the conducted DM EMI from an appliance, such as line impedance and appliance coupling behavior (specifically for appliances with low pass DM EMI filters). Further, We designed a generic model for DM EMI that can be customized to mimic actual setup to gain a better understanding of these observations. The following objectives led us towards the development of a detailed simulation model: (1) Actual measurements of DM EMI from an appliance are complicated due to the presence of several appliances in the background. Simulation models allow us to independently analyze the DM EMI from an individual appliance as well as combinations of multiple appliances; (2) Simulations allow us to analyze the impact of transmission line parameters of the mains power line which are difficult to measure in real world settings; (3) Simulation models can be, potentially, useful for generating large volumes of training databases for supervised learning techniques, for appliance level disaggregation.

In the beginning of this chapter, we gave an overview of SMPS operation, which

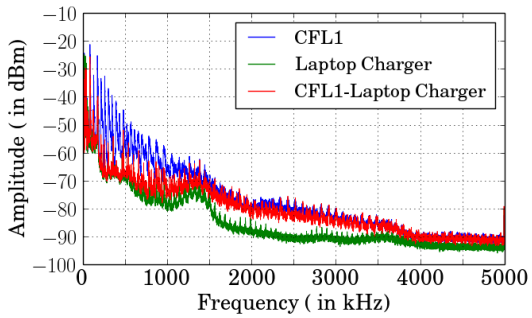

(a) CFL and Laptop Charger

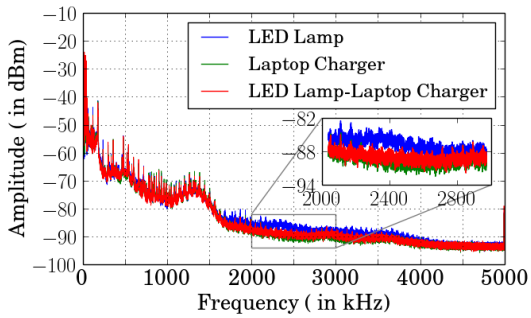

(b) LED and Laptop Charger

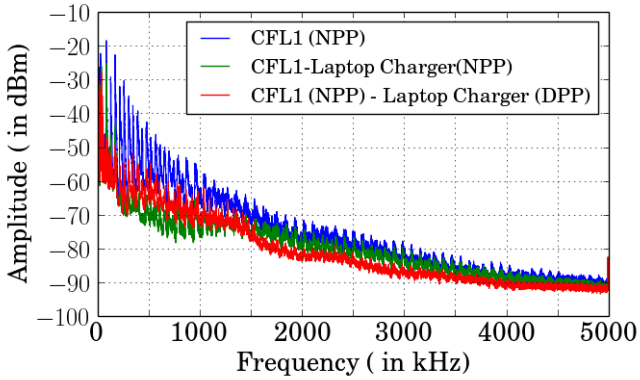

(c) CFL (NPP) and Laptop Charger (DPP)

Figure 2-9: DM EMI as observed with a combination of CFL1 and LED lamp with laptop charger on the same power line. Here, plot(a) and (b) shows the attenuation offered builtin EMI filter of laptop charger and plot (C) shows the reduced attenuation due to increased power-line impedance between CFL1 and Laptop Charger.

forms the basis of our simulation models. Now, we focus on simulating the DM EMI currents generated in the DC to DC converter (switching) section of the SMPS. These EMI currents are coupled to the mains power line through galvanic, inductive or capacitive coupling modes, within the circuit [3].

We assume that the coupling modes of the EMI to the power line are fairly uniform across multiple appliances and do not significantly alter the nature of the DM EMI spectrum, at frequencies up to 5 MHz.

To simulate the behavior of DM conducted EMI, an equivalent model for an appliance's power supply is presented here, utilizing a simplified version of a buck converter shown in Figure-2-10. A detailed description of the behavior of a buck converter is presented in [5]. A buck converter is a standard DC to DC step down

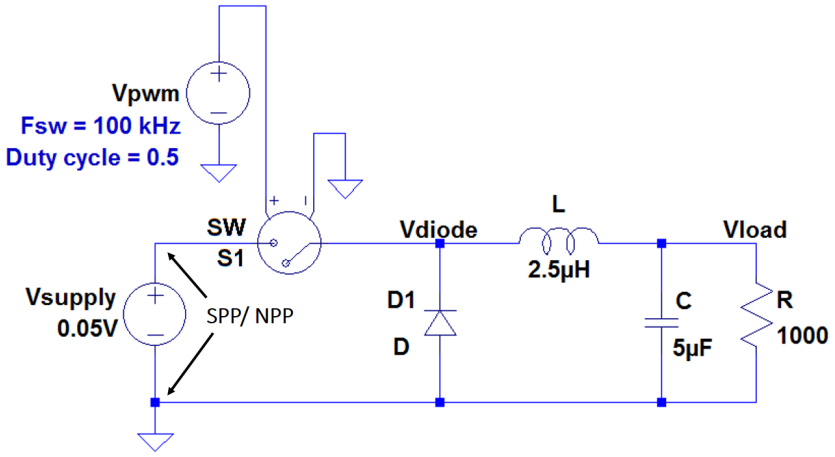

Figure 2-10: Spice model of a simplified buck convertor used as an equivalent appliance model for EMI generation

converter that utilizes a MOSFET or a transistor as a switch, $S1$, to generate a pulsating DC (V_{diode}) from input unregulated DC (V_{supply}). The switching frequency (F_{sw}) and the duty cycle of this pulsating DC are varied by a pulse width modulated (PWM) control signal driving $S1$. V_{diode} is averaged using an inductor-capacitor (LC) combination to provide a constant DC (V_{load}) at the load. The diode, $D1$, provides a path for the current through the inductor to discharge when S1 is "open". The ratio of V_{load} to V_{supply} is governed by the duty cycle of the PWM control signal. A standard buck converter may also consist of a feedback loop to maintain a constant output voltage, in the case of a fluctuating input voltage. We omit this feedback loop in our simulations and, instead, assume a constant DC supply voltage. To simplify this model, we also assume that the load impedance of the appliance is purely resistive (R). The currents ($I(V_{supply})$) drawn from the DC supply of the DC to DC converter are coupled to the mains power line giving rise to EMI. Therefore, the frequency response of $I(V_{supply})$ provides an EMI signature of the appliance.

We model the DM EMI from a specific SMPS based appliance on the basis of DM EMI measurements of the appliance when powered by a UPS. The input parameters governing the simulated DM EMI spectrum are V_{supply}, duty cycle and F_{sw} of PWM control signal, and load impedance (Z/R). F_{sw} is chosen based on the fundamental frequency component and harmonics observed in the measured DM EMI spectrum.

The baseline of the simulated DM EMI spectrum is adjusted to match the noise floor in the measured DM EMI spectrum by modifying the value of V_{supply}. V_{load} and R, are adjusted to control the amplitude of $I(V_{supply})$, which in turn, controls the magnitude of DM EMI peaks in the frequency spectrum. The component values for L & C are computed by buck converter design equations [5]. The width of the DM EMI peaks, observed in the frequency spectrum, are adjusted by introducing suitable series resistances to L and C. The main advantage of the simulation method that we have designed is that, our model is created on the basis of accurate DM EMI measurements of an appliance and not on any prior knowledge of the internal circuitry of the appliance which is usually difficult to obtain.

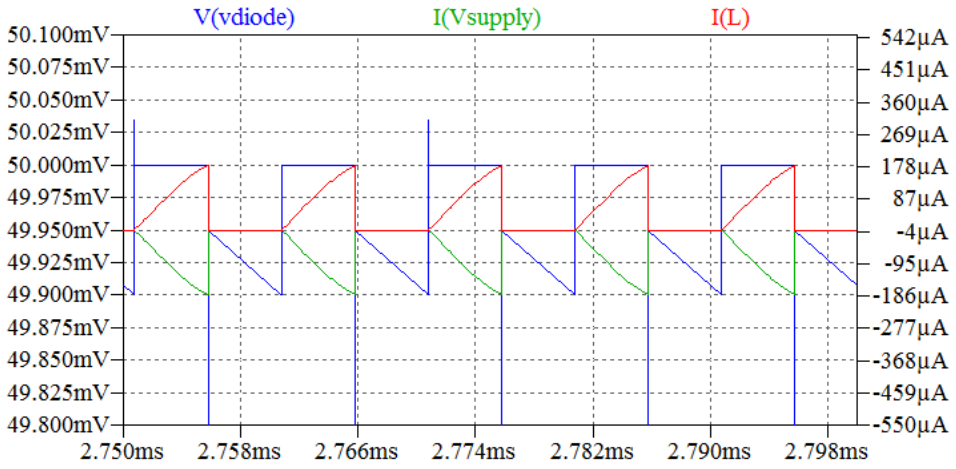

Figure 2-11: Simulated steady-state time domain behavior of a simplified buck convertor used as an equivalent appliance model. $I(V_{supply})$ is the EMI current that couples to the mains power line.

2.3.1 Appliance Specific DM EMI

We present a model to simulate the DM EMI spectrum of a router based on measurements, presented earlier in Figure-2-6d. We computed the following design parameters: V_{supply}=0.05V, duty cycle=0.5, F_{sw}=100 kHz, L=2.5uH, C=5uF and R=1000Ω. Figure-2-11 illustrates the steady-state time-domain results from the simulations. $V(v_{diode})$, the pulsating DC at the diode, has a time period of $1/F_{sw}$ and duty cycle of 0.5. $I(L)$, the current across the inductor, continually charges and discharges during

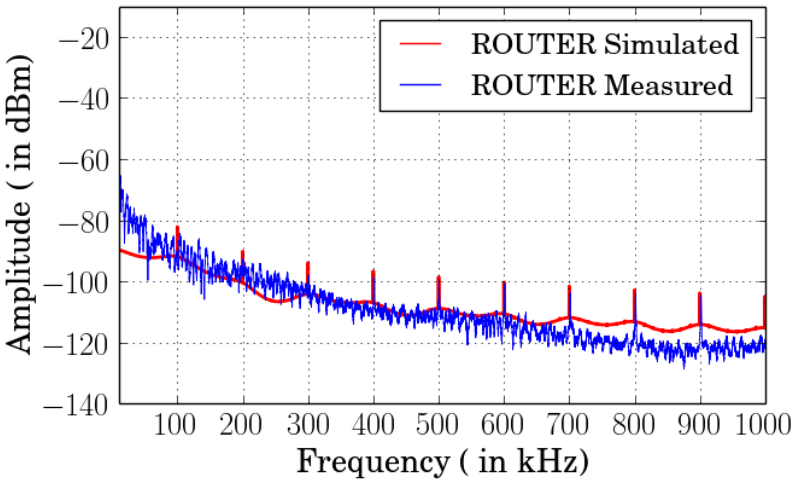

Figure 2-12: Frequency spectrum of simulated DM EMI from $I(V_{supply})$ along with DM EMI observed from router on test setup-3

the ON time and OFF time of the pulse. $I(V_{supply})$ is the current drawn from the DC power supply and is highly non-linear as indicated by the inverted triangular shaped pulses. This current is the primary component that couples to the mains power supply giving rise to DM conducted EMI. The frequency domain response of $I(V_{supply})$ is presented in Figure-2-12. Qualitatively, the simulated and measured spectrums show a good match. For instance, the DM EMI peaks, the baseline and the width of the frequency peaks are similar in both the spectrums. Although the frequency spectrum shows spectral overlap, some baseline noise features observed in the measured DM EMI are not present in the simulated model. The measured data has thermal noise which has not been modelled in simulations. By modifying the parameters of this model, we can generate unique DM EMI signatures for other SMPS based appliances for further analysis.

2.3.2 Impact of Line Impedance on DM EMI from an Appliance

We model the transmission line characteristics of the power line with a series impedance between the sensing point where the DM EMI currents are observed (near the DC supply) and the plug point where the appliance is connected as shown in Figure2-10.

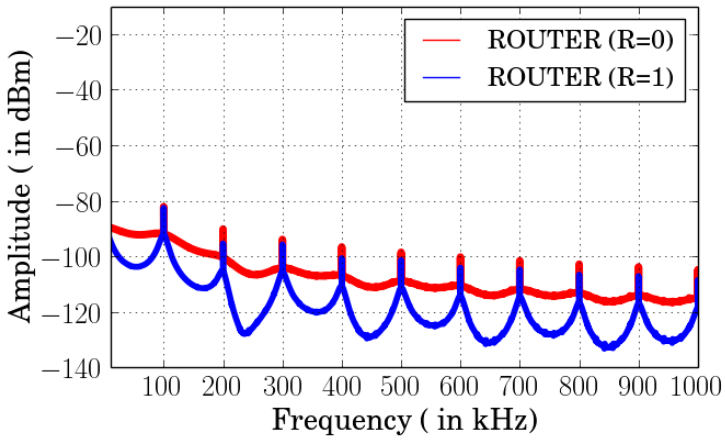

Figure 2-13: Effect of line impedance of $R = 0$ & 2Ω on DM EMI conducted by an appliance.

Though, the series impedance lies on the 230V AC power line in real world settings, we have introduced the equivalent resistance in the internal circuitry of the SMPS. Due to the low frequencies of observation, the effect of the inductance and capacitance of the transmission line are negligible. Most residential electrical lines are characterized by line impedance that varies with the thickness of wires, the number of copper strands, and the quality of shielding material [77]. We model, a 10m long electrical line with a 2Ω resistor. We compare the DM EMI signatures when an appliance is connected near the sensing point (when the line impedance is 0Ω) with the DM EMI signatures generated when an appliance is connected at a distant point, 10m from the sensing point. Figure-2-13 shows that the DM EMI signal from an appliance at a distant point is weaker (up to 7 dBm) than the DM EMI from an appliance near the sensing point. These results are similar to the line impedance effects observed on the CFL data in Section-2.2.2.3.

2.3.3 Impact of Appliance Coupling

In Section-2.2.2.2, we postulated that a DM EMI filter of an appliance can significantly impact the EMI signature of a neighbouring appliance, provided the two appliances are close together on the power line. To validate this hypothesis with simulations, we consider the following three cases which are configured as per Figure-2-14. Figure-2-

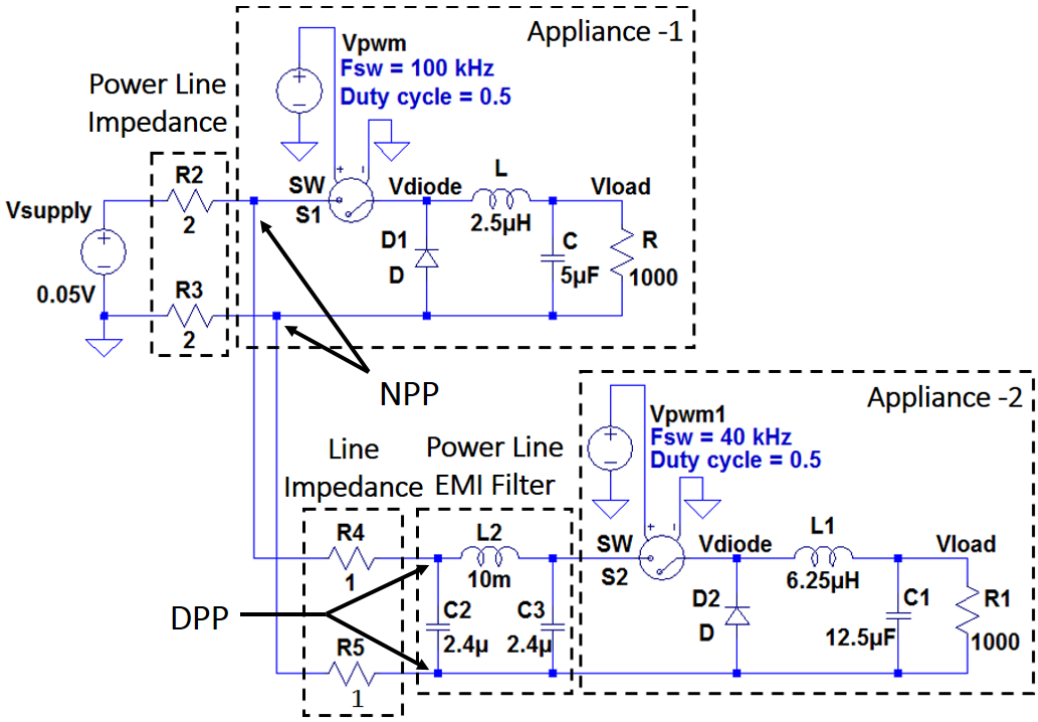

Figure 2-14: Appliance coupling model having, mains PL impedance (Case-1, 2, 3), DM EMI filter (Case-2) and line impedance & DM EMI filter (Case-3).

15 shows the frequency spectrum of the DM EMI currents (DC supply current) for all three cases.

Case-1: Two appliances-1 & 2, without DM EMI filters, are connected together on the same electric line. Appliance-1 has a switching frequency (F_{sw}) of 100 kHz, similar to the router. Appliance-2 has F_{sw} of 40 kHz. Note that in real world settings, the two appliances would be connected on the 230V AC power line. In our simulations, we instead consider the appliances connected to the same electric line from a common DC power supply. Here we are assuming that the EMI coupling mechanisms, from the DC section to AC mains power line, across different appliances are uniform. A series resistance of 4Ω is inserted between the appliances and the power supply, to model the power line impedance. Dominant frequency components in the DM EMI spectrum in Figure-2-15 include the EMI effects from both appliances i.e. 100 kHz & 40 kHz signals and their harmonics. The magnitudes of higher order harmonics decay gradually with frequency. Interestingly, we also observe inter-harmonics due to mixing of the 100 kHz and 40 kHz signals in the non-linear sections of the circuit

(such as diode).

Case-2: In this case, we consider the impact of an appliance with an inbuilt DM EMI filter on a neighbouring appliance. Therefore, a bi-directional DM EMI low pass filter, of 1 kHz cut off frequency, is incorporated into the front-end of appliance-2 (with 40 kHz switching frequency). As expected, the DM EMI filter suppresses the EMI currents (40 kHz and its harmonics) from appliance-2 at the sensing point in the circuit. However, the filter additionally suppresses the DM EMI (100 kHz and its harmonics) from appliance-1 from being observed at the sensing point. This is because the DM EMI filter of appliance-2 offers a low impedance path, compared to the electric line at the power supply, to the DM EMI currents from appliance-1. This simulation validates our earlier hypothesis, in Section-2.2.2.2, that inbuilt DM EMI filters within the module of an appliance have a two-fold effect on DM EMI based appliance disaggregation. The filters not only suppress DM EMI emanating from the appliance that they are connected to but also impact the measurability of DM EMI currents conducted by neighbouring appliances on the power line.

Case-3: In this case we consider how the line impedance between two appliances can impact the effect of the inbuilt DM EMI filter. We simulate conditions when the two appliances, considered above, are 10m apart on the power line by introducing a series resistance of 2Ω in the electric line between the two appliances. In Figure-2-15, the frequency spectrum exhibits weak DM EMI from appliance-2 and significant DM EMI (100 kHz and harmonics) from appliance-1. We observe that the impact of the DM EMI filter in appliance-2 on appliance-1 is reduced since the DM EMI currents from appliance-1 do not find a low-impedance path through the DM EMI filter when significant line impedance is introduced between the two appliances.

2.4 HFED Dataset and Spice Model Simulations

Our High Frequency EMI Dataset (HFED)[2] is also released as part of this work. It contains DM EMI traces collected from both lab and home settings, having 24

[2] `http://hfed.github.io`

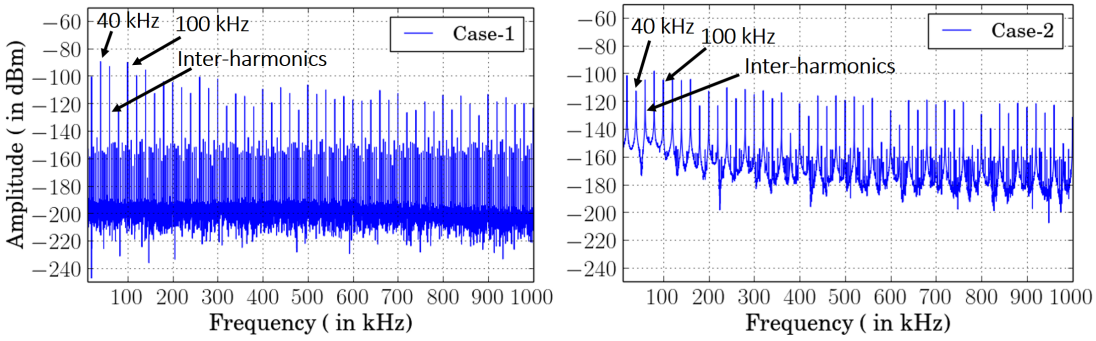

(a) Coupling with line impedance

(b) Coupling with one appliance having DM EMI filter

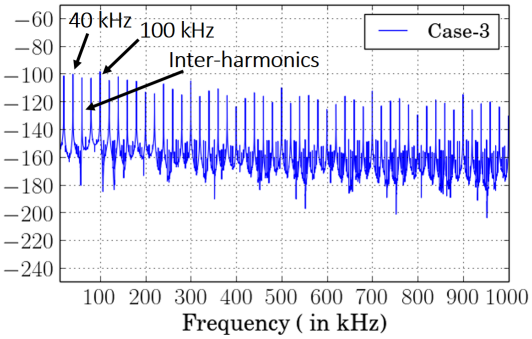

(c) Coupling with line impedance and one appliance having DM EMI filter

Figure 2-15: DM EMI spectrum, obtained from simulation model for the three used cases - Case-1, Case-2, Case-3.

appliances connected over four different test setups in lab settings and one test setup in home settings. DM EMI data from lab consists of data from signal analyser as well as USRP, while home data contains data from USRP only. DM EMI measurements from signal analyser and USRP are taken over a frequency range of 10 kHz to 5 MHz.

Parameter	Value
Frequency range	10 kHz to 5 Mhz
Number of appliances tested	24
Number of test setups	5 (4 in home, 1 in lab)
Number of FFT points	32k (Signal Analyser), 100k (USRP)

Table 2.2: Summary of HFED dataset

To further facilitate reproducible research, we also release our CAD layout files and our SPICE simulations on the dataset webpage. Our dataset is summarized in Table 2.2.

2.5 Conclusion

In this chapter, we highlight some key observations obtained from our in-depth study of DM EMI signatures over an extensive set of home appliances, tested in both laboratory and residential settings. Some of these observations either counter or qualify the observations made in earlier DM EMI related research (e.g. not all SMPS based appliances will conduct DM EMI due to high attenuation offered by inbuilt DM EMI filters) or provide novel insights (e.g. DM EMI from neighbouring appliances may significantly interfere through the DM EMI filters and line impedance along the power line). Empirical analysis, discussed in this chapter, calls for a detailed review of different factors that may impact the observed DM EMI from appliances before using the DM EMI as a signature for appliance disaggregation. Setting up controlled environments for better understanding of EMI sensing may either neglect real conditions - by isolating background noise and interference from other appliances on the power line; or would require a very extensive study accounting for all of these noise factors. To simplify the overall review process, accurate simulation models that account for several of these noise factors will significantly help in improved and thorough understanding. We made the first attempt in creating such simulation models and demonstrated their utility in explaining some of the peculiar behavior discussed in this chapter through physics. Such simulation models can further help in analyzing minute events which are otherwise not observable with standard measuring equipment.

To overcome challenges identified with DM EMI, we explore the second coupling mode demonstrated by conducted EMI i.e. CM EMI in our next chapter. Certain characteristic features of CM EMI exhibit guarantee to serve as a reliable feature for appliance detection. Hence, we carefully designed our follow-up study with CM EMI to establish its robustness over DM EMI.

Chapter 3

Common Mode Conducted EMI Signals for Appliance Detection

In the previous chapter, we showed that the DM EMI is an unreliable feature since the harmonics from the power supply and electrical infrastructure may interfere severely with the measurements. Additionally, federal regulations mandate that all appliances are fitted with sophisticated filters for rejecting their DM emissions. In this chapter, we demonstrate that high-frequency CM EMI can be used to identify specific types of electronic appliances uniquely.

On the consumption side, buildings, across the world, contribute to approximately 40% of the total energy expenditure. Offices, retail markets and educational institutes absorb roughly 50% of this energy [78]. Within these buildings, HVAC are the dominant loads (40%), followed by information technology (IT) loads and lighting (25%) [79, 80]. While there has been considerable focus on optimizing the HVAC energy consumption, there is currently little work on energy optimization for IT loads [81, 82]. A significant portion of the IT load energy consumption arises from the wasteful operations of these loads during non-working hours [83]. The detection of these appliances can enable the quantification of energy wastage and this information, when provided as consumer feedback, can motivate energy conservation. In this work, we designed a low cost sensing solution that can be used to accurately detect the operation of these IT appliances within office spaces during off-hours. Let us first

formulate the challenges that motivate and set apart this work:

1. Even a small office may have a large number of IT appliances. Therefore, the deployment and maintenance of an individual load monitor for each appliance, in a distributed setting, may quickly become prohibitive in terms of both cost and maintenance.

2. Single point sensing frameworks have been proposed (primarily for residential environments) for detecting appliances based on their energy usage patterns [7, 8, 56, 53, 54, 84, 55, 85, 86, 87]. These include permanent loads that operate throughout the day (refrigerators and thermostats); on-off appliances (fans and lamps); loads based on finite-state machines (washing machines and dimmer lamps); and time-varying loads (IT loads). State of the art single point sensing solutions mainly involve exploiting information gathered from the power consumption characteristics for appliance detection [8]. Other works in the smart grid community proposed techniques to detect appliances using either physics based models derived from voltage and current waveforms [54] or from features extracted from the real and reactive power, wave shape and harmonic content [88]. As a result, while these solutions have been effective in detecting appliances of the first 3 categories, they have been unsuccessful in detecting IT appliances due to their time-varying power consumption pattern. Also, most of these techniques are limited by signal interference in the presence of multiple appliances. The problem is even more challenging in an office environment as the number of such appliances is large.

3. In much of the previous work on single point sensing for appliance detection, the proposed detection and classification systems were evaluated based on the test and the training data gathered from the same appliance. Such approaches assume that different instances of the same appliance (e.g. 2 different CFL lamps) will likely behave in the same manner. While this may be somewhat true at low sampling frequency, it must be experimentally validated at higher sampling frequencies as well. Accuracy of a single point sensing system should ideally be proved by

training and testing on different appliance instances, for its general applicability in real world settings.

In this work, we have developed a sensor for measuring high frequency CM EMI injected by the appliances on the power lines. We also verified that we can use training data gathered from *one instance* of an appliance to classify *other instances* of the same make and model. Such a sensor offers an effective solution to detect IT appliances in office scenarios. This can eventually be used to identify their wasteful operations, thus contributing to the smartness on the consumption side in the grid. Previously [11, 76, 89, 90, 91, 92] used bulky (and expensive) systems for EMI sensing such as USRP, vector network analyzers and spectrum analyzers. These systems cannot be easily modified to support CM EMI measurements. Instead, we designed a low cost, portable, plug and play system for EMI sensing developed using commercial, off-the-shelf data acquisition systems. The classification algorithms, in prior works, were based on features extracted from frequency domain EMI data. They subsequently used a variety of algorithms such as k-nearest neighbor (k-NN) [11], neural networks [76] and support vector machines (SVM) [89] for classification. However, different appliances show considerable temporal variation in their EMI characteristics. To improve upon these results, we employed statistics learnt from histograms of the EMI data. These histograms show consistency across time and across instances of the same type. While similar statistics have been previously used on time series data [93], this is the first time they are being used to discriminate electrical appliances based on their EMI signatures.

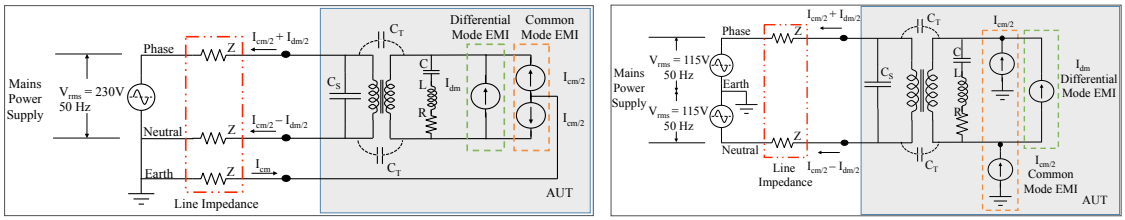

(a) Single ended power supply connected to 3-pin appliance

(b) Split phase power supply connected to 2-pin appliance

Figure 3-1: Equivalent circuit diagram of (a) single ended power supply and a (b) split phase power supply.

3.1 Description of CM and DM EMI measurements

Most consumer and power appliances with SMPS inject EMI into the power lines as shown in Figure-3-1. A single-phase power supply (or a single branch of a three phase power supply) consists of three power lines: the phase, neutral and earth, which are characterized by transmission line impedances Z. The power supply may be single ended (Figure-3-1a) or split phase (Figure-3-1b) with a 230V, 50 Hz (Indian standard) between phase and neutral. In our work, we considered the more commonly found single ended supply where the neutral and earth terminals are shorted at the distribution transformer outlet. However, the principles we have outlined in this work are equally applicable to split phase power supplies. Electrical appliances are either three pin appliances (Figure-3-1a) with earth connections or two pin appliances without an earth connection (Figure-3-1b). EMI that is generated from the switching circuits in the appliance or due to the passives may be resolved into two components - (1) the differential mode (I_{dm}) component that is inserted into the power lines across the step down transformer that interfaces between the switching circuitry and the power lines and (2) the common mode (I_{cm}) component on both the phase and neutral, with respect to the local ground of the appliance. The CM EMI noise is injected into the power lines through parasitic capacitances (C_T) in the transformer. Therefore, the current on the phase, neutral and earth lines are: $I_{cm}/2 + I_{dm}/2$, $I_{cm}/2 - I_{dm}/2$ and I_{cm} respectively. Note that the CM EMI component exists even in single-phase supplies (Figure-3-1a) due to the line impedances across the power lines. In the case of two pin appliances without an earth connection (not shown), the CM current loop is completed through a secondary coupling capacitance (C_P) between the phase and neutral terminals of the appliance and the local ground.

3.1.1 Comparison of DM and CM EMI as feature vectors for classification

The authors in [11] postulated that appliances generate a unique and time-invariant DM EMI between the phase and neutral terminals, which can be exploited as a reli-

able feature vector for classification. However, in previous chapter we showed several of the challenges associated with using the DM EMI as a reliable feature vector. First, DM noise currents, which are generated by inductive coupling through the transformer, mostly dominate high frequency bands. Therefore, these noise currents rapidly attenuate with increase in line impedance (or distance between the measurement outlet and the appliance outlet). In contrast, CM EMI currents, which are generated at low frequencies due to capacitive coupling, are likely to attenuate more gradually with the increase in line impedance. Second, higher order harmonics of the power supply (230V, 50 Hz) may dominate over the DM EMI from appliances in many cases. In [11], they tackled this issue by carrying out background subtraction in the frequency domain in the logarithmic scale (or division in the linear scale). However, this results in the emergence of spurious artifacts in the frequency domain signatures of the appliances. In contrast, the earth wire (where the CM EMI measurements can be made), is not meant for conduction of mains power supply and only meant for common mode leakage currents. As a result, the noise floor on CM EMI measurements is likely to be much lower than DM EMI. Third, there are federally mandated regulations on emission of DM noise from appliances so as to prevent the EMI from an appliance from interfering with the functioning of other appliances connected to the same grid. Therefore, most appliances come with inbuilt EMI filters that regulate the DM emission. In the previous chapter, it was observed that the DM EMI of some appliances such as laptops and CPUs was observed to be non-existent due to their EMI filters. The EMI filter of an appliance also significantly suppressed the DM EMI of neighboring appliances on the power lines by offering their DM EMI currents a low impedance path to ground. Therefore, appliances that may be detected independently may not be detected when they are powered simultaneously on the same lines. This may considerably reduce the efficacy of DM EMI as a feature vector for detecting multiple appliances. In contrast, most appliances are not fitted with CM EMI filters since CM noise is far less likely to impact the functioning of neighboring appliances. Despite this, if these appliances are fitted with CM EMI filters, the electromagnetic behavior due to CM filters do not significantly couple together. A detailed study of

the CM and DM EMI coupling between multiple appliances on a single power line is presented in Section-3.7.

3.1.2 Measurement of CM and DM EMI components

In the case of split phase power supplies, the CM and DM EMI can be measured by the sum and difference of phase (V_p) and neutral (V_n) voltages with respect to the earth measured at the power supply.

$$V_{CM} = V_p + V_n \tag{3.1}$$

$$V_{DM} = V_p - V_n \tag{3.2}$$

In single-phase power supplies, DM EMI can be measured by the potential difference between the phase and the neutral. But the measurement of CM EMI is more challenging. One method is to measure V_{dm} and V_p independently and estimate V_{cm} by subtracting V_{dm} from V_p. The advantage of this technique is that it can be applied to both two pin and three pin appliances. However, in practice, the performance of this technique is poor due to (1) the phase mismatch between DM and CM EMI components and (2) because the magnitude of DM EMI measurements usually exceeds the magnitude of CM EMI by a few orders due to power supply harmonics. A second method is to directly measure the earth currents, which correspond to the CM EMI components. The main advantage of this method is that the background noise across the earth lines is much lower than the phase and neutral lines. However, this technique can only be applied to three pin appliances due to the absence of a physical earth line connection in two pin appliances. The earth currents can be measured using either a current sense coil (such as the wide-band Rogowski coil) or through a current sense resistor. We have chosen to measure the current through the current sense resistor, to facilitate the development of a cheap sensor.

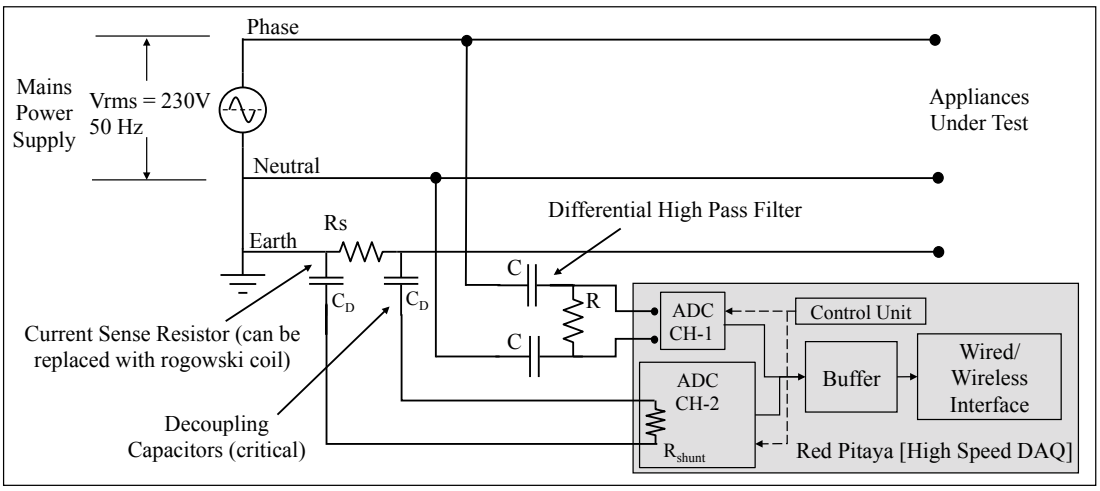

(a) Our custom EMI Sensor which is capable of simultaneously sensing CM and DM EMI on the mains power lines

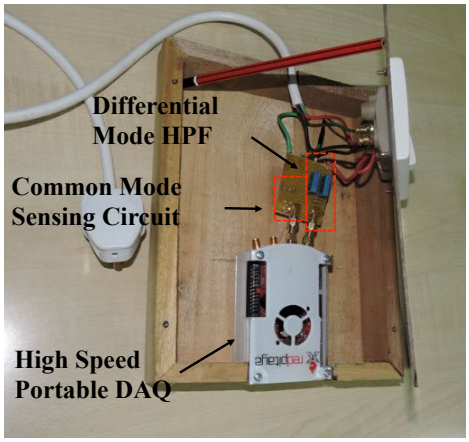

(b) Actual prototype of the proposed sensor

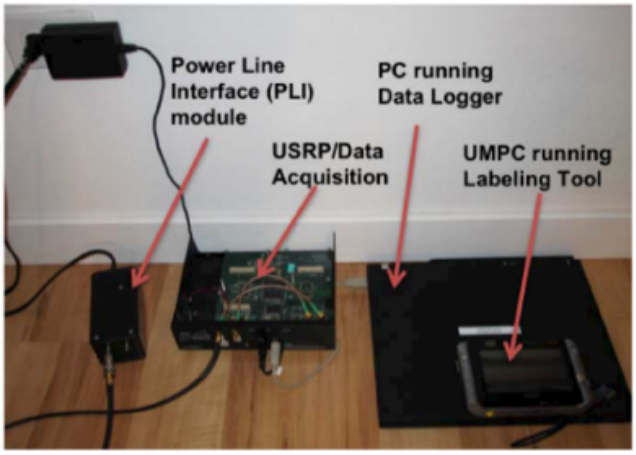

(c) Reference viewgraph of the DM EMI sensor developed previously by [11]

Figure 3-2: (a) Our custom EMI Sensor; (b) Actual prototype; (c) Reference viewgraph of the DM EMI sensor.

3.2 Plug and Play EMI Sensor Using Conducted EMI for Appliance Detection

In previous studies on EMI for NILM, measurements were made with spectrum analyzers and USRP boards [11, 76, 90]. These equipment are expensive and bulky. Hence, the measurements were mostly restricted to laboratory conditions. On the other hand, electronic manufacturers measure the DM and CM EMI emitted by appliances with expensive line impedance stabilization networks [3]. For the first time, we designed a low cost, portable sensor, made with off-the-shelf components, that is

capable of simultaneously measuring both the CM and DM EMI components from appliances on the single phase (single ended) power lines. The DM EMI component is estimated from the potential difference between the phase and neutral lines as shown in Figure-3-2a. The power signal (230V, 50 Hz) and some of its lower harmonics are removed from the signal through a differential HPF with a cut off frequency of 9 kHz. The CM EMI signal is estimated by measuring the voltage across a current sense resistor (R_s) on the earth line. Note that while the current sense resistor offers a cheap technique for measuring the CM EMI currents, the deployment introduces a break in the connection between the power supply and the appliance (or the power line feeding multiple appliances). A non-intrusive, but more expensive alternative, would be to introduce a current sensing coil around the earth line. The data acquisition is carried out with the open source high speed Red Pitaya[1] board. The choice of the value of the current sense resistor is based on the ADC resolution and the shunt resistance shown in Figure-3-3 and Figure-3-2a. The common mode voltage measured by the ADC is

$$V_{cm} = \frac{I_{cm} R_{shunt} R_s}{R_{shunt} + R_s} \tag{3.3}$$

A low value of R_s (much lower than R_{shunt}) should be chosen to ensure minimum noise injection, while ensuring that the measured voltage is greater than V_{min}.

$$V_{cm} \approx I_{cm} R_s > V_{min} \tag{3.4}$$

Here, V_{min} is the minimum voltage measurable with the ADC. In our case, the board is configured with a shunt resistance of 1MΩ and 16-bit ADC with 2V peak to peak ($\therefore V_{min} = 0.131mV$). An empirically chosen value of 100Ω satisfied both the conditions and hence was found suitable for the current sense measurements. Please note that placement of a current sense resistor in the earth line can pose a potential risk. Firstly, it can provide a path for high voltage (HV) signals to the DAQ. To avoid this safety hazard we have used two decoupling capacitors (C_D) as shown in Figure-3-2a to provide isolation from low-frequency (50 Hz) HV signals. These capacitors

[1] http://redpitaya.com/

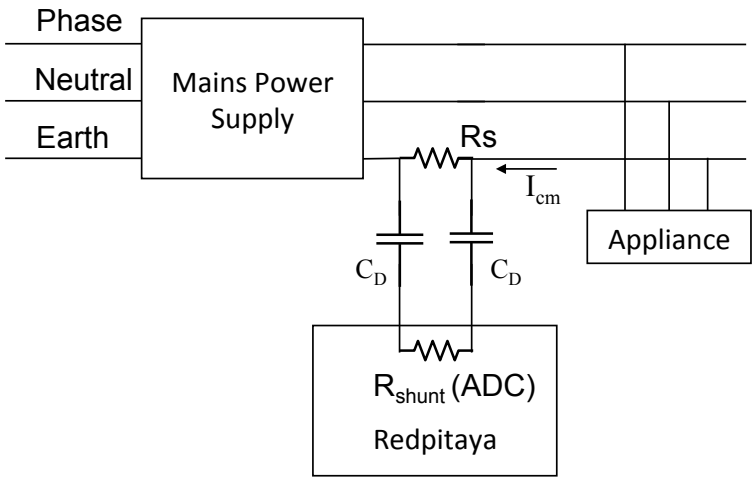

Figure 3-3: Schematic showing connection diagram for current sense resistor (R_s) with shunt resistor R_{shunt} inside ADC on Red Pitaya.

(0.1uF each) are meant for HV operation, can operate at 480VAC and provide an isolation of 1.5kVDC (EPSON Part number - B32023A3104M). Secondly, it violates the ground wire impedance regulations, which are 5Ω according to NFPA [94] and IEEE article number NEC 50.56 and 25Ω according to article number NEC 250.56 [95]. It can pose a risk to human using the appliance as 100Ω resistor grounds ground path for leakage currents. Currently, we are planning to tackle these issues in next non-intrusive version of this sensor. Both the CM and DM EMI data are acquired at a sampling frequency of 15.625 MHz and stored in internal buffers. The data from the buffers can be loaded into a server or CPU for further processing through either an Ethernet or a wireless interface. This sensor can be easily modified to measure EMI from split phase power supplies. Instead, of directly measuring the DM and CM EMI components, the phase (V_p) and neutral voltages (V_n) must be measured. The DM and CM EMI components can be estimated through (1) and (2). There is, therefore, no requirement of a current sense resistor or coil in the case of split phase power supply measurements. The sensor can be directly plugged onto any electrical outlet of the building. The equivalent circuit of our custom designed sensor is shown in Figure-3-2a, Figure-3-2b shows the actual prototype and Figure-3-2c shows a contrasting sensing solution developed in [11]. The power line interface in Figure-3-2c corresponds to the HPF in Figure-3-2b and the USRP in Figure-3-2c

corresponds to the DAQ in Figure-3-2b. All the stand-alone modules such as power line interface, data acquisition and data logging modules have been integrated into a single box in our custom sensor.

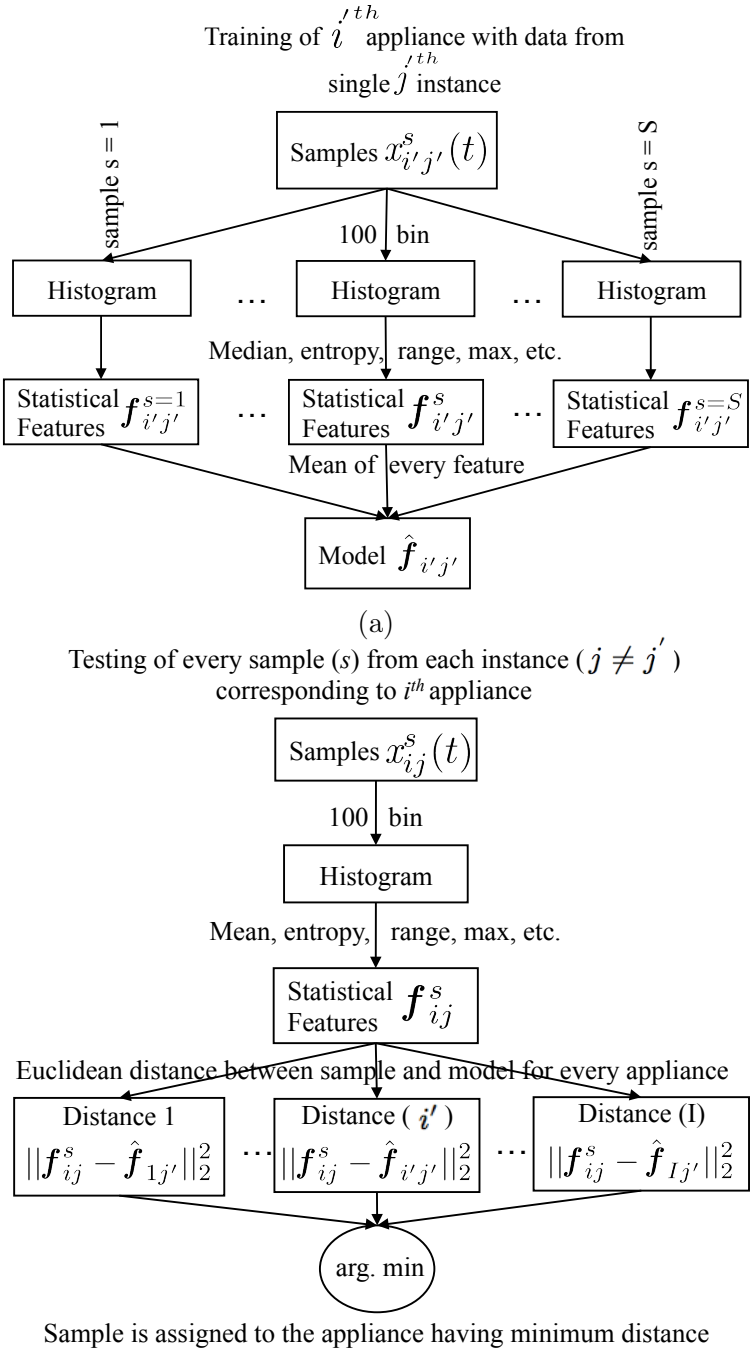

Figure 3-4: Flow chart showing the steps followed during (a) training phase and (b) test phase.

3.2.1 Signal Processing and Feature Extraction

Consider that there are I appliance categories and J instances of each category. Accordingly, $x^s_{i,j}(t)$ represents a single trace or sample from S time-domain EMI traces measured for the j^{th} instance of appliance category i. The time-domain data gathered by the sensor for each appliance are not directly used as a feature vector for classification because the measurements are not synchronized. Instead, we hypothesize that the CM EMI data from each appliance has a unique and time-invariant histogram that can be used as its signature. The histogram, derived from each sample (s), is obtained by binning the time domain data based on its magnitude. The distribution can be uniquely described by certain statistics. In this work, we extracted the following features from the histograms for classification: {entropy, skewness, interquartile range, kurtosis, percentile-75, range, maximum, median, percentile-90, mean absolute deviation}. The features are listed in the order of their effectiveness towards classification and form a vector for each sample trace ($f^s_{i,j}$). Features such as minimum and percentile-25 are not used since they look identical across multiple classes when we consider the magnitude of the measured data. Figure-3-4a shows the pipeline followed during the training phase. The data from one instance ($j^{'}$), of appliance category ($i^{'}$), are used for training while the data from the remaining instances (test instances $j \neq j^{'}$) are used for testing. The mean of the statistics, $\hat{f}_{i^{'},j^{'}}$ from all the traces corresponding to $j^{'}$, is used as the training model. Figure-3-4b shows the test procedure. Each trace of the testing instances (j), corresponding to appliance category (i), is treated as a separate test case. A test case is classified based on the minimum Euclidean distance between the test vector, $f^s_{i,j}$, and the training models for all the appliances as shown below.

$$\min_{i^{'}} \left\| f^s_{i,j} - \hat{f}_{i^{'},j^{'}} \right\|_2^2 \vee i, j \neq j^{'} \tag{3.5}$$

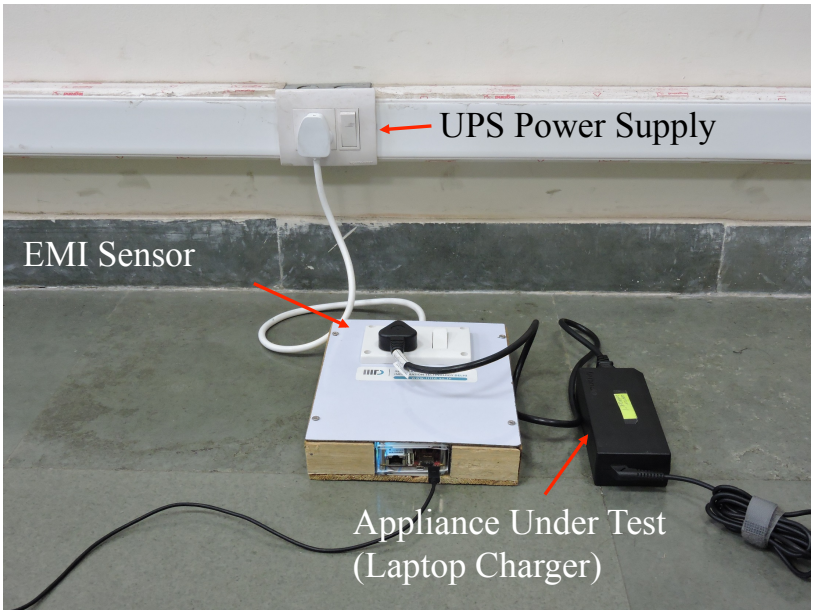

Figure 3-5: Test setup shows the conducted EMI sensor used for CM and DM EMI sensing for single ended power supply along with AUT.

List of SMPS Appliances (connected to UPS)	Quantity	Power (Watts)	Total Power
Router	23	10	230
Projector	15	250	3750
Projector Screen Controller	5	10	50
CCTV Cameras	20	5	100
Fire Control Systems	2	250	500
Desktop (CPU + Monitors) HP LE1902x Hewlett Packard Compaq 8200 Tower	91	100	9100
RFID Access Control Systems	24	5	120
Laptop and Charger (Lenovo X1 20A80056I)	150	45	6750
A4 Sheet Scanner	10	25	250
Printer (HP LaserJet P1008)	55	700	38500
CFL(Crompton Greaves)	380	18	6840

Table 3.1: IT loads within the institute. Highlighted appliances were used for the experiment.

3.3 Experimental Results

The common IT loads and lighting sources in most offices are CPUs, LCD monitors, laptops, telephones, modems, wireless routers, printers and CFL lamps. Many

published works on appliance detection note that several of these appliances, are very difficult to detect with single point sensing [53, 96, 84]. For instance, the time domain signatures of laptops and CPUs show considerable variation depending on the operational state of the appliance [13]. Hence, smart meters (with low sampling frequency) have not been successful in detecting these appliances. Additionally, these appliances are fitted with high quality EMI filters to reject DM EMI emission. Therefore, they are difficult to detect with DM EMI data. In this section, we show the utility of CM EMI feature vector for successfully detecting some of these appliances. In most office setups, multiple appliances of the same type (make and model) are used due to logistical reasons. Due to practical considerations, only a single instance of an appliance can be used for generating training data for learning the features.

However, once the features are learnt, they must be useful for detecting other instances of the same appliance type. Therefore, in this work, our classification algorithm is trained on data from a single instance of each appliance category and is used to detect other instances of the same type. This test protocol marks a significant departure from previous works in this domain.

In this work, we surveyed the SMPS based electrical appliances in our institute, which includes faculty offices, research labs, lecture halls and a small-scale data center. The complete list of appliances, their quantity, individual and aggregate power consumption are listed in Table-3.1. In this survey, we found that CFLs, LCD monitors, CPUs, printers and laptops (highlighted in the table with their make and model details) were the most commonly used appliances accounting for over 92% of the energy consumption. Hence, we focused our study on the detection of these appliances.

Servers and air conditioners used in the data center, and centralized HVAC systems used for air conditioning were not considered part of this study. In general, there is a lot of prior and ongoing research work to optimize servers [97, 98, 99], HVAC systems [81, 100], and air-conditioning systems [82, 101, 102]. Also, quite a few commercial entities like SmartJoules[2], Zenatix Solutions[3], BuildingIQ[4], and

[2]https://www.smartjoules.co.in/
[3]https://zenatix.com/
[4]https://buildingiq.com/

Building Robotics[5] focus on these loads. Hence, we tried to restrict our focus on the second most significant load in office buildings: IT and Electronic appliances.

We carried out the measurements inside the office precincts of our institute where the appliances are powered from an uninterrupted mains power supply (UPS). The EMI sensor, described in the previous Section, is connected to an outlet on an extension cord that is connected to the UPS. The AUT was connected to the EMI sensor as shown in Figure-3-5. We first examine the time-invariant characteristics of the CM EMI signal. These results are presented in Appendix-B. Additional measurements are made on the power line without connecting any of the appliances. This is useful in determining the background noise on the power lines in the absence of the AUT. The EMI data collection from the twenty five individual appliances (five instances of each of the five appliance categories) spanned over a week from which we considered a data set spanning 5-6 hours (which includes measurement and logging time). This complete dataset[6] is released as part of this work. In the next two Sections, we discuss the measurement data and classification results for all appliances.

3.4 Measurement Results

Time-domain CM and DM EMI are measured simultaneously for each individual instance of an appliance at a sampling frequency of 15.625 MHz. Each time-domain trace is 150ms long, consisting of 150 sub-frames measured and logged for 1ms duration. Each time-domain sub-frame (approximately 1ms duration) includes 16384 data points having a precision of 16-bits, which is guided by 16-bit Differential ADC that we have used in our DAQ board. The length (duration) of each sub-frame is guided by the ADC buffer size available to us. However, the total duration for each time-domain frame (150ms in this case) is decided to ensure that we have sufficient data points to analyze this signal acquired at 15.625 MHz. A total of ten traces (total duration - 1500ms) are collected for every appliance instance to account for the

[5]https://www.comfyapp.com/
[6]https://goo.gl/wpxEh9

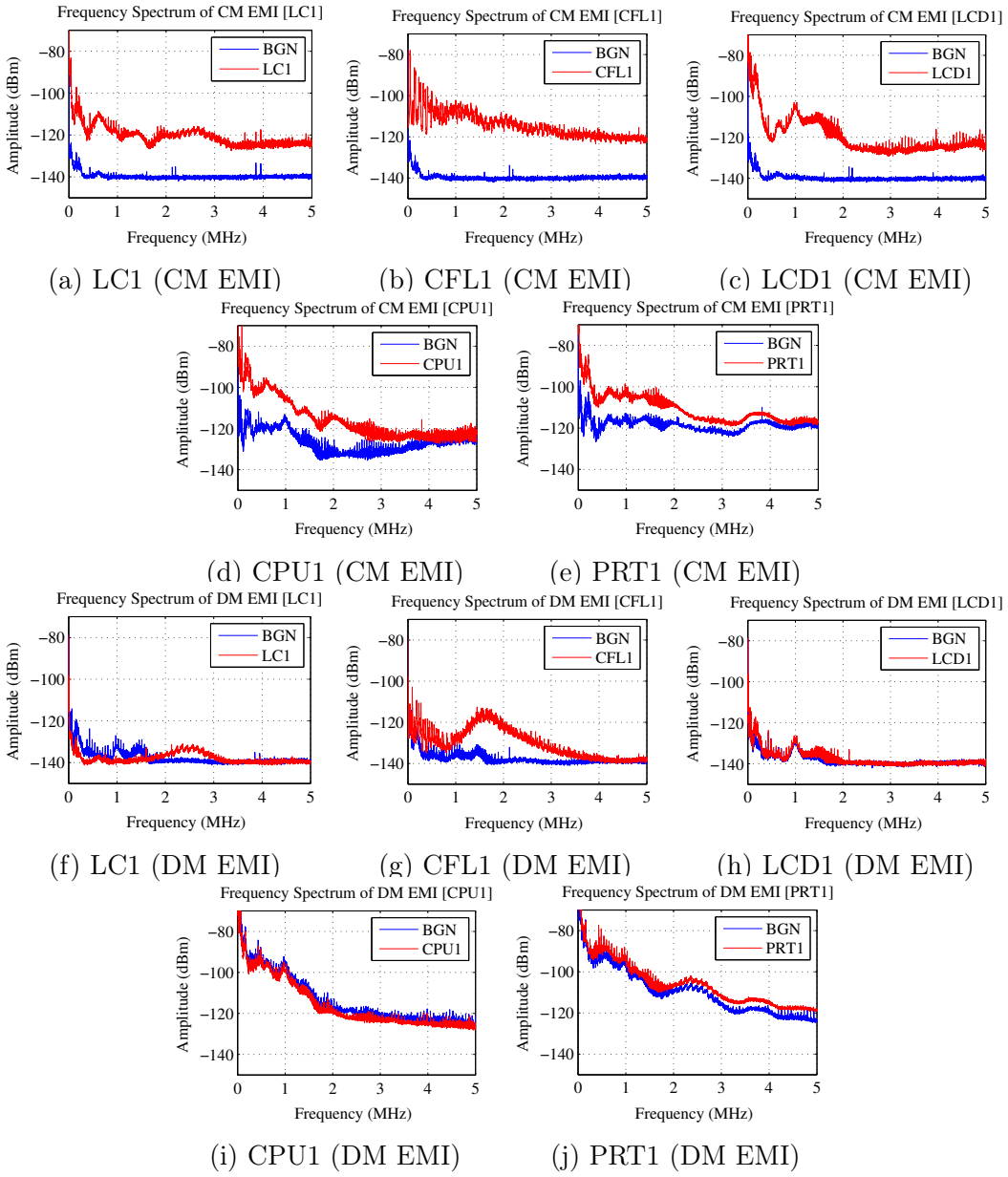

(a) LC1 (CM EMI) (b) CFL1 (CM EMI) (c) LCD1 (CM EMI)

(d) CPU1 (CM EMI) (e) PRT1 (CM EMI)

(f) LC1 (DM EMI) (g) CFL1 (DM EMI) (h) LCD1 (DM EMI)

(i) CPU1 (DM EMI) (j) PRT1 (DM EMI)

Figure 3-6: Frequency domain plots showing CM EMI and DM EMI measured from 5 appliances along with background noise on the power lines.

dynamic nature of background data (baseline noise), which can facilitate smoothing, averaging, and other signal processing operations. In total, there are 5 instances of each appliance, and the corresponding amount of background data are also collected.

3.4.1 Frequency Domain Results

Figure-3-6(a-e) and Figure-3-6(f-j) show the frequency domain CM and DM EMI signatures of an instance of each of the 5 appliances highlighted in Table-3.1. The frequency range of interest is from DC to 5 MHz. Before turning on the appliance, the background noise on the power lines are measured for each case. This exercise was carried out to monitor the change in the background noise characteristics in the power lines during the measurements. We note that across all the figures, the background noise in the CM EMI measurements (-100dBm to -130dBm) is lower than the DM EMI measurements (-60dBm to -120dBm). This is possibly because of the absence of power line harmonics and other fluctuations on the earth line where CM EMI is measured. Secondly, we observe that above 4 MHz, the frequency data look identical for all the appliances as it is dominated by the background noise on the power lines. Finally, the CM EMI signatures are reasonably consistent across multiple instances of the same appliance make and model. This is not true for the case of DM EMI. These results are not shown here due to constraints of space. In the case of the laptop charger (LC) and LCD monitor, a broad band CM EMI noise can be discerned over the background noise floor, up to 2 MHz. The average signal to noise ratio over this band of frequencies is 15dB and 20dB respectively. However, the poor DM EMI to noise ratio, clearly shows that the EMI filters in the laptops and monitors have successfully removed all DM EMI. Therefore, the detection of these appliances is likely to be very poor if DM EMI data are used as feature vectors for classification. Considerable CM and DM EMI are observed in the case of CFL. The average SNR across the entire frequency domain, are 30dB and 25dB respectively for CM and DM EMI respectively. The EMI signatures from CFL are characterized by the fundamental peak, at 41.4 kHz, corresponding to the switching frequency of the power supplies within the CFL and its higher order harmonics. Therefore, we anticipate that both CM and DM EMI data can be successfully used for identifying CFLs. In the case of the CPU and printer, the background noise on the CM EMI measurements were occasionally high. This may affect the classification results in these cases. In this work, we chose to not

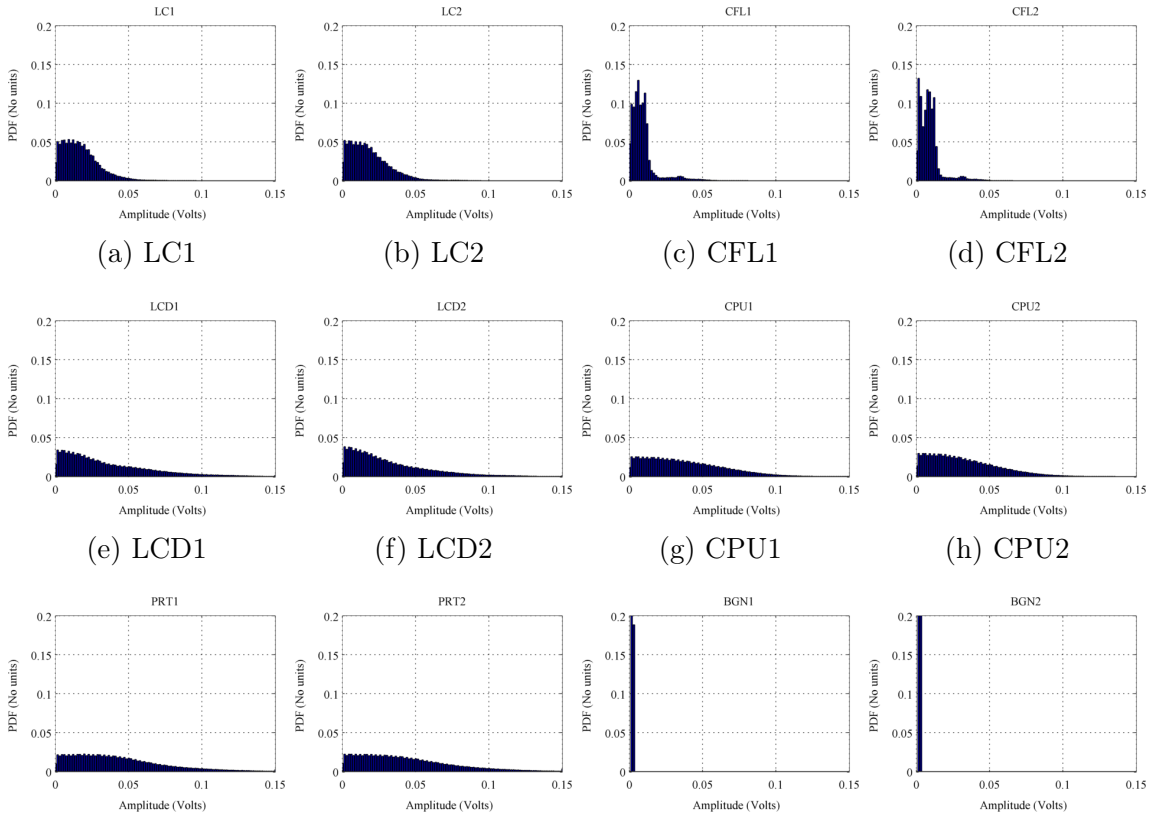

(a) LC1 (b) LC2 (c) CFL1 (d) CFL2

(e) LCD1 (f) LCD2 (g) CPU1 (h) CPU2

(i) Printer (PRT1) (j) PRT2 (k) BGN-1 (l) BGN2

Figure 3-7: Histogram of CM EMI data, of five appliances (from 2 of 5 instances) and Background noise (BGN), showing significant similarity across instances from same class of appliances.

use the frequency domain data for machine learning and classification since a large portion of the data, from 4 MHz to 7.8125 MHz (half the sampling frequency) show significant overlap across the multiple appliances.

3.4.2 Histograms

Time domain measurements are not synchronized in any manner. Hence they show considerable variation across multiple instances of the same appliance and across time depending on the starting time (and phase) of the measurements. Therefore, these traces cannot be directly used as signatures for appliance classification. On the other hand, statistical distributions derived from the time domain data from the same appliance category may show similar features. We examine this by plotting the

normalized number of counts per bin (histogram) of the magnitude of the CM EMI from each appliance category. Figure-3-7 shows the histograms from two of the five appliance categories. Each of these histograms are drawn from data from a single time-domain trace of 150ms. The figures show the following features: the histograms of the measured voltages show considerable variation across different appliance categories. The most distinct histogram belongs to the CFL and the background noise category. On the other hand, the histograms show much smaller variation across multiple instances of the same appliance category. CPU, printer and LCD have roughly similar histograms. However, due to distinct peak values and width of slope in histograms, statistics such as kurtosis and skewness are able to capture this dissimilarity. Therefore, statistics (listed in Section-3.2.1) that describe the histogram can form the basis for appliance detection and classification. DM EMI data that are dominated by background noise show very similar histograms across multiple appliance categories. These histograms are not shown here due to constraints in space.

3.5 Classification Results and Discussion

As mentioned earlier, there are 6 categories in the classification - {*LCD monitor, Laptop Charger (LC), CFL, CPU, Printer (PRT) and Background (BGN)*}. The last category, {*BGN*}, implies the absence of any of the other five IT appliances on the power line. 10 samples were measured for each of the 5 instances of every appliance category. Thus, I = 6, J = 5 and S = 10 based on the definitions provided in Section-3.2.1.

The training model is the vector formed from the mean of the statistics drawn from the histograms corresponding to the samples of the training instance (20% of measured data). Each of the samples from the remaining four test instances form an individual test case (80% of measured data). Five-fold cross validation is carried out where the training and testing instances are swapped. As a result, there are a total of 200 (4 x 10 x 5) test samples corresponding to each appliance category. Each test case is assigned to one of the 6 appliance categories on the basis of the *minimum Euclidean*

distance between the test feature vector and the training models as described in (5). We carry out the classification process using CM EMI data and then repeat the process with DM EMI data. We present the appliance confusion matrix[7] along with precision and recall results from the nearest neighbor based classification algorithm on a per appliance basis in Table-3.2(A) and Table-3.2(B). The column headers, in the tables, indicate the classification classes whereas the row headers indicate the test classes. The highlighted features in the table indicate correctly identified test cases. The precision of appliance detection is computed as the ratio of correctly classified test cases of each appliance class (i) to the total number of traces classified as that appliance class. The total number, therefore, includes test traces from other appliances that are falsely classified to this particular class. The recall of an appliance, on the other hand, is computed as the number of correctly classified test cases of each appliance class to the total number of traces from that appliance class. Therefore, some of the traces of this class have been missed (or falsely identified as belonging to another class).

$$precision|_i = \frac{correct\ class|_i \times 100}{correct\ class|_i + false\ class|_i} \tag{3.6}$$

$$recall|_i = \frac{correct\ class|_i \times 100}{correct\ class|_i + missed\ class|_i} \tag{3.7}$$

Together, the precision and recall indicate the accuracy of the classification algorithm and the efficacy of the chosen feature vector. The following inferences can be drawn from the results: the average CM EMI precision and recall results (87.3% and 86.8% respectively) are far superior to the DM EMI precision and recall results (49.6%, 45.2% respectively). This validates the key hypothesis of our work that CM EMI is a far superior feature for IT appliance detection compared to DM EMI. The poor performance of the DM EMI results can be attributed to the high background noise (-60 to -120dBm) that dominated the DM EMI measurements as seen in Figure-3-6b. The *background* results in the CM EMI case is 100% (both precision and recall) compared to the low values for DM EMI. This is because of the distinct low noise floor

[7] `https://en.wikipedia.org/wiki/Confusion_matrix`

that was observed in the CM EMI measurements due to the absence of the power signal and its higher order harmonics.

Past research efforts, using either smart meters or DM EMI, have reported the challenges in detecting IT appliances such as laptop chargers, LCD monitors and printers [103, 13]. This is because these appliances show considerable variation in their smart meter readings while operating in different modes (standby, hibernation, full operation and so on) [13]. Since these appliances are usually fitted with powerful DM EMI filters, they show very poor performance with respect to DM EMI (16.5%, 33.5% and 39.5% recall for laptop chargers, LCD monitors and printers respectively). The high precision and low recall value for printers, in the DM EMI case, is due to the poor SNR in the measurements due to the high background noise values. The classification of printers is therefore, largely on the basis of background noise rather than EMI signal itself. Nevertheless, these appliances are accurately detected with their CM EMI signatures (above 90% precision and recall for laptop chargers and printers; 72% for LCD monitors). CFLs can be accurately detected using either DM EMI or CM EMI data due to their strong and unique signatures and the absence of any type of EMI filters (DM and CM). Desktop CPUs show some improvement from DM EMI to CM EMI (from 35% to 60%). However, these appliances still remain challenging to detect. This can be attributed to the high background noise floor in the CM EMI measurements of the CPUs (refer Figure-3-6).

In this work (and all other prior works related to EMI sensing), the feature extraction for classification is carried out when the appliances are individually connected to the power lines. We have limited the study to one appliance at a time in order to evaluate the signal quality, stability and consistency across multiple instances of same appliance. In order to detect an appliance in the presence of multiple appliances on the grid, more complex appliance features (as opposed to the simple statistical features used in this work), extracted from dictionary-learning techniques may be needed. However, CM EMI will still serve as a useful signal for classification since CM EMI (unlike DM EMI) does not couple between multiple appliances. Therefore, this problem presents a unique opportunity for future research in this field. Secondly,

while the sensing solution presented in this work detects and classifies appliances on the power lines, the technique does not provide information regarding the actual energy dissipation by the appliance. The second piece of information can, however, be gathered by operating a simple energy meter in conjunction with our custom designed EMI sensor.

	BGN	LC	LCD	CFL	CPU	PRT	Recall (%)
BGN	200	0	0	0	0	0	100
LC	0	197	3	0	0	0	98.5
LCD	0	15	144	0	33	8	72
CFL	0	0	0	200	0	0	100
CPU	0	0	12	0	119	69	59.5
PRT	0	0	1	0	17	182	91
Precision (%)	100	92.9	90	100	70.4	70.3	

(B)

	BGN	LC	LCD	CFL	CPU	PRT	Recall (%)
BGN	99	30	61	0	10	0	49.5
LC	106	33	43	0	18	0	16.5
LCD	87	29	67	0	17	0	33.5
CFL	3	4	0	193	0	0	96.5
CPU	51	22	38	0	69	20	34.5
PRT	7	5	12	0	97	79	39.5
Precision (%)	28.1	26.8	30.3	100	32.7	79.6	

Table 3.2: Results from Nearest Neighbor based Classification on (A) CM EMI data and (B) DM EMI data on 6 classes (5 appliances and background): (A)

3.6 CM EMI Coupling Behavior across Multiple Appliances

In prior work, we studied how DM EMI coupled between neighboring appliances using simulation models of appliance SMPS [103]. Here, we analyze the CM EMI coupling between two appliances (AUT-1 and AUT-2) using a generalizable model shown in

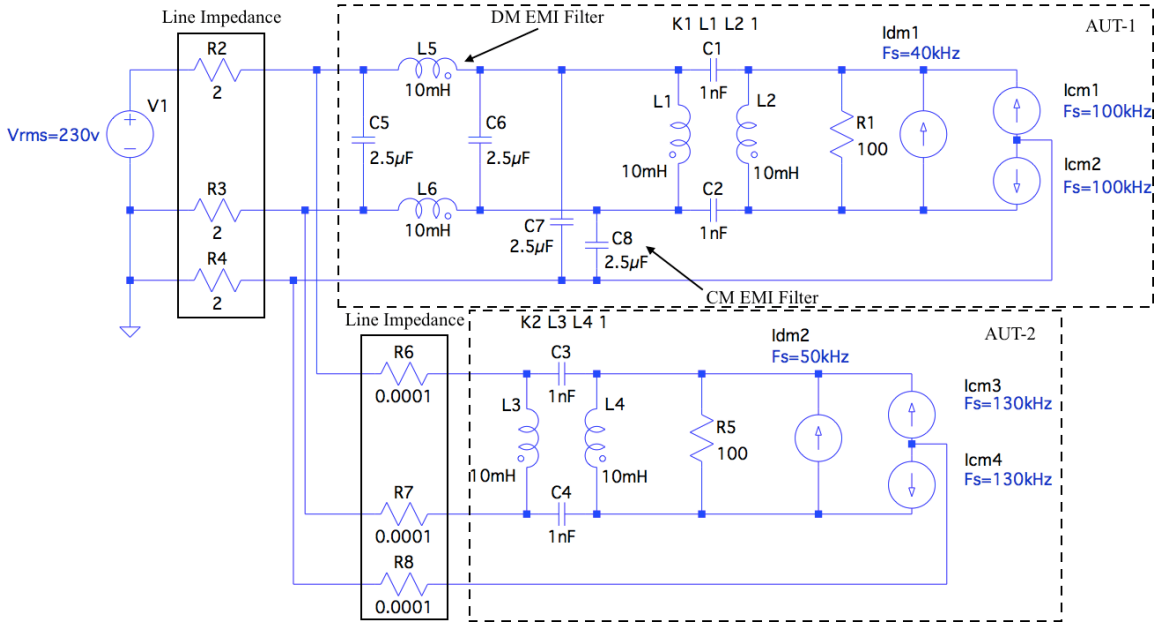

Figure 3-8: A generalizable model for analyzing CM and DM EMI coupling between two appliances (AUT1 & AUT2), having DM and CM EMI filters.

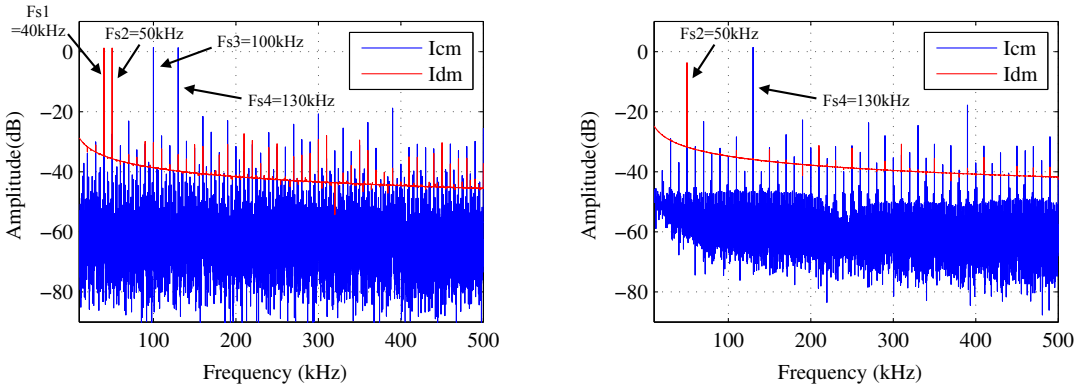

(a) (b)

Figure 3-9: CM and DM EMI spectrum showing coupling between two appliances (AUT1 & AUT2) (a) without and (b) with DM and CM EMI filter

Figure-3-8. Each appliance is fitted with a distinct CM and DM EMI source. First, we consider the case when neither of the appliances are fitted with filters (Figure-3-8 without DM and CM EMI filters). Figure-3-9a shows the corresponding CM and DM EMI spectrums. The spectrums shows superposition of signals from both the appliances - CM peaks at 100 kHz (AUT-1) and 130 kHz peaks (AUT-2) and DM EMI peaks at 40 kHz (AUT-1) and 50 kHz peaks (AUT-2). Since the amplitudes of both the CM and DM EMI current sources are assumed to be 1A, the peaks of

the corresponding signals in the EMI spectrums are of equal magnitude. Next, we consider the case when a DM EMI and CM EMI filter are applied to AUT-1 [3, 104]. In an ideal scenario, these filters should only suppress the EMI from AUT-1 and have no impact on the neighboring AUT-2. The resulting spectrums, shown in Figure-3-9b show that the DM EMI and CM EMI from AUT-1 are attenuated by approximately 40dB by their respective filters. Interestingly, the DM EMI from AUT-2 is also attenuated (by approximately 8dB) by the filter in AUT-1. This attenuation can severely impact the detection of DM EMI signals especially in low SNR scenarios as discussed in [11]. On the other hand, the CM EMI of AUT-2 is not affected by the filter in AUT-1. Therefore, this study suggests that CM EMI signals are less prone to interference between neighboring appliances and theoretically should still be detected.

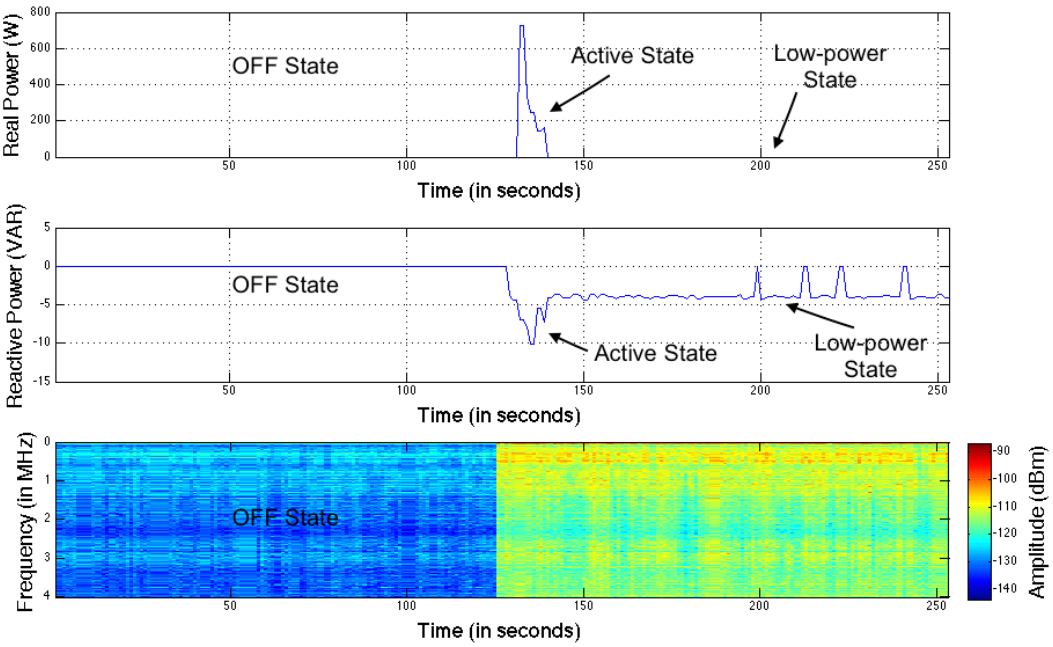

Figure 3-10: Real power (top), reactive power (middle) and CM EMI spectrum (bottom) from the printer in different states (off, active & low power).

3.7 Time-Invariance Property of the CM-EMI Signals

In this section, we investigated the time-invariance nature of the CM EMI signals of simple commonly found IT appliances that have two operational states - active and low power, besides the off state. Figure-3-10 shows the CM EMI measured from a printer along with the corresponding real and reactive power measured by a smart meter. When the SMPS is powered off (off-state), we do not observe any EMI. However, the SMPS remains active with constant EMI in both the active state and low-power state even though the actual load differs. In the low power state, there is non-zero reactive power consumption and no real power consumption while the active state has non-zero reactive and real power consumption.

Next, we considered an LCD monitor connected to a desktop CPU on which a variety of programs are run over a duration of an hour. Figure-3-11 shows the corresponding CM EMI spectrum (up to 2 MHz) measured from the monitor. The figure shows that despite the time-varying operations by the monitor, the EMI spectrum remains consistent. The findings from this work may not apply to multi-state domestic appliances that have closed loop controllers and show adaptive EMI behavior according to the instantaneous load condition [105].

3.8 Combining low-frequency smart meter data with EMI data for appliance disaggregation

Using high-frequency electromagnetic interference (EMI) emissions for detecting and extracting appliance state information of electronic loads seems to be a promising technique. Considering prior work in differential mode conducted EMI [11, 90, 105] and present work using common mode conducted EMI [106, 103], it sounds practical to infer appliances from these noise signals present on the power lines. However, it still requires more work before ensuring that appliance state information captured

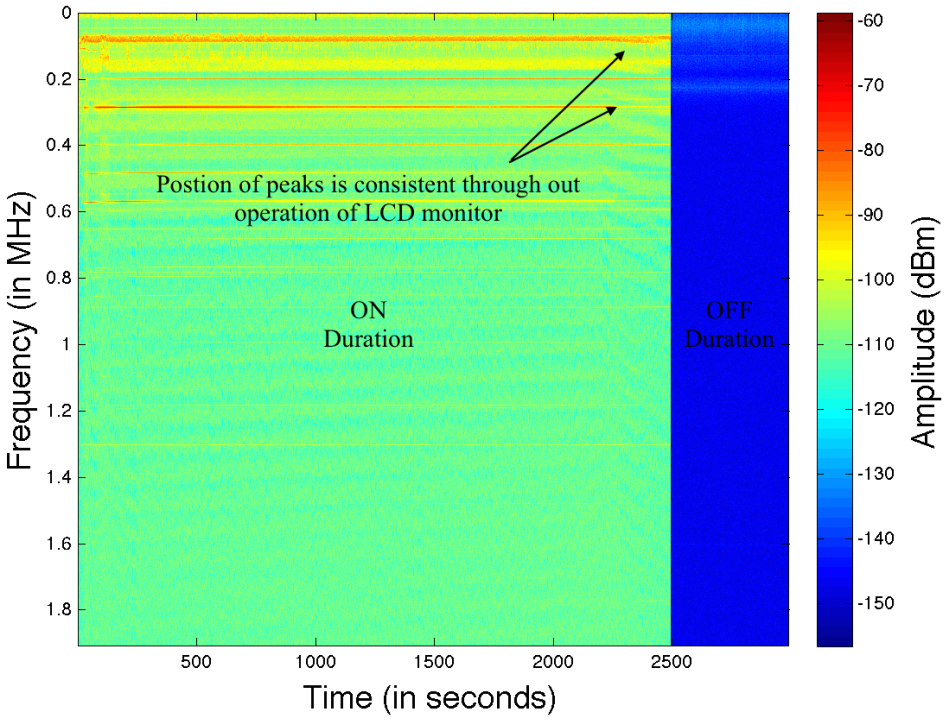

Figure 3-11: CM EMI spectrum measured from LCD monitor. This spectrum clearly shows consistent EMI peaks throughout operation of LCD monitor.

using EMI becomes useful in optimizing energy consumption.

Although, these electronic loads are the second highest consumer of electricity in office buildings after HVAC, to ensure effective energy feedback this information has to be augmented with duration of appliance usage, location inside building and amount of power consumption [10, 107]. EMI signals can be exploited to extract duration of appliance usage and type (category) of the appliance being used. However, it is hard to infer similar instances appliances and their collective power usage using EMI signals [106]. To fetch this information the appliance state information gathered from EMI data has to be combined with instantaneous low-frequency power data from conventional smart meters in a time aligned manner. This combination of low-frequency power data and appliance state information from high-frequency EMI signals can provide state of the appliance, duration of appliance usage, total instances of similar appliances which are operational and possibly the location of the appliance too.

We envision to extract appliance state information using dictionary learning based techniques [108, 109] by learning the basis matrix for each appliance category. Prior attempts of using time and frequency based features or using statistical features will not be effective in the multi-appliance scenario as when multiple appliance types are operated together EMI from one appliance interferes with other and can lead to change in EMI spectrum [103, 3]. Although CM EMI is less prone to this behavior, however, to ensure the efficacy of appliance detection we use a more robust and well-known technique (dictionary learning). Once we have the basis (dictionary) for each appliance, each time-domain EMI vector (trace) captured from EMI sensor is multiplied with the basis to extract appliance state information. This will help us to infer what all appliances were operational at that particular moment. Post this analysis of EMI data, time-aligned power data captured using smart meter is fed to a linear model having known types of appliances to infer how many instances of each appliance are operational.

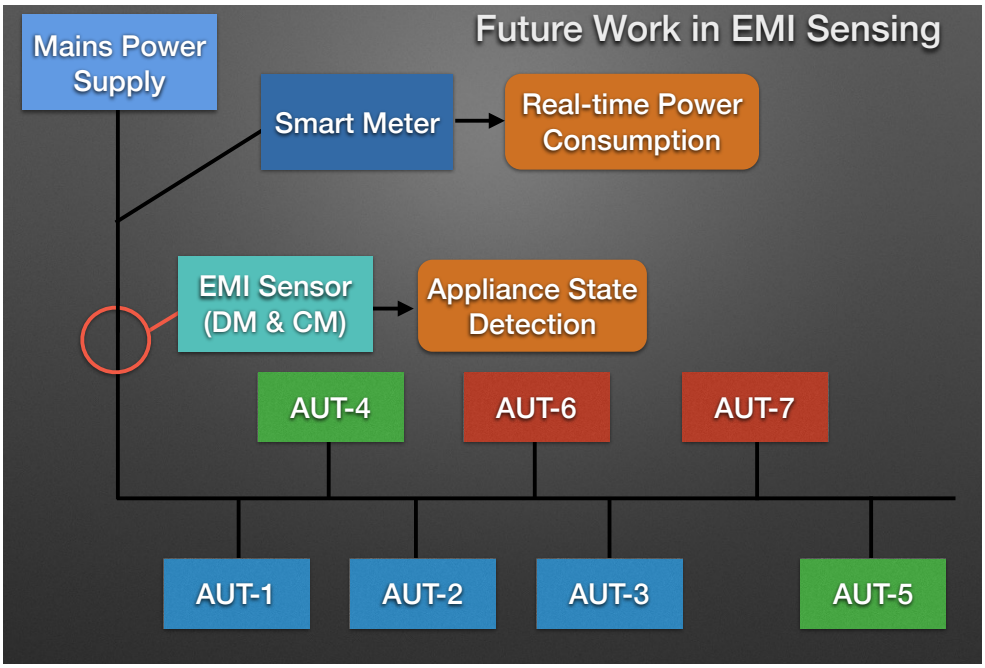

Figure 3-12: Block diagram of combination of high-frequency EMI sensing system with low-frequency smart meter based instantaneous power sensing system.

Figure 3-12 shows the block diagram of how EMI data is being collected and combined with instantaneous power data from the smart meter. The analysis and

results from the combination of these two data streams are not discussed in this thesis and they are yet to be published.

3.9 Conclusion

IT loads such as LCD monitors, laptops and desktop CPUs constitute a significant proportion of energy wastage in office spaces when they are left operational during non-working hours. Current single point sensing solutions with smart energy meters have been unsuccessful in detecting these loads, due to their dynamic power consumption patterns. All of these appliances (and many more) generate CM EMI on the phase and neutral power lines with respect to the earth at low frequencies through capacitive coupling as well as DM EMI between the phase and neutral at higher frequencies through inductive coupling. The DM EMI is difficult to detect due to the presence of EMI filters on the appliances as well as harmonics of the mains power supply. The CM EMI, on the other hand, has a much higher signal to noise ratio.

A significant advancement is made in this research in terms of the systems used for measuring EMI. Until now, bulky and expensive equipment constitute system setup for EMI measurements. In this work, both CM and DM EMI were measured simultaneously with a small and portable sensor made of commercial, off-the-shelf components. In the case of single ended power supplies, the CM EMI is estimated by measuring the earth currents. This measurement method is, however, limited to three pin appliances and not two-pin appliances. In split phase power supplies, the CM EMI can be measured by the mean of the phase and neutral voltages with respect to the earth.

Our experiments show that the histograms of CM EMI measured from IT appliances are reasonably time-invariant and consistent across multiple instances of appliances of the same make and model. Signature feature vectors of 5 IT appliances and the background electrical infrastructure are learnt from statistics extracted from their histograms. These training models are formed from data collected from a single instance of the appliance and used to classify other instances of the same make

and model. This is a rather challenging protocol that is important in office scenarios where there is a high likelihood of finding many appliances of the same make and model. We found that, CM EMI forms a better feature, than any other feature researched so far, for detecting many of the IT based appliances. Additionally, since the CM EMI signal arises from the SMPS within electrical appliances, the new method demonstrated here is not limited to IT appliances, and can be extended to other SMPS appliances in residential and office settings as well. Future directions to this work are to investigate the possibility of using these features for load disaggregation of appliances with dynamic power consumption, which is the holy grail of NILM.

Chapter 4

Radiated EMI Signals for Appliance Detection

Appliance activity recognition is an emerging domain targeted towards personalized energy feedback and individual energy apportionment. Some research studies in the past have shown the utility of providing energy feedback to the end consumers and how it can lead to significant energy savings [10, 107]. This work takes energy feedback a step further by using RFI for appliance activity recognition and associating it to an end consumer. Some prior studies in appliance activity recognition have utilized distributed sensing approach by placing individual plug load monitors at all appliances to monitor individual power consumption [110]. Another technique proposed by Hart [7], utilizes disaggregated power information from NILM based single point sensing method to do this. However, this technique underperforms in the presence of complex appliances, having time varying power consumption [13]. On similar lines, some studies have fused multiple sensor streams to extract appliance activity information; for instance, Kim et al. [111] utilized a fusion of magnetic, acoustic, temperature, and luminosity sensors to monitor the realtime status of appliance usage. The work by Taysi et al. [112] used acoustic sensor nodes to detect appliance operation. Although these studies have explored a diverse set of sensing modalities to infer appliance operation but still the goal of attributing energy consumption to individuals is not achieved as most of these methods can quantify 'which' appliance

is consuming but fails to capture 'who' is using this appliance. Further, most of these sensing methods require distributed sensing technique, having one or more than one sensor per appliance, which incurs huge deployment and maintenance cost. In this chapter, we have explored the feasibility of having a wearable sensor, which not only infers 'which' appliance is operational, but also 'who' is operating that appliance by assigning a unique id to the person wearing RFI sensor. The appliance usage data associated with the RFI sensor, having a unique identifier, can be compared with the power consumption data from the smart meter to get person level energy consumption.

Once this information is fused with power data from the smart meter, three-step information can be obtained regarding -

1. Which appliance is operational using distinct RFI signatures,
2. Who are operating this appliance by individual wearable RFI sensors,
3. How much energy is being consumed in this activity by fusing real time smart meter data.

This RFI study is one of the first detailed studies on utilizing RFI signatures for appliance activity detection, which covers sensing, feature extraction, and detection aspects along with comprehensive inferences.

4.1 Overview of RFI

RFI is a high-frequency noise radiated from nearby electronic devices that propagate in ambient RF environment [113, 114, 115]. Broadly RFI sources can be categorized into two sub-categories by their purpose of transmission (1) Intelligent sources (2) Nonintelligent sources. Intelligent sources are essentially wireless transceivers operating in adjacent or same frequency band to communicate with peers while the non-intelligent ones radiate due to high-frequency oscillators emitting RFI [116]. Wi-Fi, Bluetooth and other wireless radios operating at 2.4 GHz (license-free ISM band),

GSM etc. falls under the first category. Non-intelligent sources of RFI consist of electric and electronic appliances, buses and clocks in computing platforms. RFI sources are also categorized on the basis of the effective frequency band occupied by RFI i.e. low-high frequency emitters (< 30 MHz) and very high-frequency emitters (> 30 MHz). With increasing proliferation of such systems, RFI has become an active area of research from last two decades, especially in the wireless communications community. Although FCC has also laid down certain guidelines to maintain RFI within tolerable limits [115] but due to higher sensitivity of present day sensing systems, RFI can still be measured. RFI sensing is either blind spectrum sensing to detect nearby intruders or deterministic spectrum sensing to identify possible RF energy leakage from a known wireless device operating in same or adjacent frequency band. Our current work leverages this high frequency RFI as a signature for appliance activity recognition.

4.2 Prior work in RFI

Prior work in RFI can be classified into five subcategories as (1) Detection or sensing of RFI [117, 57, 118, 119], (2) Feature extraction and characterization of RFI [116, 120], (3) Modeling of RFI [116], (4) Techniques for mitigating RFI [116, 121] and (5) implications of RFI in a particular field of study [114, 122, 123, 124, 125, 126]. Schewabe considered RFI interference from lighting and other electronic appliances [119]. Kvasznicza also performed a similar study of RFI from public lighting sources [118]. On same lines, Hannan analyzed interference from electrical appliances (motor based loads) in smart buildings [126]. Although a substantial amount of work has been done in the past to analyze the impact of RFI. However, most of this work is restricted to analyzing interference with other electronic devices. There is a very limited amount of work that characterizes and model RFI from non-intelligent sources with a goal of appliance activity recognition. In our work, we have focused on RFI from non-intelligent sources, generated by electrical and electronic appliances. This RFI is generated due to the presence of high-speed switching circuits used in these

appliances. Switching circuits embedded in electronic appliances give rise to high-frequency noise which is either conducted into power lines as conducted EMI or radiated into ambient environment as radiated EMI (or RFI). The noise peaks of this EMI or RFI are centered around switching frequency of these circuits. Some prior work on conducted EMI has shown that these noise peaks can be used as a signature to detect appliances running on power line [11, 103]. Recently [57] and [59, 127] have also explored the possibility of using RFI to identify appliances operational in the vicinity. Our work augments this existing work significantly by characterizing and modeling RFI generated from electrical and electronic appliances emitting both low-frequency and high-frequency RF emissions.

4.3 Appliance Acivity Recognition Using RFI

This work followed a systematic pipeline as shown in Figure-4-1. The first step consists of sensing and detection of RFI from non-intelligent sources of RFI i.e. electrical AUT. The second step includes feature extraction and characterizing the spectral behavior of different appliances followed by step three, which involves feature learning from RFI measured from different appliances. Finally, step four evaluates the performance of appliance detection using k-nearest neighbor (k-NN) based classification technique. In particular, this work answers the following questions:

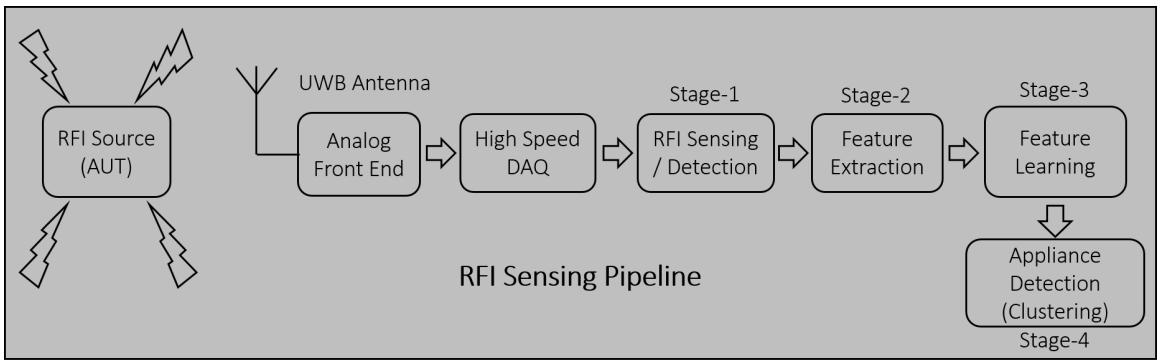

Figure 4-1: RFI Sensing Pipeline followed in this work showing different steps of execution.

1. How characteristics of RFI signatures vary for the different class of appliances?

2. How RFI signatures vary with increase in distance from the source?

3. How signatures vary for different states of appliances?

4.4 Experimental Setup

Our experimental setup, for RFI measurements, consists of Ettus N-210 USRP, low-frequency receiver (LFRX) and SBX1[1] daughter boards, two UWB dipole antennas (off-the-shelf) and an extension cord [128]. Ettus USRP N210 provides a real-time band-width of 40 MHz with an ADC resolution of 14 bits and a frequency accuracy of 2.5 ppm, with an only constraint of Gigabit Ethernet interface. In our case, we have used scripts written in GNU Radio [129] to perform RFI measurements, using USRP however it can be controlled using Matlab or Simulink. Along with USRP, two daughter boards (LFRX and SBX) are used to facilitate RFI sensing at low-frequency baseband, GSM, and Wi-Fi bands. LFRX provides a bandwidth of DC to 30 MHz, with a unity receiver gain and it doesn't include any local oscillator as down conversion is not required. SBX board provides a bandwidth of 40 MHz starting from 400 MHz going up to 4.4 GHz, thus supports sensing in GSM, Wi-Fi, and Bluetooth frequency bands. It also facilitates user defined receiver gain in the range of 0 - 31.5dB. RFI measurements are performed from a set of nine appliances mentioned in Table-4.1, at a distance of 1 cm, 10 cm, and 100 cm. Each of these measurements includes 2000 steady state traces of RFI, having 1000 data points. Along with these measurements, we have also measured (i) background noise present in ambient RF environment and (ii) transients observed in RFI spectrum. Background noise is measured to detect the presence of any unknown RFI source operating in background and transients are measured to understand the temporal change in RFI spectrum. The overall time for taking these measurements spanned over a week. Among the list of AUTs, CFL, LCD monitor, laptop charger and induction cooktop are categorized as low-frequency RFI emitters as they radiate near the baseband frequencies i.e. < 10 MHz). Printer and UPS usually radiate in LF and GSM bands and are categorized

[1]https://www.ettus.com/product/details/SBX120

as low-frequency emitters and microwave oven is considered as high-frequency RFI source as it emits in the whole Wi-Fi band. The choice of appliances is made to cover a variety of daily activities involving a distinct set of appliances thus targeting cooking, reading and operating a laptop, etc. Details of the sampling frequency and frequency band of observation are mentioned in Table-4.2. Figure-4-2a shows the measurement setup having USRP and appliance under test and Figure-4-2b shows the UWB dipole antennas used for RFI sensing [128].

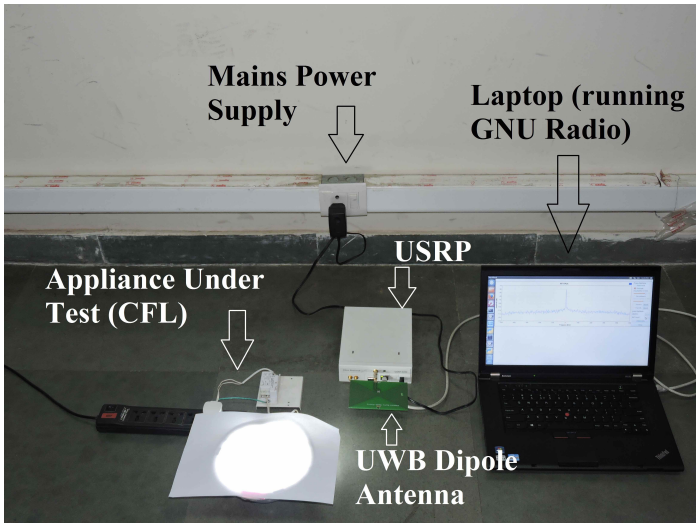

(a) Entire setup

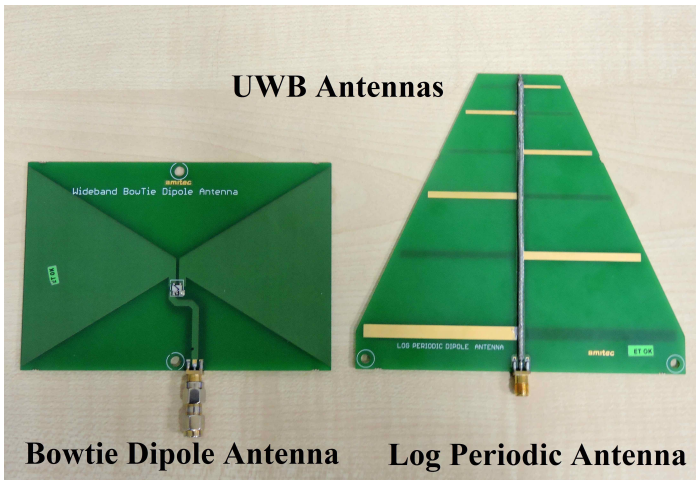

(b) Ultra wideband antennas from Amitec Electronics [130] used for RFI sensing

Figure 4-2: Test Setup used for RFI measurements having USRP, UWB antenna and AUT (top) and antennas (bottom).

S.No.	Appliance Name	Make	Model
1	Printer	Canon	MF4890DW
2	CFL	Crompton Greaves	Roof Mount
3	Laptop Charger	Dell	Inspiron 5520
4	LCD Monitor	Hewlett Packard	LE1902x
5	Microwave Oven	LG	MC2841SPS
6	UPS	Luminous	600VA
7	Hand Drill	Bosch	GSB10RE
8	CPU	Hewlett Packard	Compaq 8200 Micro Tower
9	Induction Cooktop	Philips	HD4907

Table 4.1: List of appliances (make and model) used for RFI measurements

S.No.	Frequency Band of Measurement	Sampling Frequency (MHz)	Center Frequency (MHz)	Bandwidth (in MHz)
1	Baseband	2	DC	1
2	Baseband	10	DC	5
3	GSM	25	877.5, 890, 902.5, 922.5, 935, 947.5	25
4	Wi-Fi [CH:1-7]	25	2390, 2395, 2400, 2405, 2410, 2415, 2420	25

Table 4.2: Details of RFI measurements (frequency band of measurement, sampling frequency, center frequency and bandwidth)

4.5 Observations And Analysis

Some broad observations made from RFI traces analyzed in the frequency domain are highlighted below.

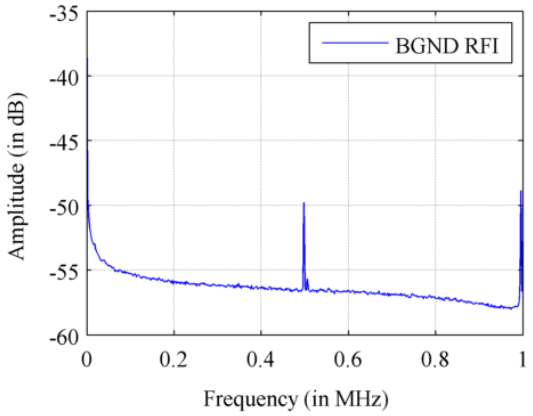

Figure 4-3: Background (BGND) RFI measured when no known appliance was operational in the vicinity.

1. Background Noise Floor in Baseband (DC-1 MHz) Range From -50 to -60dBw As shown in Figure-4-3, from baseband trace captured at Fs = 2 MHz no peaks were observed except strong 50 Hz component placed very close to DC (center frequency). This 50 Hz component was coming from nearby power supplies that were omnipresent and were hard to isolate. Another spurious having a fundamental component around 500 kHz is also observed in this trace. We assume it is coming from some adapter running in the background, as this peak was present in all the RFI traces taken over the span of multiple days.

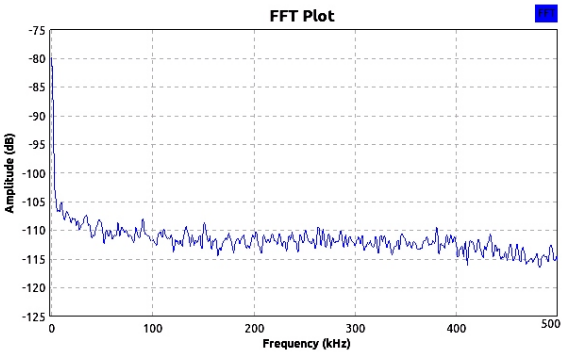

(a) Case:1 None of the appliances are operational in the vicinity

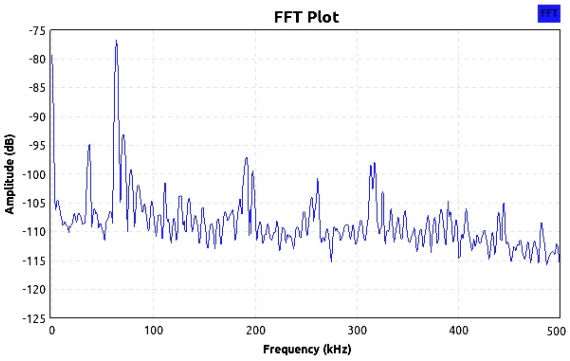

(b) Case:2 Transient's in RFI spectrum when CFL is just turned on

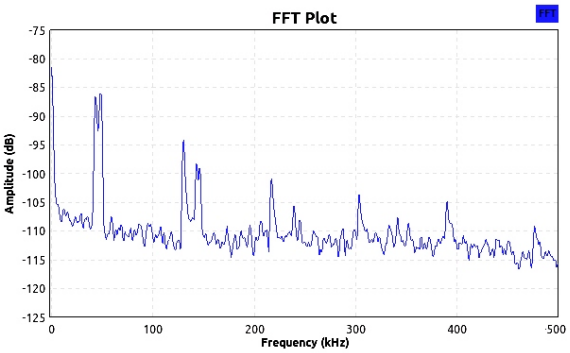

(c) Case:3 Steady state RFI measured from CFL

Figure 4-4: RFI noise floor and spectrum (DC-500 kHz) measured from CFL.

2. Appliances have distinct transient and steady state RFI characteristics Certain appliances (like CFL, hand drill and Microwave) were giving distinct characteristics in RFI during the transient duration in comparison to RFI measured

during steady state operation of the appliance. Figure-4-4a shows RFI noise floor, measured before turning on CFL, Figure-4-4b shows RFI, when CFL was just turned on (transient mode) having wide-band RFI, having first peak at 38 kHz and Figure-4-4c shows RFI examined during steady state operation of CFL having fundamental peak at 41 kHz (exact switching frequency of SMPS used inside this class of CFL).

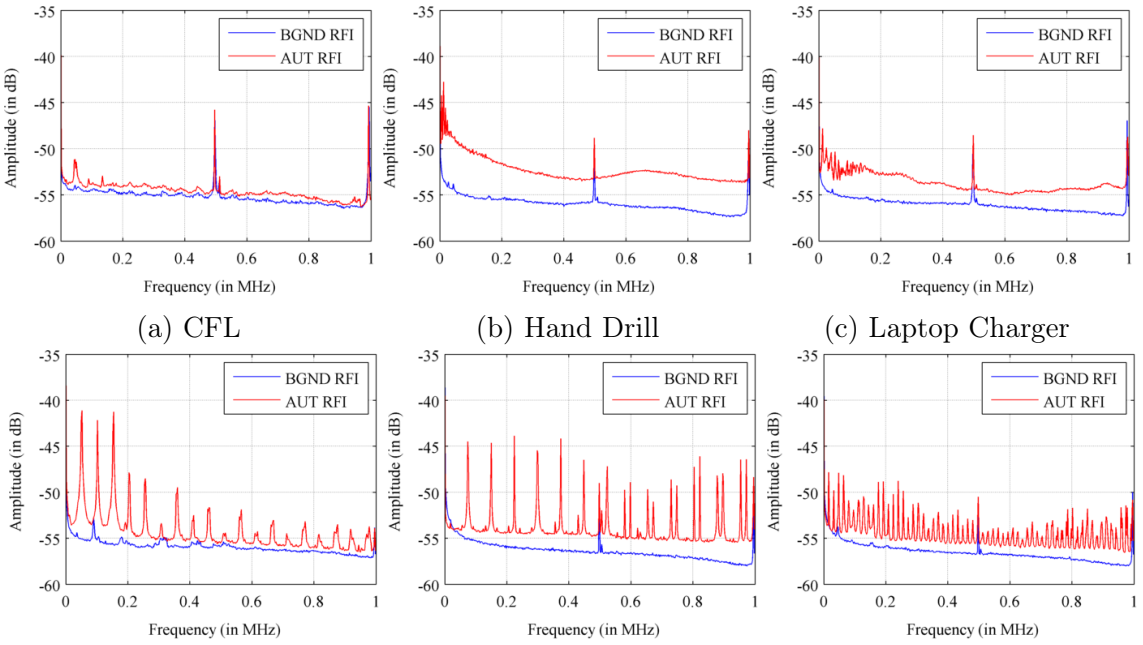

(a) CFL (b) Hand Drill (c) Laptop Charger

(d) Induction Cooktop (e) CPU SMPS (f) UPS

Figure 4-5: RFI measured in baseband (at a sampling frequency of Fs = 2 MHz) from six appliances.

3. Different appliances show unique RFI characteristics. As observed from Figure-4-5, CFL gives weak RFI (approx. 5 dB) centered at 41.4 kHz, hand drill didn't show characteristic peaks, but wideband noise is clearly observable. In case of hand drill, RFI (up to 5 dB) is observed, however, in this case instead of distinct RFI peak the whole noise floor went up and was high throughout the observation band. Laptop charger gave a band limited RFI (up to 100 kHz) but having a peak amplitude of 10 dB and was clearly discernable from baseline noise floor. Most interesting RFI signature was found from CPU, SMPS, induction cooktop and UPS having a peak amplitude of almost 20 dB w.r.t to baseline

noise. Moreover, harmonics of fundamental RFI peak were also visible. Apart from these six appliances (CFL, hand drill, microwave, CPU SMPS, UPS and laptop charger) other two appliances (LCD monitor, printer) didn't show any observable RFI signatures, we assume this is due to shielding on SMPS used inside them.

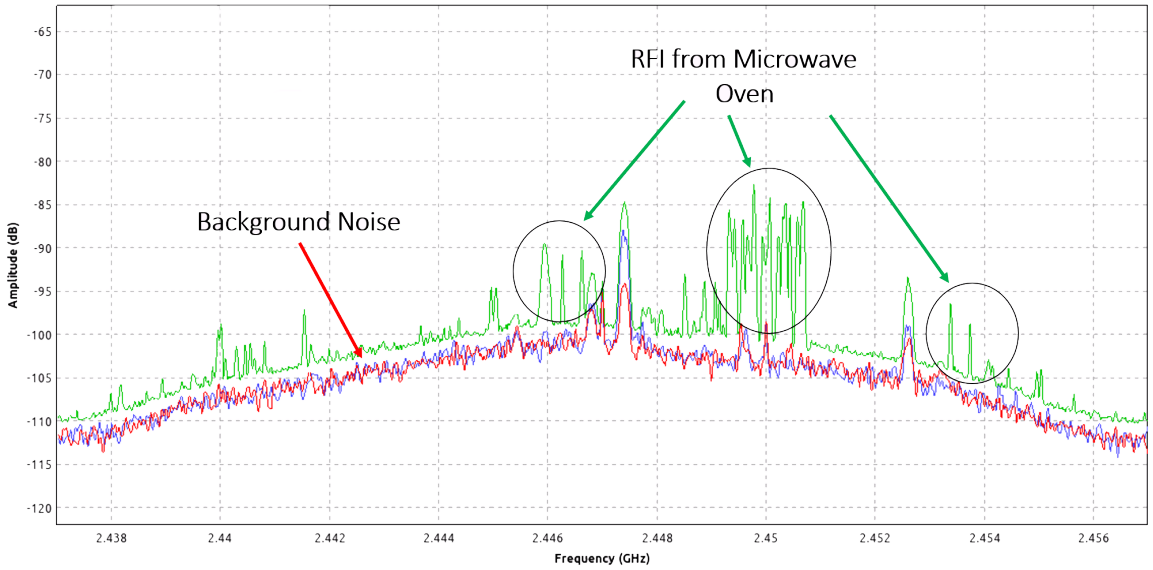

Figure 4-6: RFI measured from microwave oven in Wi-Fi band (2.412 GHz - 2.484 GHz).

4. Microwave oven exhibits time-varying RFI properties Apart from baseband certain RFI sources like microwave oven radiate significantly in higher frequency bands like 2.4 GHz but most of the RFI in 2.4 GHz is time-varying in behavior due to cyclic operation of magnetron used inside microwave oven. This kind of behavior is hard to capture using the traditional approach of RFI sensing which involves capturing of time domain RFI trace and computing averaged Fast Fourier Transform (FFT). However, we have tried to capture this behavior using spectrum analyzer application in GNU Radio as shown in the Figure-4-6. As shown in figure, microwave oven radiates a wideband RFI covering entire Wi-Fi band, and the most affected band is between 2.449 GHz - 2.451 GHz having RFI as high as 20 dB. This band also experiences a maximum burst of energy from microwave.

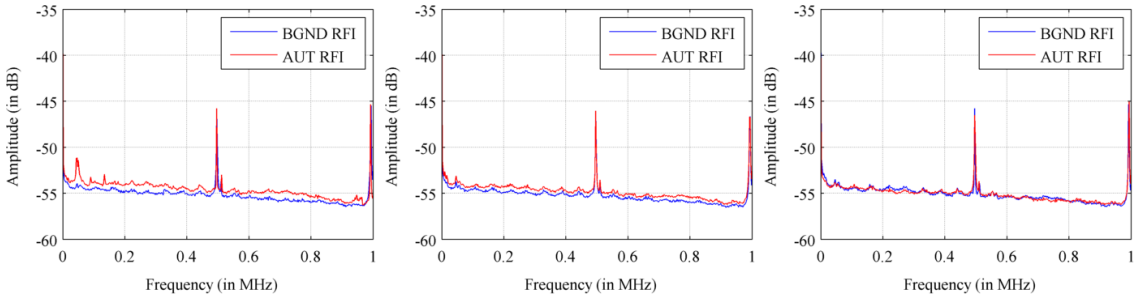

(a) (b) (c)

Figure 4-7: RFI measured in baseband from CFL (DC - 1 MHz) at varying distances (at 1 cm, 10 cm and 100 cm from left to right).

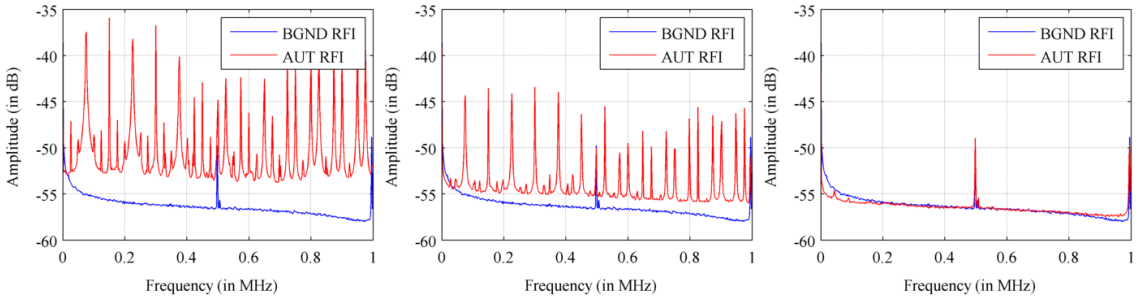

(a) (b) (c)

Figure 4-8: RFI measured in baseband from SMPS (DC - 1 MHz) at varying distances (at 1 cm, 10 cm and 100 cm from left to right).

5. RFI decays exponentially as the distance between sensing system and AUT increases. As shown in Figure-4-7a RFI plots, CFL gives RFI (approximately 5 dB) centered at 41.4 kHz which is spread across entire baseband up to 1 MHz and with increasing distance on a log scale, RFI from CFL decays rapidly. Moreover, from Figure-4-7b and Figure-4-7c it can also be seen that higher frequencies are damped at 10 cm distance, while lower band (<500 kHz) is observable up to 100 cm distance. RFI measured from SMPS, as shown in Figure-4-8 decays significantly with increase in distance from source having an amplitude of 20 dB at a distance of 1 cm, 15 dB at 10 cm and 1 dB at 100 cm, this shows RFI decays exponentially with increase in distance from RFI source. In order to verify this hypothesis, we took another set of measurement for RFI from SMPS and induction cooktop with increase in distance of separation on a linear scale. As shown in Figure-4-9, RFI from induction cooktop varies significantly from 1 cm to 30 cm (almost 20 dB decay is observable from 41 dB

to 55 dB), this shows that RFI decays exponentially. Despite of this fact that RFI decays frequently with distance, RFI still satisfies conditions required for appliance detection.

4.6 Feature Extraction From RFI and Modelling

To model and extract features from the RFI measured from non-intelligent sources, having emissions in the form of spurious Gaussian energy peaks, GMM model [131], [132] is the most likely choice. This model takes data vector along with frequency axis and fit this data in eight Gaussian curves, similar to the non-linear regression. This model returns three conventional parameters for each Gaussian curve fit i.e. mean, variance and amplitude. During our attempt to model RFI peaks using GMM, we found that for appliances with a limited number of peaks like CFL, GMM is near perfect fit as shown in Figure-4-10. However for appliances with RFI peaks followed by harmonics of fundamental frequency GMM underperformed, i.e., with an increase in the number of fits the efficacy of curve fitting started degrading. Figure-4-11 and Figure-4-12 show how GMM underperforms with RFI from SMPS and UPS when a broader frequency band is modeled. The worst fit is observed when the bandwidth is 1 MHz. To overcome this, we used k-peak finder algorithm to extract amplitude, position, and width as features from RFI peaks. Furthermore, to perform supervised learning, we have used the position of top k-peaks as a feature to train detection algorithm for all appliances uniquely.

4.7 Appliance Detection Using RFI Features

k-NN classification technique is used as a supervised learning method to learn RFI features i.e. position of top k-peaks (20 in our case) to differentiate appliances. As mentioned earlier, our data collection spanned over a couple of weeks, and it covers almost all the aspects of the temporal variations. In total, 2000 steady-state traces were collected, each having 1 thousand data points from CFL, laptop charger, UPS,

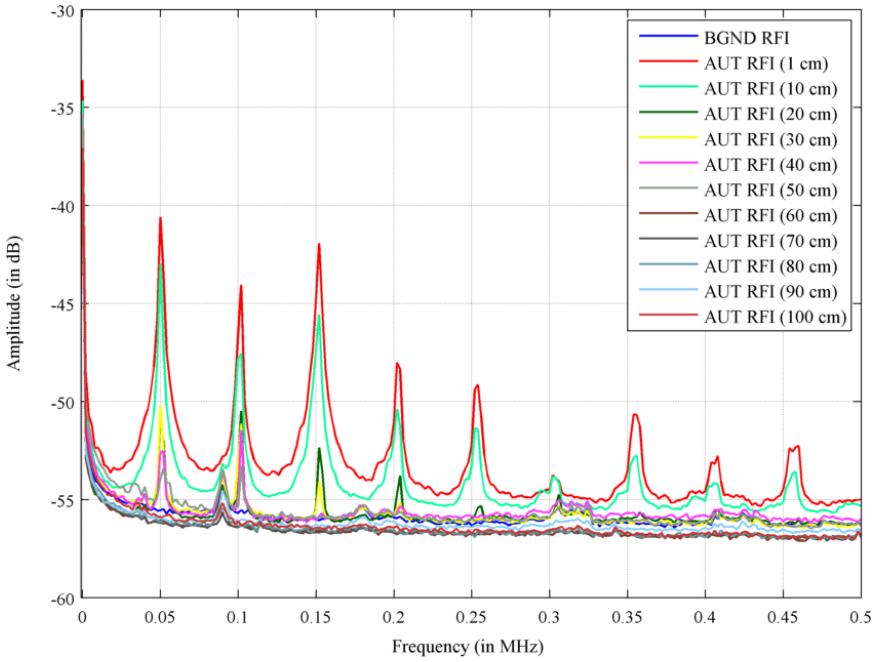

(a) Exponential decay in RFI (DC-500 kHz) with linear increase in distance from the sensing system

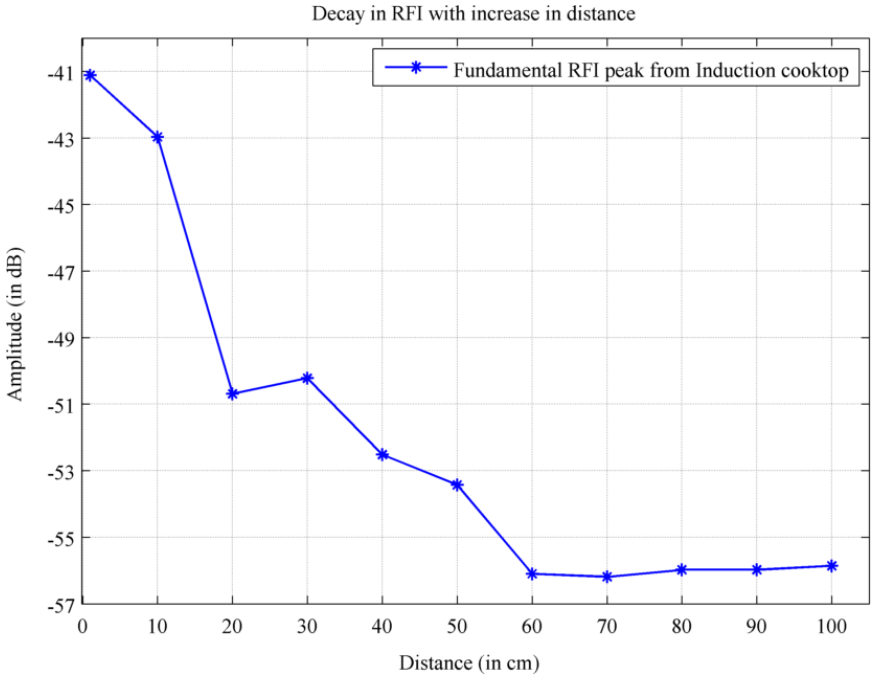

(b) Decay in fundamental component of RFI centered around 52 kHz

Figure 4-9: RFI spectrum (DC-500 kHz) measured from induction cooktop with varying distance from the sensing system from induction cooktop.

hand drill, SMPS, and induction cooktop to evaluate the performance efficacy of the appliance detection algorithm. In Stage-1, FFT spectrum is computed for all traces

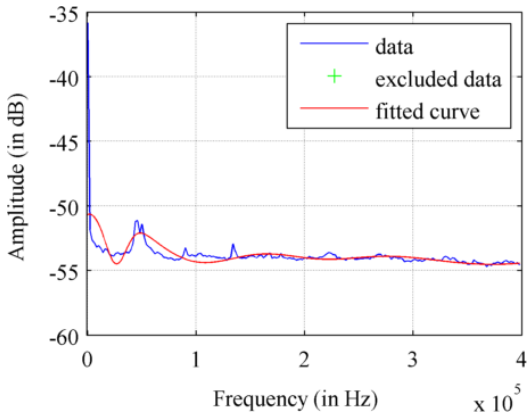

Figure 4-10: RFI measured in baseband (DC - 400 kHz) from CFL, superposed with parameters learnt using Gaussian Mixture Model (8-fit GMM).

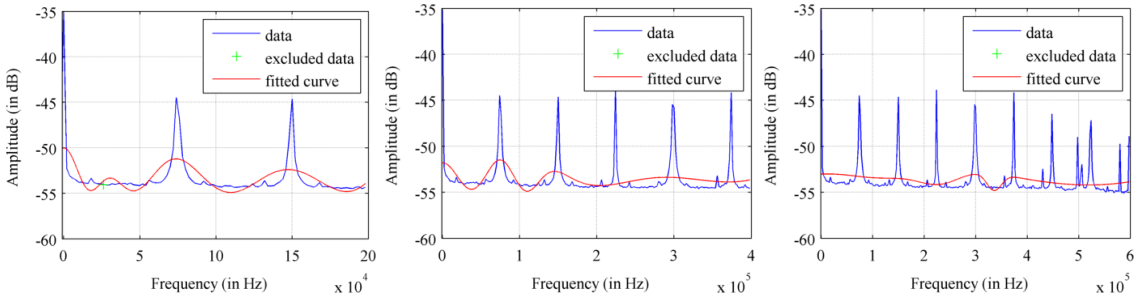

(a) Case-1: Frequency range DC - 200 kHz (b) Case-2: Frequency range DC - 400 kHz (c) Case-3: Frequency range DC - 600 kHz

Figure 4-11: RFI measured in baseband from SMPS (DC - 1 MHz) with GMM applied over different frequency bands.

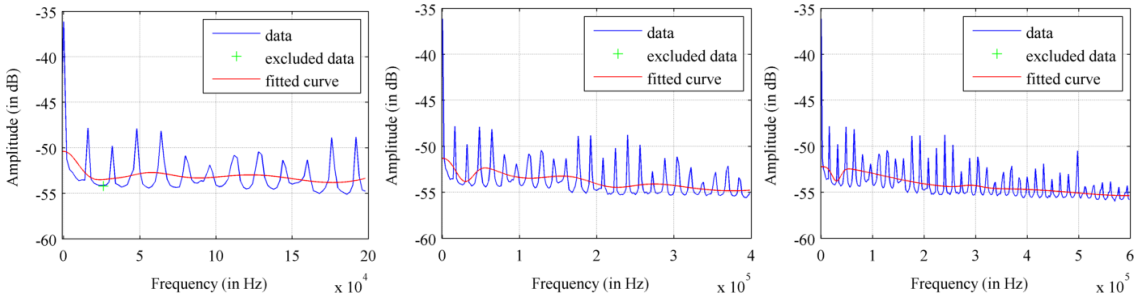

(a) Case-1: Frequency range DC - 200 kHz (b) Case-2: Frequency range DC - 400 kHz (c) Case-3: Frequency range DC - 600 kHz

Figure 4-12: RFI measured in baseband (DC - 1 MHz) from UPS with GMM applied over different frequency bands.

individually for all appliances, followed by feature extraction using top k-peak finder algorithm. Finally, the position of top 20 RFI peaks (as shown in Figure-4-13) is used for learning classes by kNN algorithm. Red marks show the position of top-k peaks used as a feature for appliance detection. Table-4.3 provides a summary of results

S.No.	Appliance Name	Mean Accuracy
1	Background Noise	52.42%
2	Induction Cooktop	78.98%
3	Laptop Charger	58.02%
4	Hand Drill	84.79%
5	UPS	54.48%
6	SMPS	100%
7	CFL	55.13%

Table 4.3: Average accuracy achieved from k-NN after 10 fold cross validation

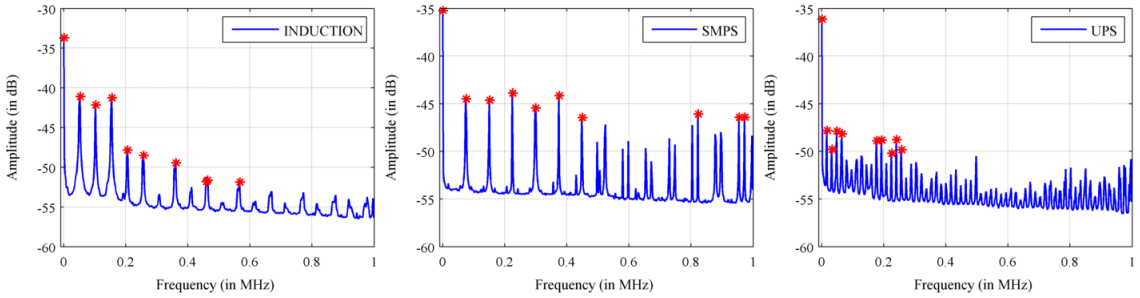

(a) Induction Cooktop (b) SMPS (c) UPS

Figure 4-13: Output of k-peak finder algorithm used for extracting RFI features (DC - 1 MHz).

obtained after 10 fold cross validation with a 7 class supervised classification process. As shown in Table-4.3 background noise, laptop charger, UPS and CFL had low detection accuracy in comparison to hand drill, induction cooktop and SMPS (which lies between 80-100%). Since laptop charger and UPS have similar RFI characteristics (around 10-20dB above baseline noise floor as seen in Figure-4-5) hence one can be easily misclassified as another. This is also evident in Table-4.4. To further extract insights on this behavior, we computed confusion matrix for 1999 trials performed (Table-4.4) during the 10-fold cross validation process. During our evaluation, we deduced that features learned from the former set of appliances are almost similar to background noise and thus are misclassified to some extent. However, despite these facts even in the worst-case scenario detection accuracy is more than 50%. On the other hand, SMPS, hand drill and induction cook-top exhibit maximum RFI with distinct characteristic peaks. Hence, the our algorithm can identify these appliances with more than 75% accuracy. This analysis shows that appliance identification using RFI as a feature will be useful in energy profiling especially for activities like cooking,

working on a computer and studying, etc. As shown in Table-4.3 background noise, laptop charger, UPS and CFL had low detection accuracy in comparison to hand drill, induction cooktop and SMPS (which lies between 80-100%). Since laptop charger and UPS have similar RFI characteristics (around 10-20 dB above baseline noise floor as seen in Figure-4-5) hence one can be easily misclassified as another. This is also evident in Table-4.4. In order to further extract insights on this behavior we computed confusion matrix for 1999 trials performed (Table-4.4) during 10-fold cross validation process. During our evaluation, we deduced that features learnt from the former set of appliances are almost similar to background noise and thus are misclassified to some extent. However, despite of these facts even in the worst case scenario detection accuracy is more than 50%. On the other hand SMPS, hand drill and induction cooktop exhibit maximum RFI with distinct characteristic peaks, hence the algorithm is able to identify these appliances with more than 75% accuracy. This analysis shows that appliance identification using RFI as a feature will be useful in energy profiling especially for activities like cooking, working on a computer and studying, etc.

AUT	BGN	CFL	Laptop Charger	UPS	Hand Drill	SMPS	Induction Cooktop
BGN	1048	920	41	0	0	0	0
CFL	675	1102	202	16	2	0	2
Laptop Charger	59	133	1160	358	236	0	53
UPS	9	22	322	1080	306	0	243
Hand Drill	0	1	102	145	1695	0	56
SMPS	0	0	0	0	0	1999	0
Induction Cooktop	0	7	45	228	140	0	1579

Table 4.4: Confusion matrix derived from k-NN classification after 10 fold cross validation (total 1999 trials)

4.8 Conclusion

In this work, RFI from nine non-intelligent sources was measured and analyzed [128]. Their behavior was characterized in terms of transients (if present) and steady-state

features of RFI. These measurements spanned across baseband, GSM and Wi-Fi bands with multiple sampling frequencies and at varying distance from RFI source. It was also demonstrated that RFI from appliance decays exponentially with the increase in separation between sensing system and the appliance under test. Gaussian mixture modeling and k-peak finder were used to extract RFI features, followed by k-nearest neighbor based classification technique to detect appliances, which is simple yet robust supervised learning technique. This work showed that using a simple k-NN classifier, it was possible to identify an appliance with a mean accuracy of 71.9%, which can be augmented further with other robust ML techniques to improve detection accuracy and also to infer other commonly used appliances.

Chapter 5

Stray Electric Field Signals from Low-Voltage Power Lines for Energy Harvesting

In the previous chapters, we showcased the applicability of stray EMI emissions originating from appliances having switch-mode power supplies for appliance detection. Appliance detection for energy monitoring and feedback is the foremost step to achieve long-term energy sustainability.

In this chapter, we exercise stray emissions from power lines for energy harvesting and leverage it to enable self-powered deploy-and-forget sensor nodes inside buildings. In our initial studies for appliance detection, we took EMI measurements in India having a 230V 50 Hz AC power supply while the later studies for energy harvesting were performed in the US on 110V 60 Hz power supply. Despite this transition, the findings from these studies are equally applicable in both of these settings having 230V 50 Hz or 110V 60 Hz power supply.

According to the 2017 forecasts by Gartner Inc, a total of 20.4 billion IoT devices will be connected to the Internet by 2020[1]. These devices demand frequent battery replacement, adding to overall deployment and maintenance costs. As the number of connected devices continues to grow, the need for scalable power management poses

[1]https://www.gartner.com/newsroom/id/3598917

a major concern. Reducing power consumption could allow small batteries to stay active for a year or two instead of months. However, keeping track of these batteries is still a tedious task. Self-powered sensor nodes have emerged as a possible solution to the problem. These nodes can harvest energy from the ambient environment in the form of light [133], temperature [134, 133, 135, 136], vibration [137, 138], RF [139, 140], and Wi-Fi [141]. Based on the availability of these ambient signals, each solution has its own benefits and constraints [142].

In this chapter, published as [143], we invented a novel battery-free, stick-on capacitive energy harvester that harvests energy from stray electric fields around the ubiquitous AC power lines as shown in Figure 5-1. Although prior preliminary work has explored harvesting energy from power lines [64, 144], these solutions have traditionally required a direct ohmic connection to ground — that is, the harvester requires an end-user to run a wire from each of the harvester devices to earth ground (achieved in prior art by connecting to a copper plate inside a wall). In contrast, our solution relies on capacitive coupling to ground, enabling easier and safer end-user deployment and use in many more scenarios, where a direct ground connection is not feasible. For instance, attics can have long insulated runs of electrical cabling with no easy access to earth ground, except at junction boxes. Although advantageous, designing a harvester without this ohmic ground connection poses a significantly more challenging problem.

To address this challenge, we use stacked capacitive electrodes to provide a local ground and design our device to effectively harvest from this nanowatt source — a significant contribution of this work. Power lines are ubiquitous inside buildings, thus facilitating a broad range of applications like monitoring ambient temperature, detecting building occupancy, monitoring appliance usage for optimizing energy consumption, environmental sensing for indoor vertical farming applications, and water leakage detection. All of these applications can be enabled with our battery-free wireless device, which is capable of periodically transmitting collected sensor data over an RF channel to a base station.

Unlike prior work [63, 62, 61], our harvester can clamp on to any *fully bundled and*

insulated AC power line without intercepting individual conductors (phase, neutral, and earth) and can harvest continuously without any active appliance operating on these power lines.

This is a notable contribution and improvement over the commonly used electromagnetic harvesters that require:

1. the user to access and clamp onto individual conductors so that the two directions of current does not produce a null field)
2. a device on the tapped conductor be consuming current in order to create a magnetic field around the wire. These requirements are obviated with CapHarvester's capacitive coupling approach, which results in a safer, more convenient device.

Our measurements in controlled lab settings and real-world environments exhibited that we can harvest up to 270 µJ in 12 min using a 14 cm-long harvester deployed at 10 cm above ground.

In summary, the contributions of this chapter are:

1. A novel stick-on capacitive energy harvester that harvests the stray electric fields from AC power lines with no need for access to ohmic earth ground thus providing increased safety and ease of use.
2. A characterization of the energy harvesting capabilities of our device in various environments and with different power cables, as well as an analysis of the trade offs in the design of the device's geometry.
3. Three real-world representative applications of this device, including distributed temperature sensing for HVAC control, non-intrusive appliance state (on/off) sensing, and environmental sensing for indoor farming.

5.1 Prior work in energy harvesting

The tradeoff between battery life and communication range is one of the foremost concerns in IoT technology [145, 146]. Extending communication range requires that devices increase their transmission power, leading to quicker battery drainage. Al-

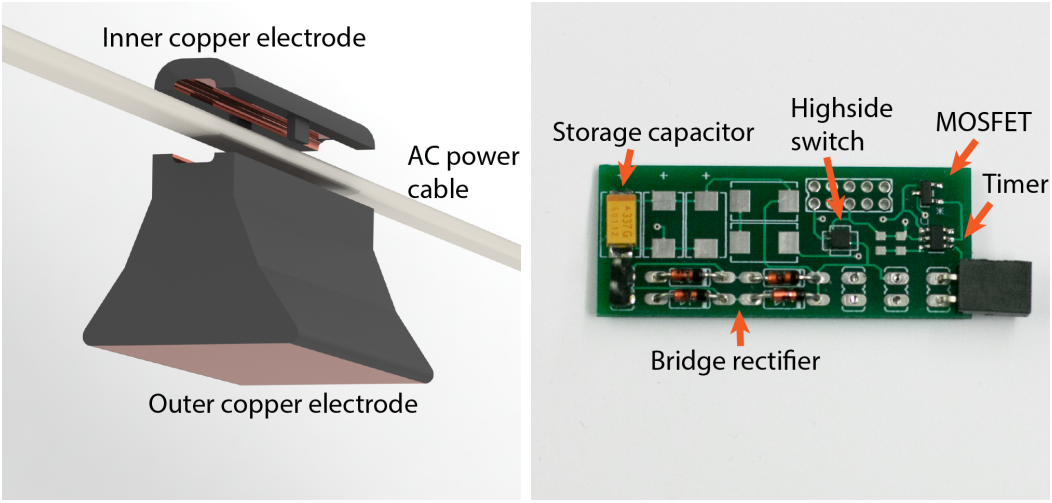

(a) The CapHarvester clamps on to a low-voltage power cable and harvests power without current flow

(b) Our power harvesting circuitry rectifies the capacitively coupled 60 Hz power line signal and stores energy in a capacitor

Figure 5-1: CapHarvester alongwith power harvesting circuitry having rectifier, storage capacitor, a high-side switch, timer, and MOSFET.

though people have proposed ultra-low power sensors and MCUs with on-chip wireless support, batteries are still the major bottleneck for power-intensive sensing. Furthermore, keeping track of the battery level in widespread, dense deployments is a major hassle.

In response, energy harvesting from the ambient environment has been explored as an alternative to battery-powered IoT. A number of different of energy sources have been leveraged, including light [133], temperature [134, 133, 135, 136], vibration [137, 138], RF [139, 140], and Wi-Fi [141]. Non-invasive energy harvesting from AC power lines, as in our work, has not been explored as thoroughly as other techniques.

In 2011, Gupta et al. explored using stray electromagnetic fields from power lines for low duty cycle sensing applications [61]. However, this work requires a large transformer placed in between conductors, which is not feasible for most applications due to space constraints. In 2013, DeBruin proposed a smart meter which uses two current transformers: one for harvesting energy to power the sensing circuit, and another for taking power measurements; this approach does not require an AC-DC transformer[62]. Campbell et al. proposed a self-powered circuit-level current

meter [63] that uses two split core current transformers, and Moon et al. proposed Vampire, which has a custom toroid-based harvester [147]. The latter three devices can be clamped onto any current-carrying conductor for harvesting local magnetic fields and measuring power consumption. The major limitation of these works is that they require isolated phase and neutral conductors for installation. This is possible for some applications, but not in general for everyday use. Another line of work has explored a low-profile power meter which connects with a 3-pin plug point for measuring the power consumption of appliances [148]. It harvests energy without making any ohmic connection with actual conductors, enabling a new dimension of plug load metering. However, this harvester design is specific to power cables that have plug points; again, it does not work for general applications. Harvesting stray electric fields from AC power lines through capacitive coupling is an exciting approach as it can continuously harvest energy and does not require any appliance to be active on the power line. However, most of the exploration in this space is limited to power lines with a high voltage overhead [149, 150, 151].

We now present a capacitively coupled stray electric field harvester with low voltage AC power lines; these power lines typically carry 110 V (North America) or 230 V (Asia Pacific) AC voltage at 60 Hz and 50 Hz respectively. Although this concept is not novel [65, 64, 144], prior work required an ohmic connection to earth ground for each harvester. In a building with painted walls, an ohmic connection requires scraping the paint off of the walls or digging a copper plate to get an earth contact, as demonstrated by Kim and Kong et al. [64, 144]. This is undesirable for ubiquitous, end-user deployable sensors. Our harvester design addresses this challenge by using stacked electrodes to generate local reference ground and leveraging an optimized power management circuit to efficiently harvest stray electric fields.

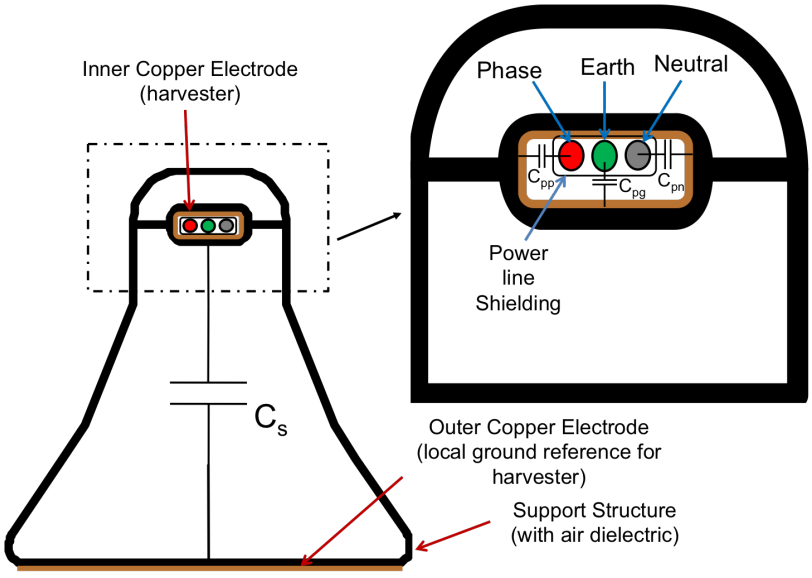

Figure 5-2: Cross-sectional model of a power line having three conductors and their respective capacitance with harvester electrodes.

5.2 Theory of operation: Stray electric field harvester

In this work [143], we designed a novel capacitive energy harvester using stray electric fields from low-voltage AC power lines for energy harvesting. Whenever an alternating voltage signal is fed through a power line (single-wire or multi-wire topology), a corresponding alternating electric field is generated on the outer surface of the cable. The strength of this field varies depending on the magnitude of the voltage signal and the dielectric constant of the shielding across the power line's conductors. Figure 5-2 illustrates the working principle for the capacitive energy harvester using a cross-sectional model of a power line having three conductors (phase, neutral, and earth). Each conductor has a primary capacitance (C_{pp}, C_{pn} and C_{pg}) with respect to the inner electrode and a secondary capacitance (C_s) exists between the inner and outer electrodes of harvester. C_{pp} represents the primary capacitive coupling between the outer surface of the power line and the phase conductor carrying a 110 V AC signal. C_{pp} serves as the driving source for an alternating electric field on the surface. The other two conductors present in a multi-wire topology, neutral and ground, are

tied to earth ground at the distribution side of the transformer. The capacitances corresponding to these two conductors, denoted as C_{pn} and C_{pg}, do not contribute any electric field.

Techniques for conventional electric field harvesting depend on the type of power line in question. For the high-voltage (HV) power lines found in industrial settings, a copper plate placed at some distance provides access to stray electric fields. For low-voltage (LV) power lines in residential and office settings, copper tape around the power line suffices. However, there are certain technical constraints that restrict the application of conventional techniques, particularly for the LV power lines we are interested in leveraging for harvesting. One of the foremost challenges is the availability of the earth ground to act as a reference. Earth ground can be accessed outdoors for HV power lines by digging a pit in the ground for a connection; for LV power lines, however, accessing earth ground requires concrete walls that lead directly to it or cumbersome infrastructure alterations to do so [64, 65]. Secondly, weak capacitive coupling limits the output power available at the harvester electrodes (a couple of volts with <1 μA of current). Typically, this capacitive coupling is weak since the voltage supply fed to the LV power lines is weaker ($\sim$100-300 V) in comparison to HV power lines ($\sim$11-33 kV); the coupled signal for LV power lines will be proportionally lower (i.e., a few volts per cm length of electrode). Also, capacitive coupling depends on the frequency of the signal and dielectric material. Coupling is weaker in most applications due to lower power signal frequencies (50 Hz or 60 Hz) and the presence of insulation material that lowers the dielectric constant of the power cables for shielding. Furthermore, in the absence of a reference to earth ground, energy harvesting becomes non-trivial and the amount of energy available at the output of the electrodes reduces significantly since in this case we tried to harvest energy from a voltage source with a really high impedance. In order to analyze the available power with local reference ground, we characterize the power harvesting capabilities of our device in various environments and with different power cables. We also analyze the trade-offs in the design of harvester. These findings are discussed in detail in Section 5.4 and Section 5.5.

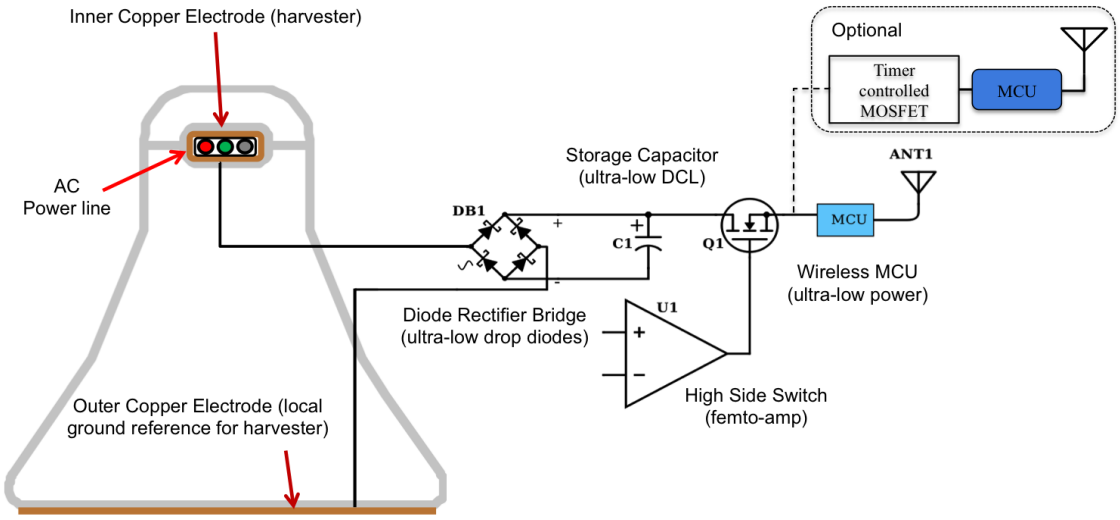

Figure 5-3: The block diagram of our CapHarvest system used for continuous and event based sensing applications.

In order to harvest energy from ubiquitous LV power lines in a continuous manner, we designed a double-layer stacked capacitor model for capacitive energy harvesting. Our approach does not require a solid earth ground for reference and generates its own reference ground. Furthermore, our approach can effectively harvest power as little as nanowatts using ultra-low power harvesting circuit.

5.3 Hardware design

We designed a capacitive energy harvester with five main components: capacitive electrodes, a diode rectifier bridge, a storage capacitor, a high-side switch, and a wireless MCU. Figure 5-3 illustrates the block diagram of the entire system and the different sections of the harvester. Before discussing the remaining blocks, we describe the double-layer stacked capacitor model of the harvesting electrodes since it is one of the most critical design choices required for the harvester.

5.3.1 Double-layer Stacked Capacitor Model of Electrodes

In order to remove the requirement of a reference earth ground, we designed a double-layer stacked capacitor model for the harvesting electrodes. Figure 5-2 shows the

primary and the secondary layer of the stacked harvester model. Primary capacitance (C_{pp}, C_{pn} and C_{pg}) exists between the power line conductors (phase, neutral and ground) and the inner electrode made up of copper tape having contact with the outer surface of the power line. The inner electrode serves as the high potential electrode in our case. In order to generate a local reference ground that can serve a lower potential than the inner electrode, we add another layer of conductive electrodes made of copper tape[2], which is propped up by a 3D-printed support structure (Figure 5-3). Ideally, the secondary capacitance between the inner and the outer electrodes (C_s) should be as low as possible. Air, with a dielectric constant of ∼1, is the primary dielectric between the inner and the outer electrodes. The area and separation of these capacitive electrodes are critical design parameters since they directly determine the voltage and power available at the output of these electrodes. In order to understand this relationship, we characterize variations in harvested power from different lengths and electrode spacings. These measurements are discussed in Section 5.4 (Analysis). Our design decisions and component selections are motivated by this power characterization. Some of these design parameters are variable and can be adjusted depending on the nature of the application. We discuss this strategic power management in more detail in Section 5.5 (Design Space).

5.3.2 Diode Rectifier Bridge

The AC voltage output from the capacitive electrodes is fed to a diode rectifier bridge consisting of small signal Schottky diodes for AC-DC conversion. Small signal Schottky diodes with ultra-low forward voltage drop are widely used in harvesting applications; however, most of them are designed to operate at fixed frequencies. In this system, we choose Vishay BAT85S diodes, which have a forward voltage drop (V_f) of around 100 mV (I_f=1 µA) at 60 Hz. The choice of a rectifier bridge over a full-wave rectifier is due to the fact that the latter requires an earth ground reference, which restricts the application space of this harvesting technique. As our harvester is de-

[2]Both the inner and outer electrodes are built using copper foil tape (3M 45J589) with a thickness of 3.50 mm, wrapped on the inner and outer surface of the support structure

signed for low frequencies (50 Hz or 60 Hz), we are not concerned about the parasitic capacitance that arises from diode leads.

5.3.3 Storage Capacitor

After AC-DC conversion, the output of the rectifier bridge is fed to a storage capacitor (C_{store}). The choice of capacitor depends highly on its DC leakage (DCL) and equivalent series resistance (ESR). The dielectric material of a capacitor is an imperfect insulator that allows a small amount of current to flow between the two conductive plates which is called the DCL. Electrolytic capacitors have large leakage currents while plastic, ceramic and tantalum capacitors have very small leakage currents. The storage capacitor should have as little DCL and ESR as possible in order to harvest effectively from a nano-watt source. We choose AVX TAJ (AVX TAJD477K004RNJ)[3] series tantalum capacitors for this reason. The maximum DCL for this capacitor is 18.8 µA. We have to note that this number is reported at the rated voltage, which is 4 volts at 80 °C. Since our system is operating at much lower temperature and voltage the DCL will reduce significantly. The other benefit of this capacitor is it's low ESR (around 0.9 Ω). Along with the dimensions of the harvesting electrodes, the ideal value of the storage capacitor C_{store} also varies depending on application's requirement. Continuous sensing applications may require a bigger capacitor (∼1-10 mF), but a sparse sensing application like temperature sensing can work with a smaller capacitor (∼220 µF to 330 µF). The data rate at which the sensing system can communicate also depends on the size of the capacitor. We discuss capacitor selection in detail under strategic power management in Section 5.5 (Design Space).

5.3.4 Charge Controller (High-side Load Switch)

Like typical energy harvesting systems, our setup also requires a charge-controller that can switch output loads once the harvested energy reaches a certain threshold.

[3] http://www.avx.com/products/tantalum/smd-tantalum-mno2/taj-series/

There are several integrated solutions for this purpose, such as TI BQ25570, Ablic (Seiko) S8823, and LT LTC3108. These solutions use dual-stage boost and buck converters or multi-stage charge pumps. However, none of them can be employed in this system as they require a cold-start. A cold-start consumes a few milliamperes of current to turn on the primary boost converter/charge pump or a quiescent current (I_q) of $\sim$1 µA, making them impractical for our harvester. Note that some of these charge controllers can perform a cold-start from a secondary storage cell or battery, but we strive towards a battery-free harvester. In order to control the output load in a hysteric manner, we explored N-MOSFET-based high-side switches. These switches drain quiescent current on the order of microamperes to facilitate the bias voltage requirements for the gate-source voltage (V_{gs}). To overcome this high drain quiescent current, we use the nano-watt high-side load switch from Semtech (TS12001-C018). This load switch has an on-state current of 70 nA and and off-state quiescent current of 100 pA. It also has a factory-programmed threshold voltage (V_{th}) for a comparator and does not require any external bias voltage like conventional N-MOSFET-based switches[4]. This high-side switch turns the output on when the storage capacitor hits V_{th}+500 mV and lets it discharge down to V_{th}, giving it a hysteric window of 500 mV. The storage capacitor is always harvesting charge, even when the high-side switch is closed); depending on the size of electrodes, though, it takes variable amounts of time to charge up to V_{th} again. Please note that V_{final} (or V_{th}) is the lower threshold voltage of the high-side switch until which it will discharge the storage capacitor while V_{init} is the turn-on voltage of the high-side switch at which it will start its operation which is typically V_{th}+500 mV.

5.3.5 Wireless MCU

During the on-state, the high-side switch powers up an ultra low-power (ULP) wireless MCU (TI CC1350) for approximately 20 ms. All the sensing and data communication tasks are handled by this MCU. We prefer the CC1350 wireless MCU over other

[4]https://www.digikey.com/en/maker/blogs/introduction-to-high-side-load-switches/9324fe174d494b9e82f733fc23884050

MCUs as it supports long-range sub-GHz band (f_c=868 MHz) communication with an integrated ULP MCU (Active Tx consumes ∼11mA at 1.95 V). It also supports a proprietary 15.4-Stack for sub-GHz band communication.

5.3.6 Charge Controller for Continuous Sensing (Nano-power Timer-based MOSFET Driver)

We also explore a continuous sensing application where we periodically turn on an ULP MCU MSP430FR5959 using a nano-power timer (TI TPL5110) and a P-MOSFET (Infineon IRLML6402), sample the ADC, and write these values to the MCU's FRAM. The timer and MOSFET are connected to the output of the high-side switch and the gate of the MOSFET is controlled with the timer. The choice of the MOSFET is very important since it needs to have extremely low on resistance. This benefit, combined with the fast switching speed and small leakage current enables continuous sensing for CapHarvester. After a known interval (12-24 hours), the data that has been stored in the FRAM can be transmitted using a low-power transmitter. Apart from these design considerations, application specific design variations are discussed in Section 5.6 (Application Space).

5.4 Analysis: Harvester specifications and efficiency

Like most energy harvesting systems, the CapHarvester operates in a duty-cycled fashion, charging a storage capacitor up to a maximum voltage (2.21 V) before activating. As shown in Figure 5-4, the system when first installed, the harvester begins its cold start period. Once the storage capacitor reaches the trigger voltage of the high-side switch (2.21 V here), the switch activates and the device becomes active until the voltage drops to the lower cutoff or threshold voltage (V_{th} = 1.8 V here). After that the recharge time of the device is significantly reduced. Because our device relies on a local ground generated by an electrode, the performance strongly depends on the electrical environment in which it is placed. In the following sections, we in-

vestigate the impact of an ohmic ground connection, explore diverse environmental effects, and characterize our device performance with different power cables.

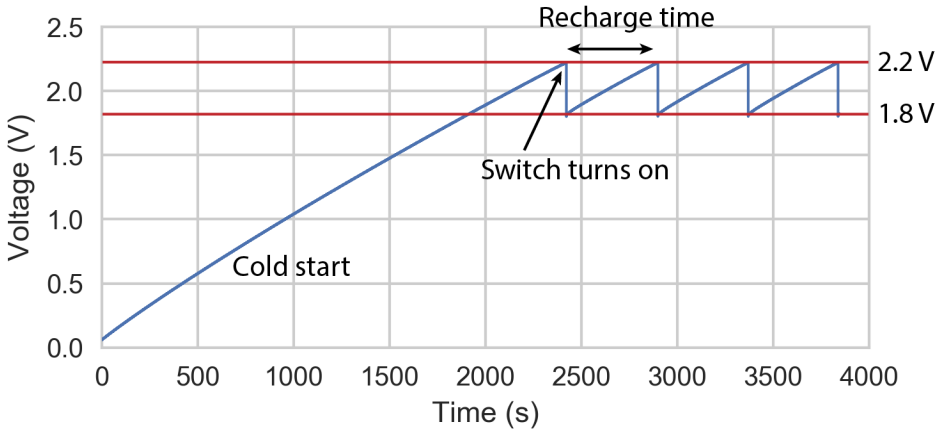

Figure 5-4: Charge discharge curve of storage capacitor in CapHarvester showing cold start period, turn-on state of high-side switch (2.21 V here) and shut-off at lower cut-off point (1.8 V here).

5.4.1 Methodology

In the following experiments, we measure the energy harvested by our device by measuring the voltage across the storage capacitor over time. For most of our applications, we use a high-side switch that remains active from $V_{th} = 1.8\ V$ to $V_{init} = 2.21\ V$. To enable a meaningful comparison, we report harvesting performance as the time it takes the capacitor to charge from 1.8 V to 2.21 V. We also report the average power, P, harvested during this time, t, according to Equation 5.1.

$$P = \frac{(V_{init}^2 - V_{th}^2)\, C_{\text{store}}}{2t} \tag{5.1}$$

Our measurement setup consists of a National Instruments (NI) USB 6003 DAQ unit configured for taking analog measurements in fully differential mode [-10 V to 10 V] at a sampling rate (F_s) of 10 kHz. We chose NI USB DAQ over a conventional digital storage oscilloscope (DSO) as the latter has a much lower input impedance (in range of tens of MΩs) and can significantly load a nano-watt source like a capacitive

ID	Location	Surface	Charge Time (s)	Average Power (uW)
A	Ground floor of cement office building	Tile floor	277	0.95
B	Fifth floor of cement office building	Carpet	731	0.36
C	Second floor of wooden house	Carpet	1308	0.20
D	Outdoors	Concrete	242	1.09
E	Wooden Stud	Wood	780	0.34
F	Wooden Attic	Wood	2356	0.11
G	Wooden floor	Wood	2500	0.11
H	Residential Basement	Carpet	653	0.40
I	Table in Residential Basement	Wood	617	0.43
J	Residential garage	Epoxy Coating	267	0.99
K	Fifth floor of a cement laboratory building	Epoxy Coating	467	0.57

Table 5.1: Charge time and average power harvested using CapHarvester in various locations in the US (110V/60 Hz)

harvester by consuming few milliamperes of current. Also, most DSO's do not allow differential measurements without referencing to earth ground. NI USB DAQ has an input impedance of >10 GΩ, consuming <1 nA for taking each measurement and allows differential measurements without referencing to earth ground. The available power is so little that even this device, with its high input impedance, has a significant impact on the charge time. Rather than leave it connected to the circuitry, we periodically connect it to sample the voltage across the storage capacitor. We use Python (PyDAQMx, SciPy and NumPy) for configuring, logging, and filtering data from the DAQ.

5.4.2 Environment

Our device relies on the capacitive coupling to the ground; hence, it is essential to characterize its performance in a variety of locations. We tested the device in 11 locations. Table 5.1 summarizes the performance in these locations. Charge time is reported using a 4 cm high and 14 cm long electrode with a 330 µF storage capacitor. These results show that performance is best when our device has a good coupling to the earth's ground. For example when tested on a concrete floor which has a good

coupling to ground the charge time of CapHarvester was only 277 second on average. When placed on wooden surfaces, or When elevated off the ground, the charge time increases significantly. In the 11 locations we tested, we observed power harvesting rates that varied by a factor of 5x - 10x. We note that this technique will not work when suspended in free air, placed on drywall, or placed on a wooden table with poor coupling to ground. This poor coupling is mostly due to lack of conducting medium between the outer electrode of CapHarvester and the earth ground. Construction materials with a higher value of the dielectric constant can serve as a better coupling medium for capacitive energy harvester in comparison to materials with lower dielectric constant (good dielectrics) like dry air or vacuum. Hence the materials like wooden table and drywall act as a non-conductive medium (good dielectrics) and offer poor coupling to earth ground.

ID	Cable Type and Make	Gauge	Length (ft)	Power Rating (W)	Charge Time (s)	Average Power (uW)
A	HDX (SPT-2)	16	12	1625	443	0.595
B	Aurum (Outdoor /Indoor)	16	15	1625	707	0.373
C	Inermatic Table top	14	2	1250	1030	0.256
D	Hanvex-HAX10G	16	10	1250	1070	0.247
E	HDX (Outdoor /Indoor)	16	50	1625	1500	0.176

Table 5.2: The available output power with different types of extension cords arranged in the order of increasing charge time.

5.4.3 Power Cable

We also characterized the amount of power harvested from different cables (extension cords) using a 14 cm long and 4 cm high CapHarvester electrode with a local reference ground. We picked five commonly used cables (of different gauge, round/flat and lengths) and also calculated the average power delivered to CapHarvester. As shown in the Table-5.2 the charge time and the amount of power delivered to capacitive harvester varied significantly even for cables having a similar gauge, this is due to

different capacitive coupling offered by these cables due to the variable length of outer shielding, inner conductors, and nature of dielectric used for shielding. In the future, a regression model can also be proposed which can help in estimating power delivered by a particular type (length, gauge, dielectric shielding) of power cable.

5.5 Design Space: Employing the Capacitive Energy Harvester

In this section, we first discuss the power management strategies for different applications that we exhibited in this work. We then discuss the design considerations for these applications, which can also be used as a reference by future designers and inventors for other applications where this capacitive harvester can be employed.

5.5.1 Strategies for Power Management

We separate the application space for capacitive harvesting into two broad categories depending on the nature of the sensing involved. We discuss the strategies for power management that we employ for these categories and then their suggested hardware design configurations.

- **Sparse Sensing:** These are scenarios when data does not need to be delivered at a specific time. Examples of scenarios in this category include distributed temperature sensing, appliance state monitoring, and sensing environmental parameters for indoor farming. For most of these applications, we use a fixed length (14 cm) and spacing (4 cm) between electrodes for ease of deployment and vary the size of the storage capacitor depending on the energy budget required for sensing and data transmission. We also occasionally include a high-side switch with a higher threshold voltage.

- **Continuous- and Event-based Sensing**: Applications like pressure monitoring in industrial scenarios require continuous sensing for data logging and

reporting anomalous events. This cannot be facilitated through a high-side switch-based charge controller as it will drive the load depending on a fixed turn-on voltage. However, continuous sensing applications require an uninterrupted supply of energy after a fixed time interval. To enable such applications, we employ an optional timer-based load driver that can be connected to the output of the high-side switch. This programmable timer can periodically drive a load for a known duration and can be turned off through an external control signal. Event-based sensing can be enabled by adding an additional firmware constraint on top of continuous sensing to transmit data whenever an anomalous event occurs or a predefined threshold is met. The size of the storage capacitor will vary depending on the energy requirements for continuous sensing and the data transmission rate.

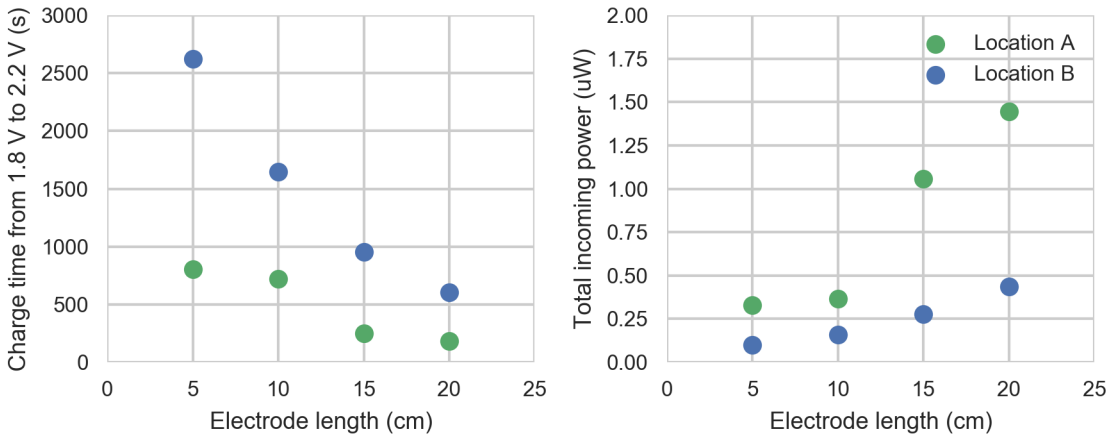

Figure 5-5: Charge time and incoming power for different lengths of electrode.

5.5.2 Design Space

In total, there are three major design variables: the length and spacing of capacitive electrodes, the size of the storage capacitor, and the configuration of the high-side switch or charge control circuit.

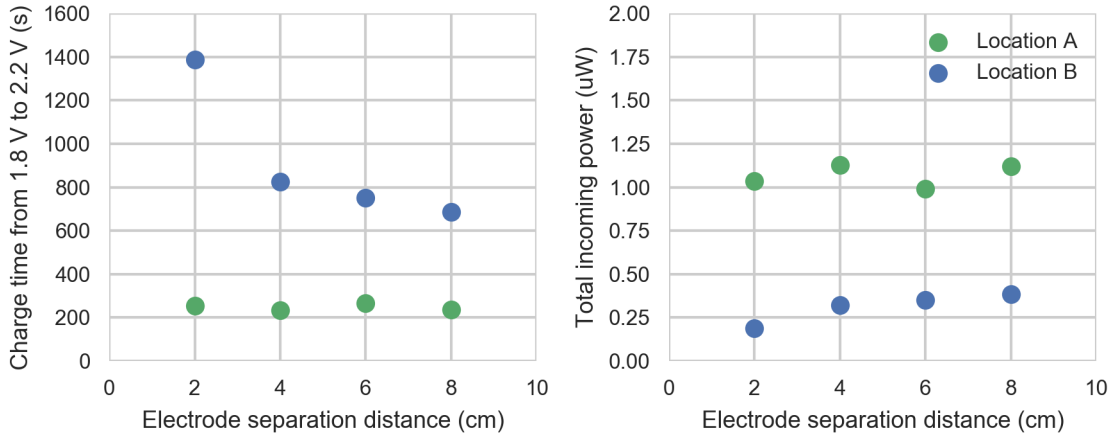

Figure 5-6: Charge time and incoming power for different separation distances between the two electrode

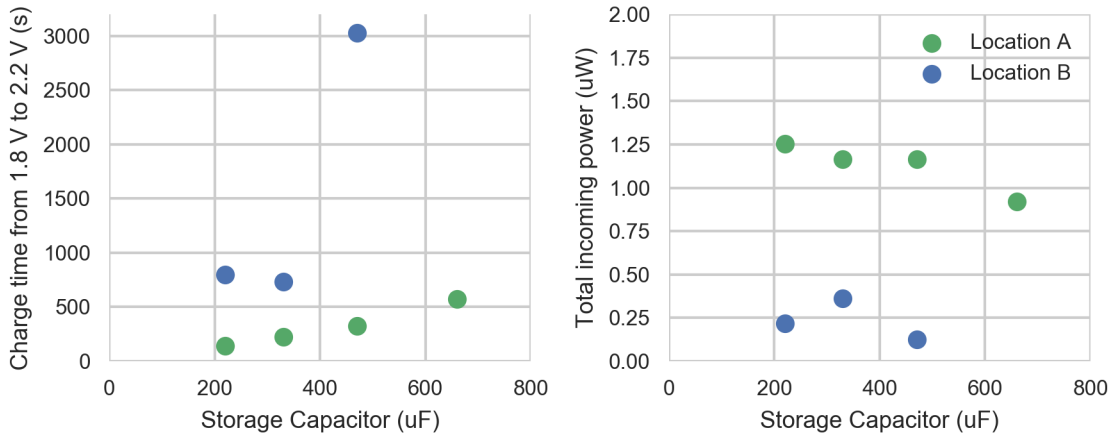

Figure 5-7: Charge time and incoming power for different capacitors size

Length and Spacing of Electrodes

The design of the electrodes is critical for determining the instantaneous power available at their output. For most applications, we prefer to use a fixed length (14 cm) and spacing (4 cm) of electrodes as they were more convenient to install than longer electrodes. Figure 5-5 shows the charge time and incoming power for different lengths of electrode and Figure 5-6 charge time and incoming power for different separation distances between the two electrode. It shows how charge time reduces with increased length and separation of electrodes. Here location A corresponds to the ground floor of cement office building having tile floor and location B corresponds to the fifth floor

of the same building having carpet surface.

Size of Storage Capacitor

We compute the capacitor required for each application according to the net energy required and equate this to the amount of energy discharged from the storage capacitor (C_{store}) using Equation 5.2.

$$E_{req} \leq E_{dis} = \frac{1}{2} \times C_{store} \times (V_{init}^2 - V_{final}^2) \tag{5.2}$$

Consider a sensor that periodically measures temperature. A CC1350 MCU requires 2 V and consumes ∼10-12 mA of current for taking one temperature measurement and transmitting this data over a sub-GHz radio. This entire process takes approximately 10 ms. Details specific to this application are discussed in Section 5.6. We use a high-side switch (Semtech TS12001) with a hysteresis window of 500 mV so we can discharge the storage capacitor by only 500 mV. As this application requires 2 V, we use a high-side switch with a threshold voltage of 1.8 V and a turn on voltage of 2.21 V. We compute energy required for this application as

$$\begin{aligned} E_{req} &= V \times I \times T \\ &= 2V \times 0.012A \times 0.010s = 240\mu J \end{aligned} \tag{5.3}$$

Next we compute the value of the storage capacitor C_{store} using Equation 5.2:

$$C_{store} = \frac{2 \times E_{dis}}{(V_{init}^2 - V_{final}^2)} \tag{5.4}$$

In this case, the turn-on voltage of the high-side switch (V_{init}) is 2.21 V and the lower threshold of the high-side switch (V_{final}) is 1.8 V. E_{dis} can be equated to E_{req}, but ideally should be greater than E_{dis}. From Equation 5.4, we compute value of storage capacitor as 292.68 µF. However, the nearest available capacitor value with low DC leakage is 330 µF (AVX TAJC337K004RNJ), which can facilitate an energy budget of 270.6 µJ. Similarly, we can select the storage capacitor size based on the application's

energy budget. Note that the time required to store energy on the capacitor will depend on the length of electrodes as the instantaneous power would vary with the length of the harvesting electrodes. Figure 5-7 shows the charge time and incoming power for different capacitors size.

Configuration of the Charge Control Circuit

The threshold voltage of the high-side switch is the third design variable which controls the output voltage of this harvester. For sparse sensing applications, the discharge time from V_{init} to V_{final} is a few ms and the average voltage output is around $(V_{init} + V_{final})/2$. For most of the applications, we rely on a high-side switch that has a threshold voltage of 1.8 V and turn on voltage of 2.21 V as it can serve most of the sensing applications unless they require greater than 2 V on an average. For applications which require more than a 2 V input, like sensing environmental parameters or powering a time-lapse camera, we use a high-side switch with a threshold of 3 V and a turn-on voltage of 3.5 V which can provide an average voltage of 3.25 V. For sparse sensing applications which do not have any timing constraints for sensing, we only vary these three design parameters. However, apart from these three design variables, we optionally add a timer (TI TPL5110) controlled MOSFET driver (IRLML6402) for specific applications which require a continuous or event-based power draw. This timer can be programmed to the drive output load in a periodic manner for a known duration, thus facilitating continuous sensing by delivering a small amount of energy after a known time interval.

5.6 Application Space

In order to exhibit the applicability of this capacitive energy harvester, we developed three different applications: appliance state (on/off) monitoring for energy sustainability; sensing environmental parameters like temperature, humidity, and light intensity for indoor vertical farming applications; and distributed temperature sensing inside buildings for HVAC control. Each of these applications requires optimization of

certain design parameters of the CapHarvester in order to facilitate a variable energy budget.

5.6.1 ApplianceTag

ApplianceTag, an exciting application of CapHarvester, allows for non-invasive stick-on appliance state monitoring. It uses an inductive pick-up (Bourns SDR1806-102KL[5]) connected to an ADC (CC1350) to detect appliance state (on/off) using stray magnetic fields present around power cords. This approach to appliance state

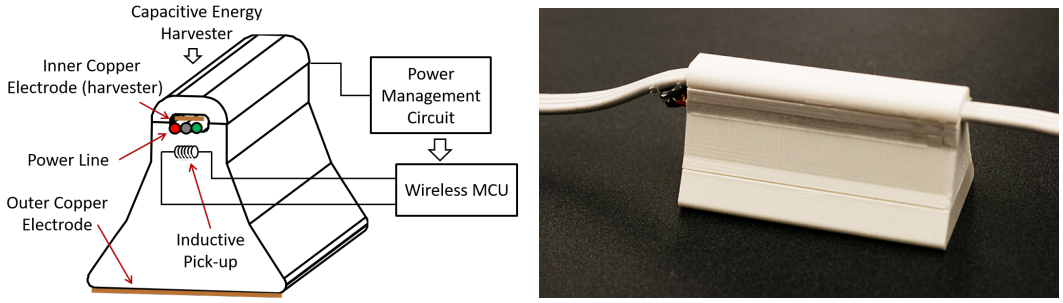

(a) ApplianceTag having inductive pick-up for sensing appliance state (on/off) and capacitive electrodes for energy harvesting

(b) ApplianceTag powered using CapHarvester installed on a power cord for measuring appliance state information

Figure 5-8: Block diagram (left) and actual prototype (right) of ApplianceTag

sensing is based on work by Rowe et al. [152]. Intuitively, as per KCL, one expects the net magnetic field present around multi-wire power cables with phase, neutral and earth wires bundled together to be zero. However, depending on the position of the inductive pick-up around a wire bundle and the bundle's asymmetry, stray magnetic fields, albeit with low SNR, can be sensed. In our application, this is sufficient to detect loads of approximately 500 W. We note that with an appropriate low power amplifier, we can significantly lower this detection threshold.

Key features of the ApplianceTag include:

- Potentially possible to install on any power line with no ohmic connection for appliance state monitoring and for energy harvesting.
- Likely to harvest energy even when appliance is not active or drawing any current.

[5]http://www.bourns.com/docs/Product-Datasheets/SDR1806.pdf

- Does not require a junction box for installation and can go behind walls for infrastructure mediated sensing.

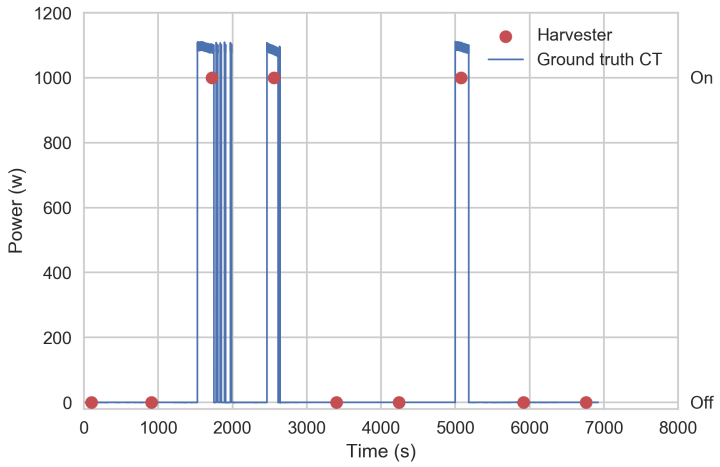

Figure 5-9: Appliance state information (on/off) for a 1 kW hot plate measured using ApplianceTag

Once the storage capacitor reaches a certain threshold (2.21 V in this case), the CC1350 wireless MCU turns on, which is programmed to immediately take 56 ADC samples at a sampling rate of 3.360 kHz. These parameters were chosen to ensure that an entire 60 Hz AC cycle is captured. Next, the signal is de-meaned and the signal energy is computed. This value is transmitted back to a base station over an RF link. A threshold is used to detect the appliance ON/OFF state followed. This application requires an energy budget of 250 µJ, which is facilitated by the use of a 330 µF storage capacitor. In our testing, this resulted in an average duty cycle of 1 transmission every 13 minutes. Figure 5-8a shows the block diagram of ApplianceTag. We tested this scenario by monitoring the state of a 1 kW hot plate, which was manually turned on and off. We compare our data against ground truth data collected using a current transformer (CR3100)[6] for two hours in Figure 5-9.

5.6.2 HeatMap

In this application, distributed temperature across a building is gathered to create an hourly heat map of the building. Most building managers perform temperature

[6]http://www.crmagnetics.com/Assets/ProductPDFs/CR3100.pdf

Figure 5-10: A possible implementation of a temperature monitor deployed on a stud (location E)

logging on an hourly basis for fine grained control of HVAC systems. HVAC, being the most energy-expensive load in any commercial or residential building, requires indoor temperature sensing for an effective scheduling of different zones. This requires putting temperature loggers in each and every zone and as the deployment scales, keeping track of batteries becomes a challenging job. We alleviate this by enabling temperature sensing powered by the capacitive energy harvester connected to power lines that are close to air handling units (AHUs). For this application, we chose a 220 uF storage capacitor which results in an average transmission every 6 min with a standard capacitive electrode (14 cm long with a 4 cm separation between electrodes). Figure-5-10 shows a self-powered temperature monitor installed on a stud.

Figure 5-11 shows the temperature variation logged using an on-chip (TI CC1350) temperature sensor powered via the capacitive harvester along with the ground truth data logged using a high resolution temperature sensor (TI HDC1000[7])

[7]http://www.ti.com/lit/ds/symlink/hdc1000.pdf

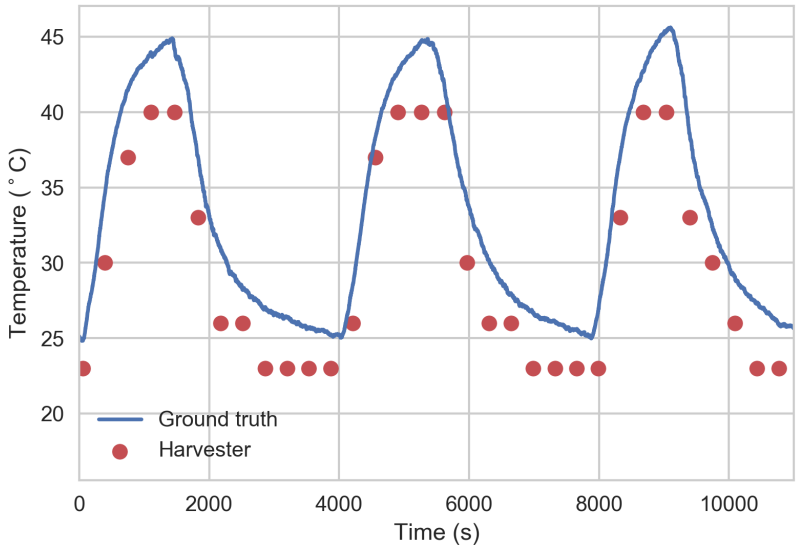

Figure 5-11: Temperature variation logged using on-chip temperature sensor powered using capacitive harvester along with the ground truth data logged using high resolution temperature sensor (TI HDC1000)

5.6.3 FarmCheck

FarmCheck exhibits sensing environmental parameters like temperature, humidity, and light intensity for indoor vertical farming applications. We make use of the TI CC1350 SensorTag[8] platform for this application. SensorTag is a development board that is fitted with ten different ambient sensors including high resolution temperature (TMP007), humidity (HDC1000YPA), and light sensors (OPT3001). In contrast to previous applications, FarmCheck requires the most power and a 3 V power supply for operation. These requirements were met by designing a circuit that employs a high-side switch with a threshold voltage (V_{th}) of 3 V and a 660 µF storage capacitor resulting in being able to produce 1072 µJ. On an average, this results in a RF transmission every 27 minutes. Figure 5-12 shows the temperature, humidity, and light intensity variation for 36 hrs of a kitchen garden.

[8]https://www.mouser.com/publicrelations_ti_cc1350_devkits_2016final/

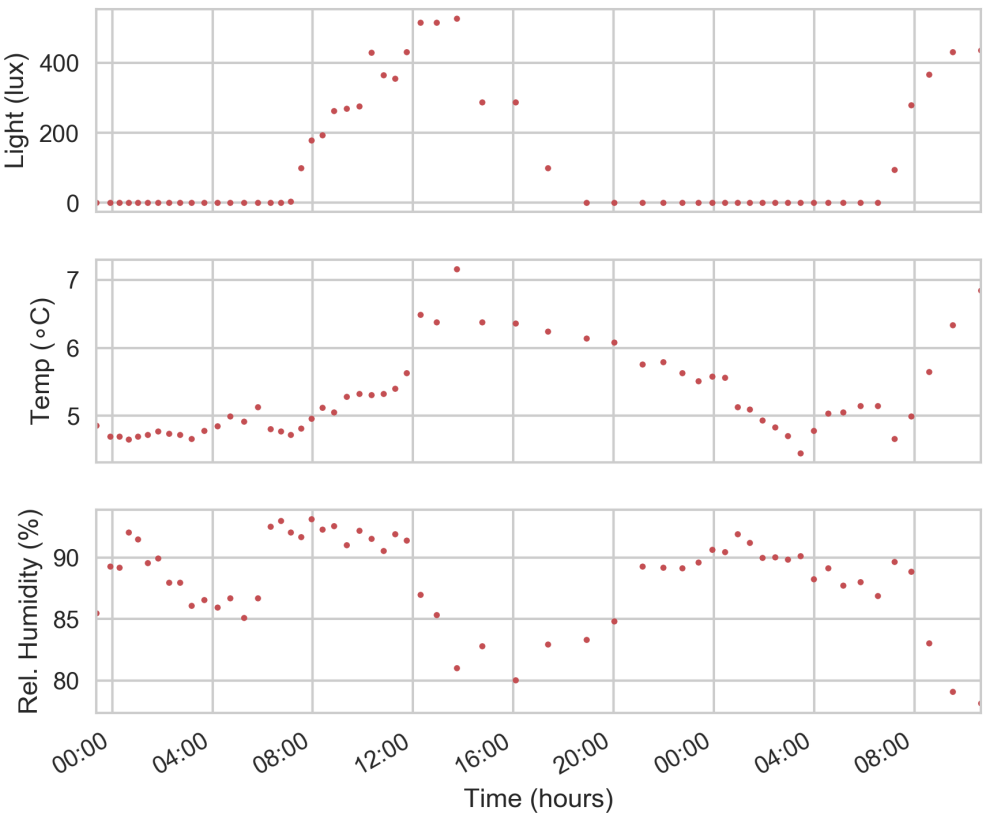

Figure 5-12: Environmental parameters logged by our harvester and wirelessly streamed to a base station over a period of over 36 hours.

5.7 Discussion

Previous capacitive energy harvesters using stray electric fields required a direct (ohmic) connection to earth ground which has severely limited their applications on low voltage AC power lines. In this work [143], we have designed a stick-on capacitive energy harvester that does not require an ohmic connection to earth ground and generates a local reference ground using stacked capacitive electrodes. Our experiments exhibit that our device can harvest 270.6 µJ of energy in 12 min. We also exhibited several applications, such as distributed temperature monitoring, appliance state monitoring, and environmental parameter logging for indoor farming.

- **Study Limitations**: The experiments performed in the residential setting involved environments with variable humidity; the attic, garage, and house had humidities of 63%, 39%, and 30% respectively. We hypothesize that higher humidity increases

the harvesting potential of our system. As an environment becomes more humid, the material of the floor and walls become more wet, which improves their coupling to earth's ground.

Our study was only conducted in the United States. North American AC power lines operate at 110V, while AC power lines in other regions operate at 230V (Asia-Pacific) and 220-240V (Europe). Although we have done all the experiments with 110 V AC power lines, our same electronic design can also be used with 220 V AC power lines since the reverse voltage of the diodes in the rectifier bridge is high enough. Also, the junction capacitance of these diodes supports the range of frequencies available in other countries. If someone wants to use our design for more HV power lines, they need to customize the layout of harvesting electrodes a bit to ensure that voltage output from capacitive harvester along with the available earth ground is enough to sustain the DCL of storage capacitors, i.e.>10-12V. Also, the output of electrodes should be less than the maximum reverse voltage of these diodes. The stray electric field generated on the outer surface of the power line is proportional to the magnitude of the alternating voltage fed through the power line, so the capabilities of this harvester will scale up in regions with AC power lines that have higher voltage ratings.

- **Hardware Limitations**: Our novel capacitive energy harvester relies on the local reference ground generated by the stacked capacitive electrodes and relies weakly on coupling with the earth ground available through nearby metallic or concrete structures. Our harvester under performs in certain scenarios when there is a huge air gap between earth ground and the local reference (outer electrode of harvester). Since air is the worst dielectric possible (ϵ_r=1.0), the gap provides negligible coupling to earth ground and the outer electrode becomes a floating electrode. Our harvester struggles to collect energy in scenarios where power lines are dangling in the air or do not have any surface in contact with them. For example, our harvester is less effective on a table with wooden legs than it is on a shelf with vertical boards.
- **Unexplored Applications**: We outlined three different application categories for our harvester - sparse, continuous, and event-based - but our evaluation focuses

on three different sparse sensing applications. We informally evaluated a continuous sensing application on a breadboard where a timer based MOSFET driver is connected on the output of the high-side switch. The setup included an ADC (MSP430) that was triggered by a timer-based MOSFET driver every 5 minutes. We found that taking each ADC sample and writing it to FRAM consumes 20 µJ of energy. These results to do not translate to real-world applications given the controlled setup and different grounding; however, we were encouraged by these results. Our harvester can collect 270.6 µJ in 12 minutes (across a 330 µF storage capacitor), which is more than enough given our informal results. Hence, we can enable applications which sample data every minute and do delayed transmission by computing the appropriate size of the storage capacitor to do a transmission every 12 or 24 hours. Similarly, we can enable event-based sensing by adding soft constraints on continuous sensing and enable an event-based transmission, such as an occupancy sensor or pressure gauge trigger.

5.8 Conclusion

The increase of smart devices due to the popularity of Internet of Things applications demands devices that can operate without the need for frequent battery maintenance. To support battery-free applications, we made a novel battery-free, stick-on capacitive energy harvester that harvests the stray electric field generated around AC power lines without a reference connection to earth ground. Also, our harvester does not require an active load on the power line, making it more widely applicable and easier and safer to deploy. Our controlled lab measurements and real-world deployments affirmed that our device can harvest 270.6 µJ of energy from a 14 cm long interface in 12 min. We foresee a number of possible applications, ranging from sparse sensing of temperature in houses to event-driven appliance state monitoring. We plan to improve upon our initial designs and make them work in other countries as well. We also look forward to other researchers and engineers doing the same.

Chapter 6

Thesis Conclusion and Future Work

This thesis emphasizes on leveraging stray EMI emissions (conducted and radiated) from appliances and power lines to improve state-of-the-art appliance detection and energy harvesting.

Specific research contributions, their impact and scope for future extensions are discussed below:

1. DM EMI signals, that originates through inductive coupling from switching power supply circuits within appliances, are unreliable feature for appliance detection. The signal is sensed between the phase and neutral power lines and is considerably affected by power line impedance; interference due to filters present inside neighboring appliances connected on the same power line; and power line harmonics. The common mode conducted EMI from appliances, that originate from capacitive coupling, can be sensed through earth wire carrying only leakage signals. Hence these signals are not prone to interference from power line artifacts. Besides this, most appliances are not fitted with common mode chokes because of which the CM EMI signals from multiple appliances do not interfere with each other.

2. We demonstrated a novel sensor capable of simultaneously measurements of DM and CM EMI signals from appliances. Based on our measurements, we found

that the CM EMI is a far more robust feature for appliance detection than DM EMI. CM EMI outperformed DM EMI with higher detection accuracy of 87% in comparison to an accuracy of 45% in the case of DM EMI. In future, simultaneous measurement and fusion of CM conducted EMI data and low-frequency power data from smart meters can yield several new functions such as real-time appliance identification, tracking instances of anomalies in appliance operation, load segregation and fine-grained energy breakdown. As discussed earlier in the thesis, these inferences can facilitate direct energy feedback to all energy stakeholders; cater to data-driven load scheduling and peak load balancing. Further, these inferences can provide insights into daily activities, which can be used for an assisted and improved living for elderly and disabled people.

3. We demonstrated that statistical features derived from time-domain EMI signals are unique signatures which are useful for classifying complex appliances even under considerably challenging scenarios - where the algorithms were trained on data gathered from one appliance instance and used to infer other instances of similar make and model. We achieved good results with a very basic classification algorithm based on nearest neighbors. We believe that further improvement of the classification performance can be achieved when the features are derived from time-frequency representations of the EMI data. Additionally, instead of naive machine learning techniques like nearest neighbor more robust technologies like sparse dictionary learning or deep neural networks (RNN and CNN) can be employed for supervised learning of EMI features and subsequent appliance classification. To facilitate future research using conducted EMI signals, we have released two data sets (HFED and ComBED) in the open-source community.

4. Through the development and deployment of a custom sensor, we demonstrated the effectiveness of radiated EMI for appliance detection. We showed that these signals are detectable up to an approximate range of 30 cm for commonly found

appliances such as laptop chargers and desktop CPUs. RFI based appliance detection could be a key enabling technology for applications such as PEA. PEA is critical in shared spaces having multiple stakeholders typically having ill utilization of resources. It is not far from reality, when we will see a person operating appliances in a shared kitchen or living room and all those appliances with their corresponding electricity usage will be assigned to that person. All this can be made possible with a wearable band having RFI sensors, which can tag appliance activity to the end-users. Some follow-up work already exists in literature which leveraged insight from our initial study with RFI signals to design a near-field wearable sensor specifically for PEA.

5. We demonstrated a novel ultra-low power non-intrusive capacitive circuit (CapHarvest) for continuously harvesting energy using stray electric field signals, of the order of a few nano-watts, from ubiquitous AC power lines. Our circuit handled all the challenges associated with prior techniques associated with energy harvesting from stray fields like finding an earth ground for electric field harvesting or requiring bulky transformers for capturing stray magnetic fields.

6. The CapHarvest circuit demonstrated a nice blend of sensing and harvesting with two sample applications. First is Appliance Tag - a stick-on sensing system for detecting appliance states and second is Farm Check, which monitors ambient parameters for indoor farming applications. Future possibilities around this fusion of simultaneous sensing and harvesting are numerous. For example, applications like active beaconing using tags placed inside walls for indoor localization; powering ambient sensor nodes placed during construction for HVAC control; anomaly detection in appliances and other similar energy sustainability applications. Apart from this, energy harvested from outdoor AC power lines can enable traffic monitoring and time-lapse cameras. CapHarvest can also facilitate event-based sensing applications like pressure valve or thermostat failure notifications, which rarely occur and require a significant chunk of energy for communication. These applications are just some samples that we envisioned in

this thesis. However, the work carried out as part of this thesis can enable many more such exciting applications, which we leave up to the research community to explore.

Chapter 7

List of Publications

All the publications (first author) accepted during the course of this thesis dissertation are listed in reverse chronological order below.

2018

- Gulati, M., Parizi, F. S., Whitmire, E., Gupta, S., Ram, S. S., Singh, A., & Patel, S. N. (2018). **CapHarvester: A stick-on capacitive energy harvester using stray electric field from AC power lines**. Proceedings of the ACM on Interactive, Mobile, Wearable and Ubiquitous Technologies (ACM IMWUT), 2(3), 1-20 [143].

2016

- Gulati, M., Ram, S. S., Majumdar, A., & Singh, A. (2016). **Single point conducted EMI sensor with intelligent inference for detecting IT appliances.** IEEE Transactions on Smart Grid, 9(4), 3716-3726 [106].
- Gulati, M., Singh, V. K., Agarwal, S. K., & Bohara, V. A. (2016). **Appliance activity recognition using radio frequency interference emissions.** IEEE Sensors Journal, 16(16), 6197-6204 [128].
- Gulati, M., Ram, S. S., Majumdar, A., & Singh, A. (2016, May). **Detecting IT and lighting loads using common-mode conducted EMI signals.** In Proceedings of 3rd International Workshop on Non-Intrusive Load Monitoring (NILMW) (p. 5) [92].

2014

- Gulati, M., Ram, S. S., & Singh, A. (2014, November). An in depth study into using EMI signatures for appliance identification. In Proceedings of the 1st ACM Conference on Embedded Systems for Energy-efficient Buildings (pp. 70-79) [103].

Other Publications (Non-first Author)

- Bhattacharjee, P., Banerjee, S., Gulati, M., Majumdar, A., & Ram, S. S. (2017, March). **Supervised analysis dictionary learning: application in consumer electronics appliance classification.** In Proceedings of the Fourth ACM IKDD Conferences on Data Sciences (pp. 1-10) [153].
- Arjunan, P., Saha, M., Choi, H., Gulati, M., Singh, A., Singh, P., & Srivastava, M. B. (2015, August). **SensorAct: a decentralized and scriptable middleware for smart energy buildings.** In 2015 IEEE 12th Intl Conf on Ubiquitous Intelligence and Computing (UIC) (pp. 11-19). IEEE [154].
- Batra, N., Gulati, M., Singh, A., & Srivastava, M. B. (2013, November). **It's Different: Insights into home energy consumption in India.** In Proceedings of the 5th ACM Workshop on Embedded Systems For Energy-Efficient Buildings (pp. 1-8) [85].

Poster Publications

- Arjunan, P., Saha, M., Gulati, M., Batra, N., Singh, A., & Singh, P. (2013). Sensoract: Design and implementation of fine-grained sensing and control sharing in buildings. In the poster track of 10th USENIX Symposium on Networked Systems Design and Implementation (NSDI'13) [155].
- Batra, N., Gulati, M., Jain, P., Whitehouse, K., & Singh, A. (2014, November). Bits and Watts: Improving energy disaggregation performance using power line communication modems. In Proceedings of the 1st ACM Conference on Embedded Systems for Energy-Efficient Buildings (pp. 210-211) [87].

Bibliography

[1] Tutorials-Point. Electronic circuits smps. `http://www.tutorialspoint.com/electronic_circuits/electronic_circuits_smps.htm`, 2017 [Date accessed: 12.12.2018].

[2] Electronic-Environment. A review of the principal emi coupling paths. `https://www.electronic.nu/2015/12/08/a-review-of-the-principal-emi-coupling-paths-the-key-to-understanding-and-preventing-or-solving-emi-problems/`, 2015 [Date accessed: 15.12.2018].

[3] Clayton R Paul. *Introduction to electromagnetic compatibility*, volume 184. John Wiley & Sons, 2006.

[4] Norman Violette. *Electromagnetic compatibility handbook*. Springer, 2013.

[5] Christophe Basso. *Switch-mode power supplies spice simulations and practical designs*. McGraw-Hill, Inc., 2008.

[6] Shwetak N. Patel. `https://www.ece.uw.edu/colloquia/your-noise-is-my-signal/`, 2019 [Date accessed: 14.09.2019].

[7] George William Hart. Nonintrusive appliance load monitoring. *Proceedings of the IEEE*, 80(12):1870–1891, 1992.

[8] Michael Zeifman, Craig Akers, and Kurt Roth. Nonintrusive appliance load monitoring (nialm) for energy control in residential buildings: Review and outlook. In *IEEE transactions on Consumer Electronics*. Citeseer, 2011.

[9] Sidhant Gupta. *ElectriSense: Single-Point Sensing Using EMI for Electrical Event Detection and Classification in the Home*. PhD thesis, 2014.

[10] Sarah Darby et al. The effectiveness of feedback on energy consumption. *A Review for DEFRA of the Literature on Metering, Billing and direct Displays*, 486(2006):26, 2006.

[11] Sidhant Gupta, Matthew S Reynolds, and Shwetak N Patel. Electrisense: single-point sensing using emi for electrical event detection and classification in the home. In *Proceedings of the 12th ACM international conference on Ubiquitous computing*, pages 139–148. ACM, 2010.

[12] Ahmed Zoha, Alexander Gluhak, Muhammad Ali Imran, and Sutharshan Rajasegarar. Non-intrusive load monitoring approaches for disaggregated energy sensing: A survey. *Sensors*, 12(12):16838–16866, 2012.

[13] Sean Barker, Sandeep Kalra, David Irwin, and Prashant Shenoy. Empirical characterization and modeling of electrical loads in smart homes. In *Green Computing Conference (IGCC), 2013 International*, pages 1–10. IEEE, 2013.

[14] Niraniini Rajagopal, Suman Giri, Mario Berges, and Anthony Rowe. A magnetic field-based appliance metering system. In *2013 ACM/IEEE International Conference on Cyber-Physical Systems (ICCPS)*, pages 229–238. IEEE, 2013.

[15] Suman Giri and Mario Berges. Virtual metering of electrical appliances through analysis of data from contactless sensing. In *2015 IEEE Global Conference on Signal and Information Processing (GlobalSIP)*, pages 348–352. IEEE, 2015.

[16] Suman Giri and MA Berges. Study on the feasibility of automated data labeling and training using an emf sensor in nilm platforms. In *Proceedings of the 2012 International EG-ICE Workshop on Intelligent Computing, Munich, Germany*, volume 46, 2012.

[17] Suman Giri, Mario Bergés, and Anthony Rowe. Towards automated appliance recognition using an emf sensor in nilm platforms. *Advanced Engineering Informatics*, 27(4):477–485, 2013.

[18] Matias Quintana, Henning Lange, and Mario Bergés. Design and implementation of a low-cost arduino-based high-frequency ac waveform meter board for the raspberry pi. In *Proceedings of the 4th acm international conference on systems for energy-efficient built environments*, pages 1–2, 2017.

[19] T Kriechbaumer, AU Haq, M Kahl, and HA Jacobsen. Towards a cost-effective high-frequency energy data acquisition system for electric appliances-google search. In *International Workshop on Non-Intrusive Load Monitoring*, 2016.

[20] Thomas Kriechbaumer, Anwar Ul Haq, Matthias Kahl, and Hans-Arno Jacobsen. Medal: A cost-effective high-frequency energy data acquisition system for electrical appliances. In *Proceedings of the eighth international conference on future energy systems*, pages 216–221, 2017.

[21] Anwar Ul Haq, Thomas Kriechbaumer, Matthias Kahl, and Hans-Arno Jacobsen. Clear—a circuit level electric appliance radar for the electric cabinet. In *2017 IEEE International Conference on Industrial Technology (ICIT)*, pages 1130–1135. IEEE, 2017.

[22] Jingkun Gao, Suman Giri, Emre Can Kara, and Mario Bergés. Plaid: a public dataset of high-resoultion electrical appliance measurements for load identification research: demo abstract. In *proceedings of the 1st ACM Conference on Embedded Systems for Energy-Efficient Buildings*, pages 198–199, 2014.

[23] Roberto Medico, Leen De Baets, Jingkun Gao, Suman Giri, Emre Kara, Tom Dhaene, Chris Develder, Mario Bergés, and Dirk Deschrijver. A voltage and current measurement dataset for plug load appliance identification in households. *Scientific Data*, 7(1):1–10, 2020.

[24] Matthias Kahl, Christoph Goebel, Anwar Ul Haq, Thomas Kriechbaumer, and Hans-Arno Jacobsen. Nofare: A non-intrusive facility resource monitoring system. In *DA-CH Conference on Energy Informatics*, pages 59–68. Springer, 2015.

[25] Simon Henriet, Umut Simsekli, Gaël Richard, and Benoit Fuentes. Synthetic dataset generation for non-intrusive load monitoring in commercial buildings. In *Proceedings of the 4th ACM International Conference on Systems for Energy-Efficient Built Environments*, pages 1–2, 2017.

[26] Simon Henriet, Umut Şimşekli, Benoit Fuentes, and Gaël Richard. A generative model for non-intrusive load monitoring in commercial buildings. *Energy and Buildings*, 177:268–278, 2018.

[27] Simon Henriet, Umut Simsekli, Gaël Richard, and Benoit Fuentes. Energy disaggregation for commercial buildings: A statistical analysis. In *», International Workshop on Non-Intrusive Load Monitoring (NILM2018)*, 2018.

[28] Nipun Batra, Oliver Parson, Mario Berges, Amarjeet Singh, and Alex Rogers. A comparison of non-intrusive load monitoring methods for commercial and residential buildings. *arXiv preprint arXiv:1408.6595*, 2014.

[29] June Young Park, Xiya Yang, Clayton Miller, Pandarasamy Arjunan, and Zoltan Nagy. Apples or oranges? identification of fundamental load shape profiles for benchmarking buildings using a large and diverse dataset. *Applied energy*, 236:1280–1295, 2019.

[30] Matias Quintana, Pandarasamy Arjunan, and Clayton Miller. Islands of misfit buildings: Detecting uncharacteristic electricity use behavior using load shape clustering. Springer.

[31] Matthias Kahl, Anwar Ul Haq, Thomas Kriechbaumer, and Hans-Arno Jacobsen. Whited-a worldwide household and industry transient energy data set. In *3rd International Workshop on Non-Intrusive Load Monitoring*, 2016.

[32] Matthias Kahl, Veronika Krause, Rudolph Hackenberg, Anwar Ul Haq, Anton Horn, Hans-Arno Jacobsen, Thomas Kriechbaumer, Michael Petzenhauser, Mikhail Shamonin, and Anton Udalzow. Measurement system and dataset for in-depth analysis of appliance energy consumption in industrial environment. *tm-Technisches Messen*, 86(1):1–13, 2019.

[33] Thomas Picon, Mohamed Nait Meziane, Philippe Ravier, Guy Lamarque, Clarisse Novello, Jean-Charles Le Bunetel, and Yves Raingeaud. Cooll: Controlled on/off loads library, a public dataset of high-sampled electrical signals for appliance identification. *arXiv preprint arXiv:1611.05803*, 2016.

[34] J Zico Kolter and Matthew J Johnson. Redd: A public data set for energy disaggregation research. In *Workshop on Data Mining Applications in Sustainability (SIGKDD), San Diego, CA*, volume 25, pages 59–62. Citeseer, 2011.

[35] Adrian Filip et al. Blued: A fully labeled public dataset for event-based nonintrusive load monitoring research. In *2nd Workshop on Data Mining Applications in Sustainability (SustKDD)*, page 2012, 2011.

[36] Jack Kelly and William Knottenbelt. The uk-dale dataset, domestic appliance-level electricity demand and whole-house demand from five uk homes. *Scientific data*, 2(1):1–14, 2015.

[37] Douglas Renaux, Robson Linhares, Fabiana Pottker, Andre Lazzaretti, Carlos Lima, Adil Coelho Neto, and Mateus Campaner. Designing a novel dataset for non-intrusive load monitoring. In *2018 VIII Brazilian Symposium on Computing Systems Engineering (SBESC)*, pages 243–249. IEEE, 2018.

[38] Suman Giri and Mario Bergés. An energy estimation framework for event-based methods in non-intrusive load monitoring. *Energy Conversion and Management*, 90:488–498, 2015.

[39] Suman Giri and Mario Bergés. Towards automatic classification of appliances: Tackling cross talk in emf sensors using blind source separation techniques.

[40] Suman Giri and Mario Bergés. An error correction framework for sequences resulting from known state-transition models in non-intrusive load monitoring. *Advanced Engineering Informatics*, 32:152–162, 2017.

[41] Henning Lange and Mario Bergés. Bolt: Energy disaggregation by online binary matrix factorization of current waveforms. In *Proceedings of the 3rd ACM International Conference on Systems for Energy-Efficient Built Environments*, pages 11–20, 2016.

[42] Henning Lange, Mario Bergés, and Zico Kolter. Neural variational identification and filtering for stochastic non-linear dynamical systems with application to non-intrusive load monitoring. In *ICASSP 2019-2019 IEEE International Conference on Acoustics, Speech and Signal Processing (ICASSP)*, pages 8340–8344. IEEE, 2019.

[43] Bingqing Chen, Jingxiao Liu, Henning Lange, and Mario Bergés. Dyna-bolt: Domain adaptive binary factorization of current waveforms for energy disaggregation. In *ICASSP 2020-2020 IEEE International Conference on Acoustics, Speech and Signal Processing (ICASSP)*, pages 3262–3266. IEEE, 2020.

[44] Matthias Kahl, Anwar Ul Haq, Thomas Kriechbaumer, and Hans-Arno Jacobsen. A comprehensive feature study for appliance recognition on high frequency energy data. In *Proceedings of the Eighth International Conference on Future Energy Systems*, pages 121–131, 2017.

[45] Matthias Kahl, Thomas Kriechbaumer, Anwar Ul Haq, and Hans-Arno Jacobsen. Appliance classification across multiple high frequency energy datasets. In *2017 IEEE International Conference on Smart Grid Communications (SmartGridComm)*, pages 147–152. IEEE, 2017.

[46] Daniel Jorde, Matthias Kahl, and Hans-Arno Jacobsen. Meed: An unsupervised multi-environment event detector for non-intrusive load monitoring. In *2019 IEEE International Conference on Communications, Control, and Computing Technologies for Smart Grids (SmartGridComm)*, pages 1–6. IEEE, 2019.

[47] Matthias Kahl, Thomas Kriechbaumer, Daniel Jorde, Anwar Ul Haq, and Hans-Arno Jacobsen. Appliance event detection-a multivariate, supervised classification approach. In *Proceedings of the Tenth ACM International Conference on Future Energy Systems*, pages 373–375, 2019.

[48] Simon Henriet, Umut Simsekli, Sérgio Santos, Benoît Fuentes, and Gael Richard. Factorisation matricielle semi non-négative: Applicationà la décomposition de consommations electriques. In *Colloque francophonede traitement du signal et des images (GRETSI)*, 2019.

[49] Simon Henriet, Umut Şimşekli, Sergio Dos Santos, Benoît Fuentes, and Gael Richard. Independent-variation matrix factorization with application to energy disaggregation. *IEEE Signal Processing Letters*, 26(11):1643–1647, 2019.

[50] Amy Cortese, Cathy Higgins, and Mark Lyles. Getting to zero: The 2014 net zero energy status report findings for commercial buildings. `https://www.aceee.org/files/proceedings/2014/data/papers/5-1224.pdf`, 2020 [Date accessed: 22.07.2020].

[51] U.S. Energy Information Administration. Commercial buildings energy consumption survey, 2003. `https://www.eia.gov/consumption/commercial/data/2003/index.php?view=microdata`, 2020 [Date accessed: 22.07.2020].

[52] Shwetak N Patel, Thomas Robertson, Julie A Kientz, Matthew S Reynolds, and Gregory D Abowd. At the flick of a switch: Detecting and classifying unique electrical events on the residential power line (nominated for the best paper award). In *International Conference on Ubiquitous Computing*, pages 271–288. Springer, 2007.

[53] Ming Dong, Paulo CM Meira, Wilsun Xu, and Walmir Freitas. An event window based load monitoring technique for smart meters. *IEEE transactions on smart grid*, 3(2):787–796, 2012.

[54] Dawei He, Liang Du, Yi Yang, Ronald Harley, and Thomas Habetler. Front-end electronic circuit topology analysis for model-driven classification and monitoring of appliance loads in smart buildings. *IEEE Transactions on Smart Grid*, 3(4):2286–2293, 2012.

[55] Jon Froehlich, Eric Larson, Sidhant Gupta, Gabe Cohn, Matthew Reynolds, and Shwetak Patel. Disaggregated end-use energy sensing for the smart grid. *IEEE Pervasive Computing*, 10(1):28–39, 2011.

[56] Jessie M Gillis, Sami M Alshareef, and Walid G Morsi. Nonintrusive load monitoring using wavelet design and machine learning. *IEEE Transactions on Smart Grid*, 7(1):320–328, 2016.

[57] Anand Sunil Kulkarni, Cindy K Harnett, and Karla Conn Welch. Emf signature for appliance classification. *IEEE Sensors Journal*, 15(6):3573–3581, 2015.

[58] Gierad Laput, Chouchang Yang, Robert Xiao, Alanson Sample, and Chris Harrison. Em-sense: Touch recognition of uninstrumented, electrical and electromechanical objects. In *Proceedings of the 28th Annual ACM Symposium on User Interface Software & Technology*, pages 157–166. ACM, 2015.

[59] Edward J Wang, Tien-Jui Lee, Alex Mariakakis, Mayank Goel, Sidhant Gupta, and Shwetak N Patel. Magnifisense: Inferring device interaction using wrist-worn passive magneto-inductive sensors. In *Proceedings of the 2015 ACM International Joint Conference on Pervasive and Ubiquitous Computing*, pages 15–26. ACM, 2015.

[60] Navneet Soin. Magnetic nanoparticles-piezoelectric polymer nanocomposites for energy harvesting. In *Magnetic Nanostructured Materials*, pages 295–322. Elsevier, 2018.

[61] Vikram Gupta, Arvind Kandhalu, and Ragunathan Raj Rajkumar. Energy harvesting from electromagnetic energy radiating from ac power lines. In *Proceedings of the 6th Workshop on Hot Topics in Embedded Networked Sensors*, page 17. ACM, 2010.

[62] Samuel DeBruin, Bradford Campbell, and Prabal Dutta. Monjolo: An energy-harvesting energy meter architecture. In *Proceedings of the 11th ACM Conference on Embedded Networked Sensor Systems*, page 18. ACM, 2013.

[63] Bradford Campbell and Prabal Dutta. Gemini: A non-invasive, energy-harvesting true power meter. In *Real-Time Systems Symposium (RTSS), 2014 IEEE*, pages 324–333. IEEE, 2014.

[64] Hoseong Kim, Dongkil Choi, Sungmin Gong, and Kyungjin Park. Stray electric field energy harvesting technology using mems switch from insulated ac power lines. *Electronics letters*, 50(17):1236–1238, 2014.

[65] Keun-Su Chang, Sung-Muk Kang, Kyung-Jin Park, Seung-Hwan Shin, Hyeong-Seok Kim, and Ho-Seong Kim. Electric field energy harvesting powered wireless sensors for smart grid. *Journal of Electrical Engineering and Technology*, 7(1):75–80, 2012.

[66] What is electromagnetic interference? `https://www.sunpower-uk.com/glossary/whait-is-electromagnetic-interference/`, 2019 [Date accessed: 14.09.2019].

[67] V Prasad Kodali and V Prasad. *Engineering electromagnetic compatibility: principles, measurements, technologies, and computer models*. IEEE, 2001.

[68] Emi in power supplies. `https://www.fairchildsemi.com/technical-articles/Electromagnetic-Interference-EMI-in-Power-Supplies.pdf`.

[69] IECA. Smps design guide. `http://www.ieca-inc.com/images/smps_design_guide.pdf`, 2005 [Date accessed: 12.12.2018].

[70] Microchip. Smps ac/dc reference design user's guide. `http://ww1.microchip.com/downloads/en/devicedoc/70320a.pdf`, 2008 [Date accessed: 12.12.2018].

[71] ON-Semiconductor. Smps reference manual. `https://www.onsemi.com/pub/Collateral/SMPSRM-D.PDF`, 2014 [Date accessed: 12.12.2018].

[72] Electronics-notes. Electromagnetic interference (emi) in power supplies. `https://www.electronics-notes.com/articles/analogue_circuits/emc-emi-electromagnetic-interference-compatibility/what-is-emi-basics-tutorial.php`, 2006 [Date accessed: 15.12.2018].

[73] Electronic-design. Understanding common-mode and differential-mode interference. `https://www.electronicdesign.com/communications/understanding-common-mode-and-differential-mode-interference`, 2009 [Date accessed: 15.12.2018].

[74] Hassan Farhangi. The path of the smart grid. *IEEE power and energy magazine*, 8(1), 2010.

[75] Steven B Leeb, Steven R Shaw, and James L Kirtley. Transient event detection in spectral envelope estimates for nonintrusive load monitoring. *IEEE Transactions on Power Delivery*, 10(3):1200–1210, 1995.

[76] Miro Enev, Sidhant Gupta, Tadayoshi Kohno, and Shwetak N Patel. Televisions, video privacy, and powerline electromagnetic interference. In *Proceedings of the 18th ACM conference on Computer and communications security*, pages 537–550. ACM, 2011.

[77] Michael J Russell, Consulting Electrical Engineer, and P PowerLines. The impact of mains impedance on power quality. In *Power Quality*, 2000.

[78] B Sisson and C Van Aerschot. Energy efficiency in buildings: Business realities and opportunities; summary report. *World Business Council Sustainable Development (WBCSD)*, 2007.

[79] IEA. Etechnology roadmap energy-efficient buildings: Heating and cooling equipment. 2011.

[80] Luis Pérez-Lombard, José Ortiz, and Christine Pout. A review on buildings energy consumption information. *Energy and buildings*, 40(3):394–398, 2008.

[81] Yuvraj Agarwal, Bharathan Balaji, Seemanta Dutta, Rajesh K Gupta, and Thomas Weng. Duty-cycling buildings aggressively: The next frontier in hvac control. In *Information Processing in Sensor Networks (IPSN), 2011 10th International Conference on*, pages 246–257. IEEE, 2011.

[82] Milan Jain, Amarjeet Singh, and Vikas Chandan. Non-intrusive estimation and prediction of residential ac energy consumption. In *2016 IEEE International Conference on Pervasive Computing and Communications (PerCom)*, pages 1–9. IEEE, 2016.

[83] OT Masoso and Louis Johannes Grobler. The dark side of occupants' behaviour on building energy use. *Energy and buildings*, 42(2):173–177, 2010.

[84] Zhenyu Wang and Guilin Zheng. Residential appliances identification and monitoring by a nonintrusive method. *IEEE transactions on Smart Grid*, 3(1):80–92, 2012.

[85] Nipun Batra, Manoj Gulati, Amarjeet Singh, and Mani B Srivastava. It's different: Insights into home energy consumption in india. In *Proceedings of the 5th ACM Workshop on Embedded Systems For Energy-Efficient Buildings*, pages 1–8. ACM, 2013.

[86] Nipun Batra, Jack Kelly, Oliver Parson, Haimonti Dutta, William Knottenbelt, Alex Rogers, Amarjeet Singh, and Mani Srivastava. Nilmtk: an open source toolkit for non-intrusive load monitoring. In *Proceedings of the 5th international conference on Future energy systems*, pages 265–276. ACM, 2014.

[87] Nipun Batra, Manoj Gulati, Puneet Jain, Kamin Whitehouse, and Amarjeet Singh. Bits and watts: improving energy disaggregation performance using power line communication modems: poster abstract. In *Proceedings of the 1st ACM Conference on Embedded Systems for Energy-Efficient Buildings*, pages 210–211. ACM, 2014.

[88] Taha Hassan, Fahad Javed, and Naveed Arshad. An empirical investigation of vi trajectory based load signatures for non-intrusive load monitoring. *IEEE Transactions on Smart Grid*, 5(2):870–878, 2014.

[89] Shane S Clark, Hossen Mustafa, Benjamin Ransford, Jacob Sorber, Kevin Fu, and Wenyuan Xu. Current events: Identifying webpages by tapping the electrical outlet. In *European Symposium on Research in Computer Security*, pages 700–717. Springer, 2013.

[90] Ke-Yu Chen, Gabe A Cohn, Sidhant Gupta, and Shwetak N Patel. utouch: sensing touch gestures on unmodified lcds. In *Proceedings of the SIGCHI Conference on Human Factors in Computing Systems*, pages 2581–2584. ACM, 2013.

[91] Gabe Cohn, Daniel Morris, Shwetak N Patel, and Desney S Tan. Your noise is my command: sensing gestures using the body as an antenna. In *Proceedings of the SIGCHI Conference on Human Factors in Computing Systems*, pages 791–800. ACM, 2011.

[92] Manoj Gulati, Shobha Sundar Ram, Angshul Majumdar, and Amarjeet Singh. Detecting it and lighting loads using common-mode conducted emi signals. In *Proc. NILM2016 3rd International Workshop on Non-Intrusive Load Monitoring*, page 5, 2016.

[93] Theodore Wilbur Anderson. *The statistical analysis of time series*, volume 19. John Wiley & Sons, 2011.

[94] Fluke. Ground impedance. `https://support.fluke.com/find-sales/Download/Asset/2633834_6115_ENG_A_W.PDF`, 2016 [Date accessed: 19.12.2018].

[95] NEC. `http://fyi.uwex.edu/mrec/files/2011/04/W4.-Biesterveld-NEC-grounding-MREC2010.pdf`, 2016 [Date accessed: 19.12.2018].

[96] Dawei He, Weixuan Lin, Nan Liu, Ronald G Harley, and Thomas G Habetler. Incorporating non-intrusive load monitoring into building level demand response. *IEEE Transactions on Smart Grid*, 4(4):1870–1877, 2013.

[97] Miyuru Dayarathna, Yonggang Wen, and Rui Fan. Data center energy consumption modeling: A survey. *IEEE Communications Surveys & Tutorials*, 18(1):732–794, 2015.

[98] Faraz Ahmad and TN Vijaykumar. Joint optimization of idle and cooling power in data centers while maintaining response time. *ACM Sigplan Notices*, 45(3):243–256, 2010.

[99] Lei Rao, Xue Liu, Le Xie, and Wenyu Liu. Minimizing electricity cost: optimization of distributed internet data centers in a multi-electricity-market environment. In *2010 Proceedings IEEE INFOCOM*, pages 1–9. IEEE, 2010.

[100] Rachel Kalaimani, Milan Jain, Srinivasan Keshav, and Catherine Rosenberg. On the interaction between personal comfort systems and centralized hvac systems in office buildings. *Advances in Building Energy Research*, 14(1):129–157, 2020.

[101] Milan Jain, Amarjeet Singh, and Vikas Chandan. Portable+ a ubiquitous and smart way towards comfortable energy savings. *Proceedings of the ACM on Interactive, Mobile, Wearable and Ubiquitous Technologies*, 1(2):1–22, 2017.

[102] Milan Jain and Amarjeet Singh. *PACMAN: predicting AC consumption minimizing Aggregate eNergy consumption.* PhD thesis, IIIT Delhi, 2014.

[103] Manoj Gulati, Shobha Sundar Ram, and Amarjeet Singh. An in depth study into using emi signatures for appliance identification. In *Proceedings of the 1st ACM Conference on Embedded Systems for Energy-Efficient Buildings*, pages 70–79. ACM, 2014.

[104] TDK. All about emi filters. `https://us.tdk-lambda.com/ftp/other/all_about_emi_epmag.pdf`, 2016 [Date accessed: 19.12.2018].

[105] Ke-Yu Chen, Sidhant Gupta, Eric C Larson, and Shwetak Patel. Dose: Detecting user-driven operating states of electronic devices from a single sensing point. In *Pervasive Computing and Communications (PerCom), 2015 IEEE International Conference on*, pages 46–54. IEEE, 2015.

[106] Manoj Gulati, Shobha Sundar Ram, Angshul Majumdar, and Amarjeet Singh. Single point conducted emi sensor with intelligent inference for detecting it appliances. *IEEE Transactions on Smart Grid*, 9(4):3716–3726, 2018.

[107] Clive Seligman and John M Darley. Feedback as a means of decreasing residential energy consumption. *Journal of Applied Psychology*, 62(4):363, 1977.

[108] Michal Aharon, Michael Elad, Alfred Bruckstein, et al. K-svd: An algorithm for designing overcomplete dictionaries for sparse representation. *IEEE Transactions on signal processing*, 54(11):4311, 2006.

[109] Julien Mairal, Jean Ponce, Guillermo Sapiro, Andrew Zisserman, and Francis R Bach. Supervised dictionary learning. In *Advances in neural information processing systems*, pages 1033–1040, 2009.

[110] Mario Berges, Ethan Goldman, H Scott Matthews, and Lucio Soibelman. Training load monitoring algorithms on highly sub-metered home electricity consumption data. *Tsinghua Science and Technology*, 13(S1):406–411, 2008.

[111] Younghun Kim, Thomas Schmid, Zainul M Charbiwala, and Mani B Srivastava. Viridiscope: design and implementation of a fine grained power monitoring system for homes. In *Proceedings of the 11th international conference on Ubiquitous computing*, pages 245–254. ACM, 2009.

[112] Z Cihan Taysi, M Amac Guvensan, and Tommaso Melodia. Tinyears: spying on house appliances with audio sensor nodes. In *Proceedings of the 2nd ACM Workshop on Embedded Sensing Systems for Energy-Efficiency in Building*, pages 31–36. ACM, 2010.

[113] Bernd W Jaekel, Ana Mladenovic, Mirjana Peric, Dusan Vuckovic, Nenad Cvetkovic, and Slavoljub Aleksic. Assessment of emissions from electrical equipment regarding human exposure-approaches for application of the generic standard iec 62311. In *Electromagnetic Compatibility (EMC), 2010 IEEE International Symposium on*, pages 697–701. IEEE, 2010.

[114] Iman Morsi and Hassan Elkamchouchi. Noise field measurements for safety use of environmental electronic and electrical equipment. In *Innovations in Information Technology, 2007. IIT'07. 4th International Conference on*, pages 621–625. IEEE, 2007.

[115] Michel Mardiguian. Generalities on radiated interference. In *Controlling Radiated Emissions by Design*, pages 1–15. Springer, 2014.

[116] Kapil Gulati. *Radio frequency interference modeling and mitigation in wireless receivers*. PhD thesis, 2011.

[117] Ammar Ahmed Alkahtani, Farah Hani Nordin, ZAM Sharrif, Nur Badariah Bte, and Ahmad Mustafa. Analysis on rf emission of electrical appliances. In *Control System, Computing and Engineering (ICCSCE), 2012 IEEE International Conference on*, pages 539–543. IEEE, 2012.

[118] Zoltan Kvasznicza and Gyorgy Elmer. Radio frequency emissions of public lighting devices. In *Power Electronics and Motion Control Conference, 2006. EPE-PEMC 2006. 12th International*, pages 1340–1344. IEEE, 2006.

[119] RJ Schwabe, S Zelingher, T Key, and K Phipps. Interference between electronic lighting and other appliances. In *Industry Applications Conference, 1995. Thirtieth IAS Annual Meeting, IAS'95., Conference Record of the 1995 IEEE*, volume 3, pages 2076–2082. IEEE, 1995.

[120] Sabih Güzelgöz, Hasan B Çelebi, Tayyar Güzel, Hüseyin Arslan, and M Kivanç Mihçak. Time frequency analysis of noise generated by electrical loads in plc. In *Telecommunications (ICT), 2010 IEEE 17th International Conference on*, pages 864–871. IEEE, 2010.

[121] Jonathan Ryan Wilkerson and Frederick Vosburgh. Methods and devices for reducing radio frequency interference, March 4 2014. US Patent 8,666,347.

[122] S Shihab and KL Wong. Detection of faulty components on power lines using radio frequency signatures and signal processing techniques. In *Power Engineering Society Winter Meeting, 2000. IEEE*, volume 4, pages 2449–2452. IEEE, 2000.

[123] Valerio De Santis, Pierre A Beeckman, Domenico Alessandro Lampasi, and Mauro Feliziani. Assessment of human body impedance for safety requirements against contact currents for frequencies up to 110 mhz. *IEEE Transactions on Biomedical Engineering*, 58(2):390–396, 2011.

[124] Sevda Soker, Cemil Sert, Mustafa Deniz, Isl Tekmen, Murat Akkus, Yusuf Nergiz, S SOKER, C SERT, M DENIZ, I TEKMEN, et al. The effects of electromagnetic fields on the ultrastructure of heart. *Int. J. Morphol*, 29(3):960–964, 2011.

[125] Yuanyuan Sun, Li Wang, and Zhiming Yin. Research on detrimental effects of the using of home electrical appliances to the human beings. In *Electric Utility Deregulation and Restructuring and Power Technologies (DRPT), 2011 4th International Conference on*, pages 577–582. IEEE, 2011.

[126] Md Abdul Hannan and Kamran Arshad. An experimental study of interference in smart buildings. In *Communications, Signal Processing, and their Applications (ICCSPA), 2013 1st International Conference on*, pages 1–5. IEEE, 2013.

[127] Chouchang Jack Yang and Alanson P Sample. Em-comm: Touch-based communication via modulated electromagnetic emissions. *Proceedings of the ACM on Interactive, Mobile, Wearable and Ubiquitous Technologies*, 1(3):118, 2017.

[128] Manoj Gulati, Vibhutesh Kumar Singh, Sanchit Kumar Agarwal, and Vivek Ashok Bohara. Appliance activity recognition using radio frequency interference emissions. *IEEE Sensors Journal*, 16(16):6197–6204, 2016.

[129] Eric Blossom. Gnu radio: tools for exploring the radio frequency spectrum. *Linux journal*, 2004(122):4, 2004.

[130] Amit Sharma. Amitec electronics ltd. (india). `https://amitec.co`, 2016 [Date accessed: 19.12.2018].

[131] Christopher KI Williams and Carl Edward Rasmussen. Gaussian processes for regression. In *Advances in neural information processing systems*, pages 514–520, 1996.

[132] Carl Edward Rasmussen. The infinite gaussian mixture model. In *Advances in neural information processing systems*, pages 554–560, 2000.

[133] Yen Kheng Tan and Sanjib Kumar Panda. Energy harvesting from hybrid indoor ambient light and thermal energy sources for enhanced performance of wireless sensor nodes. *IEEE Transactions on Industrial Electronics*, 58(9):4424–4435, 2011.

[134] Vijay Raghunathan, Aman Kansal, Jason Hsu, Jonathan Friedman, and Mani Srivastava. Design considerations for solar energy harvesting wireless embedded systems. In *Information Processing in Sensor Networks, 2005. IPSN 2005. Fourth International Symposium on*, pages 457–462. IEEE, 2005.

[135] Henry A Sodano, Garnett E Simmers, Remi Dereux, and Daniel J Inman. Recharging batteries using energy harvested from thermal gradients. *Journal of Intelligent material systems and structures*, 18(1):3–10, 2007.

[136] Chen Zhao, Sam Yisrael, Joshua R Smith, and Shwetak N Patel. Powering wireless sensor nodes with ambient temperature changes. In *Proceedings of the 2014 ACM International Joint Conference on Pervasive and Ubiquitous Computing*, pages 383–387. ACM, 2014.

[137] Xudong Wang. Piezoelectric nanogenerators-harvesting ambient mechanical energy at the nanometer scale. *Nano Energy*, 1(1):13–24, 2012.

[138] Jing-Quan Liu, Hua-Bin Fang, Zheng-Yi Xu, Xin-Hui Mao, Xiu-Cheng Shen, Di Chen, Hang Liao, and Bing-Chu Cai. A mems-based piezoelectric power generator array for vibration energy harvesting. *Microelectronics Journal*, 39(5):802–806, 2008.

[139] Daniel J Yeager, Alanson P Sample, Joshua R Smith, and Joshua R Smith. Wisp: A passively powered uhf rfid tag with sensing and computation. *RFID handbook: Applications, technology, security, and privacy*, pages 261–278, 2008.

[140] Matthai Philipose, Joshua R Smith, Bing Jiang, Alexander Mamishev, Sumit Roy, and Kishore Sundara-Rajan. Battery-free wireless identification and sensing. *IEEE Pervasive computing*, 4(1):37–45, 2005.

[141] Vamsi Talla, Bryce Kellogg, Benjamin Ransford, Saman Naderiparizi, Shyamnath Gollakota, and Joshua R Smith. Powering the next billion devices with wi-fi. In *Proceedings of the 11th ACM Conference on Emerging Networking Experiments and Technologies*, page 4. ACM, 2015.

[142] Faisal Karim Shaikh and Sherali Zeadally. Energy harvesting in wireless sensor networks: A comprehensive review. *Renewable and Sustainable Energy Reviews*, 55:1041–1054, 2016.

[143] Manoj Gulati, Farshid Salemi Parizi, Eric Whitmire, Sidhant Gupta, Shobha Sundar Ram, Amarjeet Singh, and Shwetak N Patel. Capharvester: A stick-on capacitive energy harvester using stray electric field from ac power lines. *Proceedings of the ACM on Interactive, Mobile, Wearable and Ubiquitous Technologies*, 2(3):110, 2018.

[144] S Kang, S Yang, and H Kim. Non-intrusive voltage measurement of ac power lines for smart grid system based on electric field energy harvesting. *Electron. Lett*, 53(3):181–183, 2017.

[145] Joseph M Kahn, Randy H Katz, and Kristofer SJ Pister. Next century challenges: mobile networking for "smart dust". In *Proceedings of the 5th annual ACM/IEEE international conference on Mobile computing and networking*, pages 271–278. ACM, 1999.

[146] G Asada, M Dong, TS Lin, F Newberg, G Pottie, WJ Kaiser, and HO Marcy. Wireless integrated network sensors: Low power systems on a chip. In *Solid-State Circuits Conference, 1998. ESSCIRC'98. Proceedings of the 24th European*, pages 9–16. IEEE, 1998.

[147] Jinyeong Moon, John Donnal, Jim Paris, and Steven B Leeb. Vampire: A magnetically self-powered sensor node capable of wireless transmission. In *Applied Power Electronics Conference and Exposition (APEC), 2013 Twenty-Eighth Annual IEEE*, pages 3151–3159. IEEE, 2013.

[148] Samuel DeBruin, Branden Ghena, Ye-Sheng Kuo, and Prabal Dutta. Powerblade: A low-profile, true-power, plug-through energy meter. In *Proceedings of the 13th ACM Conference on Embedded Networked Sensor Systems*, pages 17–29. ACM, 2015.

[149] Hubert Zangl, Thomas Bretterklieber, and Georg Brasseur. Energy harvesting for online condition monitoring of high voltage overhead power lines. In *Instrumentation and Measurement Technology Conference Proceedings, 2008. IMTC 2008. IEEE*, pages 1364–1369. IEEE, 2008.

[150] Hubert Zangl, Thomas Bretterklieber, and Georg Brasseur. A feasibility study on autonomous online condition monitoring of high-voltage overhead power lines. *IEEE Transactions on Instrumentation and Measurement*, 58(5):1789–1796, 2009.

[151] Michael J Moser, Thomas Bretterklieber, Hubert Zangl, and Georg Brasseur. Strong and weak electric field interfering: Capacitive icing detection and capacitive energy harvesting on a 220-kv high-voltage overhead power line. *IEEE Transactions on Industrial Electronics*, 58(7):2597–2604, 2011.

[152] Anthony Rowe, Mario Berges, and Raj Rajkumar. Contactless sensing of appliance state transitions through variations in electromagnetic fields. In *Proceedings of the 2nd ACM workshop on embedded sensing systems for energy-efficiency in building*, pages 19–24. ACM, 2010.

[153] Protim Bhattacharjee, Shisagnee Banerjee, Manoj Gulati, Angshul Majumdar, and Shobha Sundar Ram. Supervised analysis dictionary learning: application in consumer electronics appliance classification. In *Proceedings of the Fourth ACM IKDD Conferences on Data Sciences*, pages 1–10, 2017.

[154] Pandarasamy Arjunan, Manaswi Saha, Haksoo Choi, Manoj Gulati, Amarjeet Singh, Pushpendra Singh, and Mani B Srivastava. Sensoract: a decentralized and scriptable middleware for smart energy buildings. In *2015 IEEE 12th Intl Conf on Ubiquitous Intelligence and Computing and 2015 IEEE 12th Intl Conf on Autonomic and Trusted Computing and 2015 IEEE 15th Intl Conf on Scalable Computing and Communications and Its Associated Workshops (UIC-ATC-ScalCom)*, pages 11–19. IEEE, 2015.

[155] Pandarasamy Arjunan, Manaswi Saha, Manoj Gulati, Nipun Batra, Amarjeet Singh, and Pushpendra Singh. Sensoract: Design and implementation of fine-grained sensing and control sharing in buildings.